1-1-2003

De-noising the CN Tower lightning current signal using short term Fourier transform-based spectral substraction

Mohammed Jahirul Islam
Ryerson University

De–Noising The CN Tower Lightning Current Signal Using Short Term Fourier Transform–Based Spectral Subtraction

By

Mohammed Jahirul Islam
(MSc. in Electronics and Computer Science, Shahjalal University of Science and Technology, Sylhet, Bangladesh, July 1997)

A Thesis Submitted in Partial Fulfillment of the Requirements for the Degree of
Master of Applied Science in Electrical and Computer Engineering

School of Graduate Studies
Ryerson University
Toronto, ON, Canada
August 2003

Abstract

De-Noising The CN Tower Lightning Current Signal

Using Short Term Fourier Transform-Based Spectral Subtraction

© Mohammed Jahirul Islam 2003

Master of Applied Science in Electrical and Computer Engineering

Ryerson University

The CN Tower is a transmission tower and it is not unexpected that recorded lightning current signals be corrupted by noise. The existence of noise may affect the calculation of current waveform parameters (current peak, 10-90% risetime to current peak, maximum steepness, and pulse width at half value of current peak). But accurate statistics of current waveform parameters are required to design systems for the protection of structures and devices, especially those with electrical and electronic components, exposed to hazards of lightning. Since more electrical devices are used nowadays, lightning protection becomes more important. So to determine accurate statistics of current waveform parameters, the interfering noise must be removed. In this thesis, we describe a technique for de-noising the CN Tower lightning current by modifying its Fourier Transform (FT) where a simulated current waveform (Heidler function) is used to represent the lightning current signal. The limitations of Discrete Fourier Transform (DFT) for removal of non-stationary noise signals, including the noise connected with CN Tower lightning current signals and its properties are discussed.

The Short Term Fourier Transform (STFT) is explored to analyze non-stationary signals and to deal with the limitations of DFT. Last of all, an STFT-based Spectral Subtraction method is developed to de-noise the CN Tower lightning current signal. In order to evaluate the Spectral Subtraction method, a simulated current derivative waveform (obtained by differentiating Heidler function) is artificially distorted by a noise signal measured at the CN Tower in the absence of lightning. The Spectral Subtraction method is then used to de-noise the distorted waveform. The de-noised waveform proved to be very close to the original simulated waveform.

A signal-peak to noise-peak ratio (SPNPR) of the CN Tower lightning current signal is defined and calculated before and after the de-noising process. For example, for a typical measured current derivative signal, the SPNPR before de-noising is 7.27, and after de-noising it becomes 151.30. Similarly for its current waveform (obtained by numerical integration), the SPNPR before de-noising is 20.16 and it becomes 361.39 after de-noising. Statistics of current waveform parameters are obtained from the de-noised waveforms. The Spectral Subtraction method is also applied for de-noising the electric and magnetic field waveforms generated by lightning to the CN Tower which enables the calculation of their waveform parameters.

Acknowledgements

I would like to express my deep gratitude and appreciation to my supervisor, Professor Ali M. Hussein for his invaluable guidance, encouragement and advice throughout my graduate studies.

The financial support of Dr. Ali M. Hussein, School of Graduate Studies and the Electrical and Computer Engineering Department of Ryerson University, which made my study possible, are greatly appreciated.

Special thanks go to Professor Sridhar Krishnan, Professor A. Anpalagan and Professor K. Raahemifar of the Electrical and Computer Engineering Department of Ryerson University, and Professor W. Janischewskyj of the University of Toronto.

I would like to express my gratitude to Ms. Dawn Wright, Program Assistant of Electrical and Computer Engineering and Spatial Analysis Department, School of Graduate Studies, Ryerson University for her full-fledged support and encouragement.

I would like to thank Mariusz Milewski, Petros Liatos, Kristopher Bitner and Ouarda Nedjah for their involvement in the Lightning Studies Project that enriched my experiences.

Last, but not the least, I would like to express my sincere appreciation to my parents, wife and best friend, Niru and my son, Raeid, for their patience, continual support and understanding over the years of my graduate studies.

Table of Contents

List of Figures

List of Tables

Chapter 1

Introduction

Lightning is one of the fascinating events of nature. Although the preliminary understanding of the lightning phenomenon was established by Benjamin Franklin early in the eighteenth century, it is still one of the major subjects in modern research [1]. The present research interest in the lightning area is mostly concerning on the protection of electrical and electronic components that are exposed to hazards of lightning such as those used in electric power lines, telecommunication systems, aircrafts and spacecrafts. Since more sensitive electronic devices are used nowadays, lightning protection has become more important than ever. In the meantime the development of high speed, high quality measuring instruments and advanced analysis methods make it possible to study lightning characteristics more precisely and efficiently.

1.1 Background

It is observed that tall structures receive more lightning strikes than plain ground. Traditionally they are very useful in studying characteristics of lightning. The Toronto Canadian National (CN) Tower, with a height of 553 m, is the tallest manmade freestanding structure in the world. While the local lightning flash density in Toronto area is less than 2 flashes per square kilometer per year, the tower usually receives many tens of direct strikes during a lightning season. For example, during the summer of 1991, the CN Tower was hit with 72 flashes, 24 of which occurred within 100 minutes in the early morning of July 7. Therefore, the CN Tower presents one of the best sites in the world to study the lightning phenomenon [2, 3].

Lightning Parameters Measuring Instrumentation

Lightning strikes to the CN Tower have been monitored since 1978, two years after its erection [3]. Successful simultaneous measurements of significant parameters of CN Tower lightning strikes have been performed since the summer of 1991 [2]. By the beginning of the summer of 1991, five measuring stations were operating to simultaneously measure seven of the most important lightning parameters [2].

The current derivative measuring station is one of the five measuring stations, and it is installed at the CN Tower. A 40-MHz Rogowaski coil, placed at the 474-m above ground level (AGL), captures approximately 20% of the current derivative since it encircles one fifth of the Tower's steel structure. The coil is connected, via a tri-axial cable, to a 10-bit, 10-ns, computer controlled double channel digitizer with segmented memory (Tektronix 710A) as shown in Fig. 1.1, presently placed at the 403-m AGL. The digitizer has two channels and it provides a 10-bit signal at ±0.4% accuracy and 200 MHz maximum sampling rate for a single channel operation or 100 MHz maximum sampling rate for both channels.

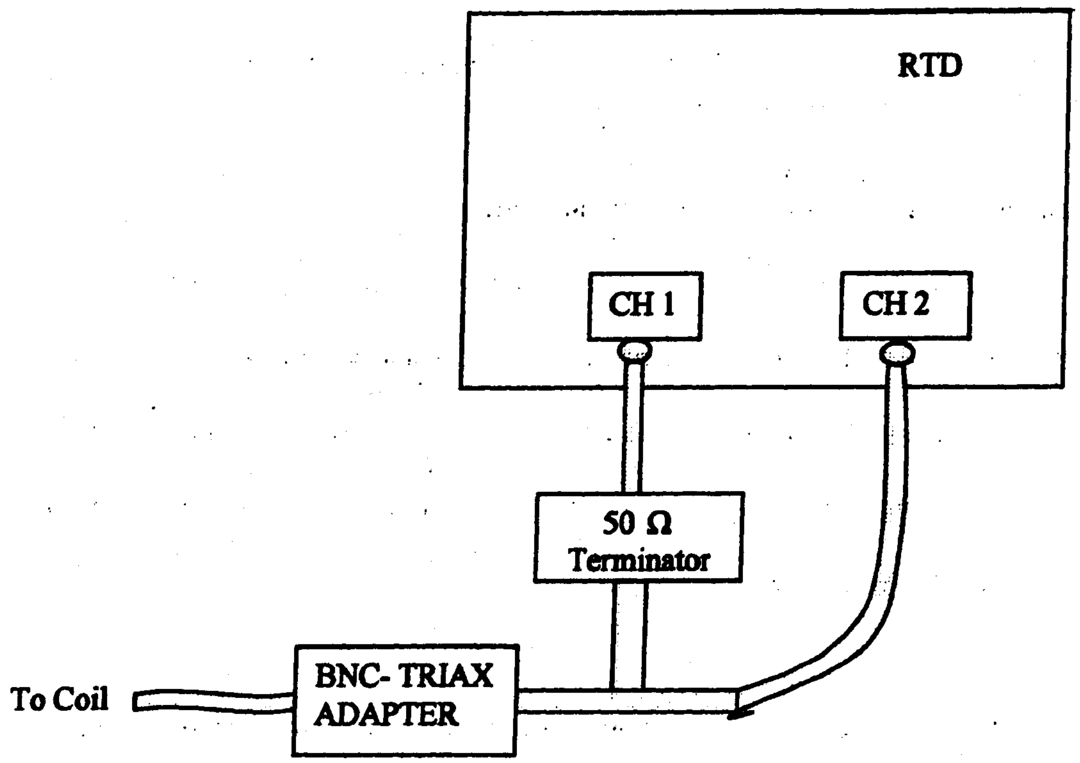

Figure 1.1: RTD (Real Time Digitizer) Connections at the CN Tower.

During the summer of 1997, a noise-protected current measuring system was placed at the Tower. This system features a new Rogowaski coil surrounding the whole steel structure of the Tower at the 509-m AGL and is connected to the recording station via an optical fiber link. The lightning current derivative *(di/dt)* measurement system at CN Tower is shown in Fig. 1.2.

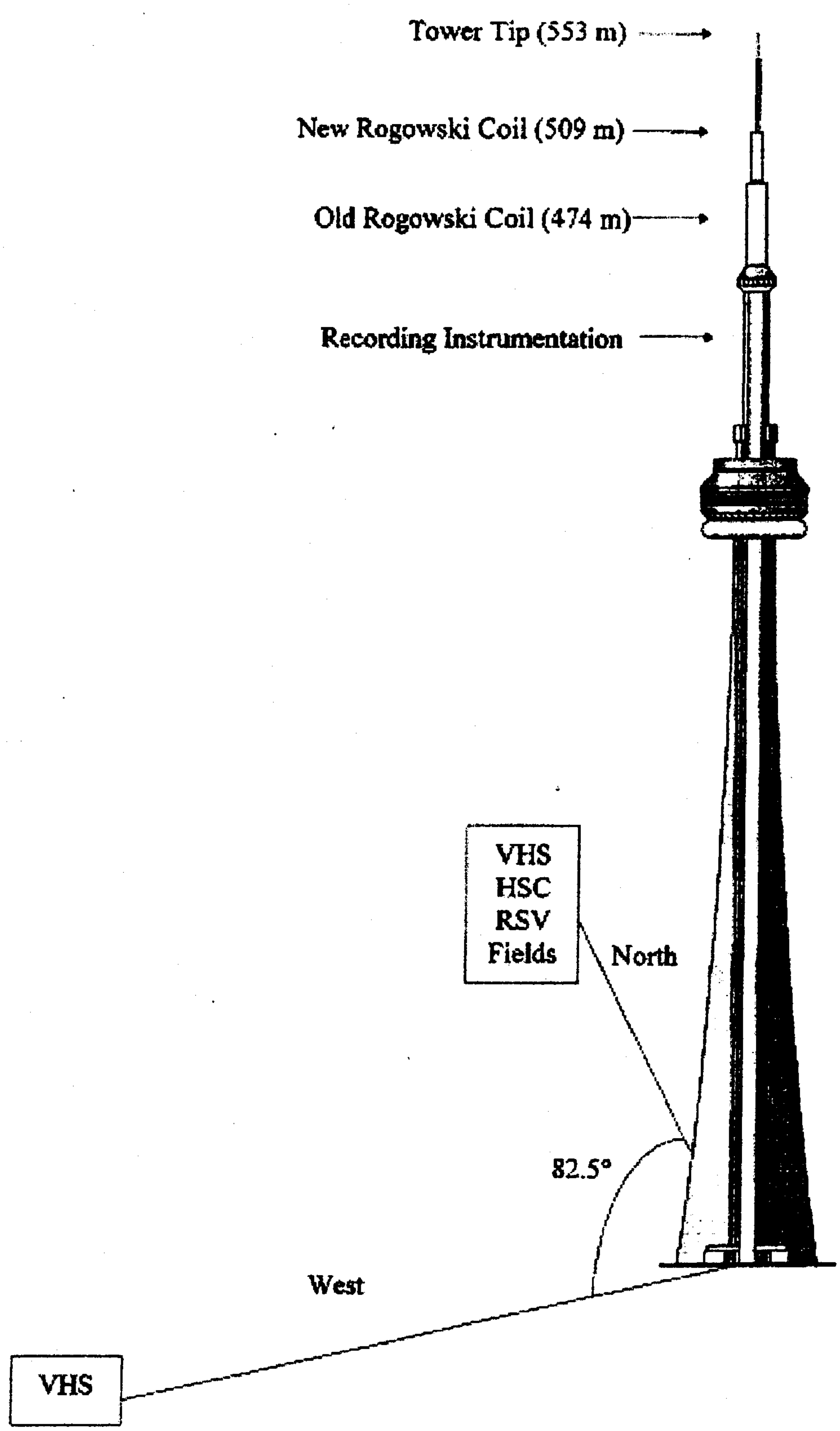

Figure 1.2: CN Tower lightning current derivative measuring system.

A typical current derivative waveform (recorded by the old coil) and its corresponding current waveform (obtained through time integration) of a CN Tower lightning stroke are, respectively, shown in Figs. 1.3 and 1.4. Each *di/dt* record contains 16 kilobytes (kB) of data recorded at 100 MHz (10 ns resolution). In some cases the last 2 kB of data recorded at 20 MHz (50 ns resolution). The digitized data is transferred and stored in a computer at the same time. Fig. 1.5 is the magnitude spectrum of the lightning current waveform of Fig. 1.4.

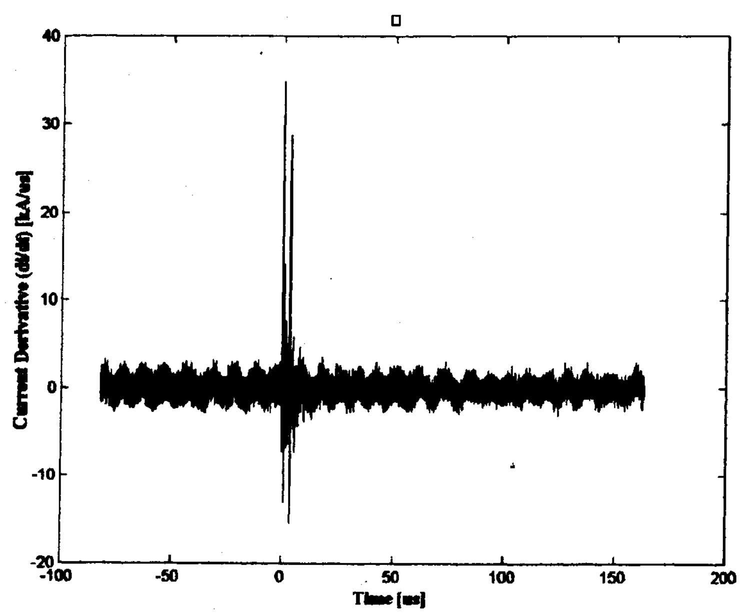

Figure 1.3: A typical lightning current derivative *(di/dt)*, File: F2050091.997 (1997).

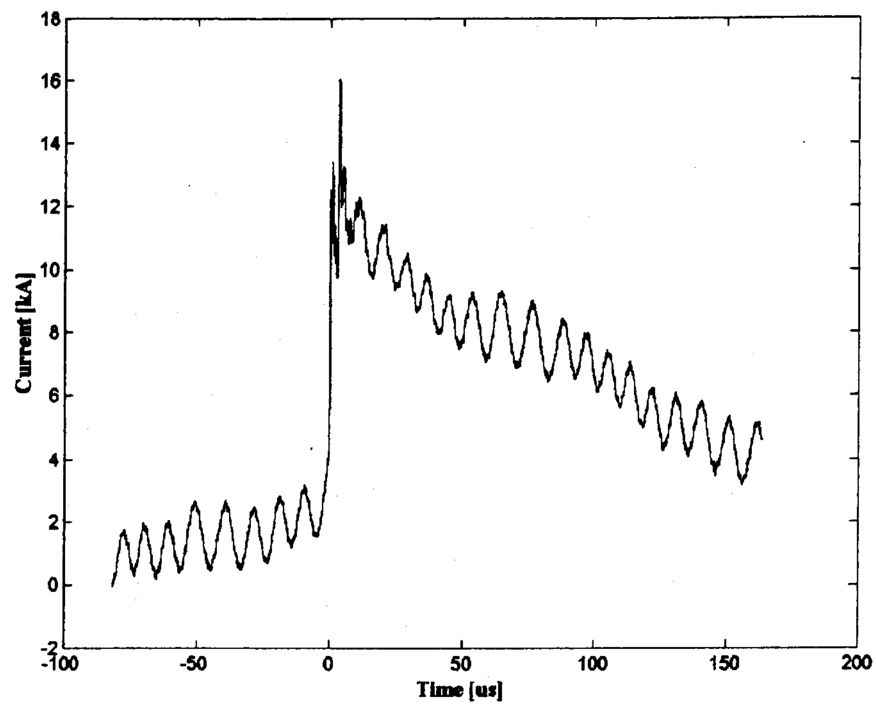

Figure 1.4: The lightning current waveform of the signal shown in Fig. 1.3.

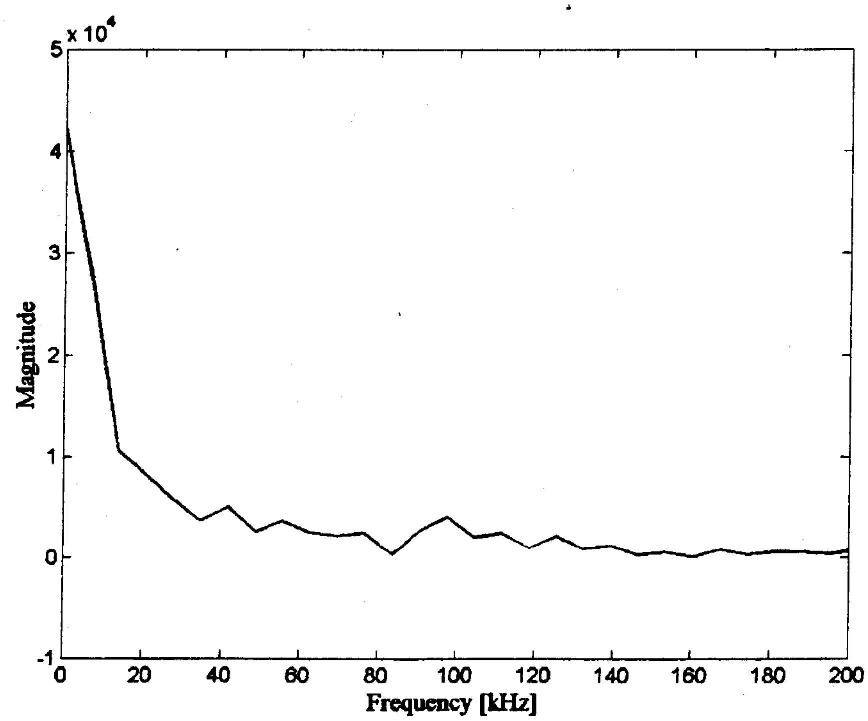

Figure 1.5: FFT of the CN Tower lightning current waveform of Fig. 1.4.

1.2 Motivations

The CN Tower itself is a transmission tower and it is not unexpected that recorded lightning current signals be corrupted by noise. From the waveforms Fig. 1.3 and Fig 1.4 and the magnitude response of the current waveform in Fig. 1.5, it is obvious that the measured current derivative and the current waveform is affected by various types of noise. These are as follows:

1. *DC Offset*

There is a noticeable DC offset in the typical *di/dt* and current waveform and this interference is projected as a noticeable ramp after integration (Fig. 1.4). This offset may be caused by the lightning charge to the measuring circuit.

2. *High Frequency Noise*

This type of noise does not have much effect on the waveforms with high peak values of *di/dt*. It does make the waveform shape unclear and peaks indistinct.

3. *Low Frequency Noise around 100 kHz*

The interference oscillating around 100 kHz is normally slow in comparison with fast-rising current waveforms. Nevertheless, with this interference present, it is hard to calculate the current waveform parameters (peak, maximum steepness and 10%- 90% risetime) [4].

4. *Reflections*

The discontinuities of the tower's structure cause several reflections when the lightning current is transmitted through the tower. It can be seen from the *di/dt* (Fig. 1.3) and current waveform (Fig. 1.4) waveforms that they have several distinct peaks after the first peak. The peaks appearing after the first peak are results of reflections from abrupt changes of the towers' structure. This is the reason why the absolute peak of current waveform is not considered as the injected current peak. However, for slow-rising injected current, the first peak may not represent the injected current peak, because the injected current reaches its peak after the first reflection arrives [5].

Lightning current data collected at the CN Tower since 1991 are corrupted with noise. Because of these kind of noise, there have been serious limitations concerning the use of the CN Tower current data captured during more than one decade (1991-2003). In order to determine statistics concerning current waveform parameters, these parameters (maximum steepness, current peak, 10%- 90% risetime to current peak, absolute peak and pulse width) must be accurately determined. Cumulative statistics based on extensive data and accurate current waveform parameters are needed to help in the establishment of more sophisticated protective measures against lightning hazards. This major objective cannot be realized without de-noising the measured current signal.

1.3 Existing Solutions

For the current derivative signal measured by the old Rogowski coil, the value of the usual background noise is about 50 mV [4]. However there were periods of time when the noise level was much higher, reaching up to 500 mV. The source of high amplitude noise that appears often has not yet been identified. The source of low frequency (100 kHz) noise is still unknown and the source of the high frequency noise is the broadcast antennas.

The noise embedded in a lightning waveform contains a broad spectrum of frequencies which makes it very difficult to eliminate without losing part of the lightning signal itself. To date attempts to de-noise CN Tower lightning current signals have not yielded satisfactory results.

Among different types of interference, DC offset is easy to remove by subtracting the average of the pre-stroke portion of the current derivative signal.

Most of the high frequency noise is removed when the numerical integration of the recorded current derivative is performed to determine the current waveform.

The low frequency noise is difficult to remove using existing software filters because of its frequency modulated nature which lies within the wideband frequency response of the measured signal.

Interference due to reflections is basically dependent on the structural discontinues of the tower and it is possible to remove using the transmission line model of the tower. So the low frequency noise, oscillating around 100 kHz is the dominant one that should be removed to get the accurate statistics of the lightning current waveform parameters.

In order to remove the interference from the lightning current signal adaptive filtering technique [7] has been tried to de-noise low frequency components and the success is limited. Because, the proposed algorithm is more suitable for signal of unlimited length. Therefore, for unlimited signal no difficulty is encountered in estimating and eliminating the interference; in such cases, the algorithm has enough time to identify the interference. However, signals with limited length may be affected by unidentified interferences of short duration like CN tower lightning current signals. In such cases, the algorithm loses its effectiveness in eliminating the noise due to the fact that it lacks enough information for proper identification of the noise.

It is evident from the limitations of the adaptive filtering technique that a new method needs to be devised to de-noise low frequency noise components around 100 kHz. This thesis proposes a method of de-noising the CN Tower lightning current signal by applying STFT-based Spectral Subtraction.

The proposed method takes the measured current derivative as its input and outputs the de-noised current derivative that can be used to obtain the values of current derivative and current waveform parameters, which eventually helps to design a protection systems to deal with hazards of lightning.

1.4 Objective of Studies

The main objectives of this thesis are:

1. To develop an appropriate method for de-noising the CN Tower lightning current signal.
2. To determine waveform parameters from the de-noised waveforms and establish a set of statistics data.
3. To apply the proposed method for de-noising the electric and magnetic field signals generated by lightning strikes to the CN Tower and to obtain their waveform parameters.

1.5 Outline of the Thesis

In chapter 2, Continuous Time Fourier Transform (CTFT), Aliasing and Nyquist theorem, Discrete Fourier Transform (DFT) and its properties are described to analyze the frequency components of a signal. Fast Fourier Transform (FFT) is a computational tool of Fourier transform. So FFT is used for the above purpose and the limitations of DFT are described. For non-stationary signal analysis, Short Term Fourier Transform (STFT) is suitable which is the advanced form of Fourier Transform. In this chapter STFT is also described. The properties and relative merits of various window functions are described in this chapter to select the best window for our problems.

In chapter 3, the STFT-based Spectral Subtraction is described. A simulated current waveform, called Heidler function, is used to model the lightning current signal. This function is basically used to propose the final method called STFT- based Spectral Subtraction method for de-noising the CN Tower lightning current signal. This STFT- based Spectral subtraction method is formulated and implemented in this chapter. We compared the de-noised waveforms to those measured by the new coil. Results of the proposed method applied on the measured *di/dt* are also reported in this chapter.

In chapter 4, lightning current derivative and integrated current waveform parameters and their statistics are obtained from the waveform de-noised by the proposed method. The proposed method is applied on the electric and magnetic field waveforms, generated by lightning strikes to the tower and their corresponding parameters are obtained in this chapter.

Final Conclusions, including discussions, major contributions, main features and future work are reported in Chapter 5.

Chapter 2

Introduction to Non-Stationary Signal Analysis

In this chapter, Continuous Time Fourier Transform (CTFT), Aliasing and Nyquist Theorem, Discrete Fourier Transform (DFT), its properties and pitfalls, Short Term Fourier Transform, different window functions, their properties and the relative merits that will eventually help to formulate the proposed method are described.

2.1 Continuous Time Fourier Transform (CTFT)

The Fourier transform is used to transform a continuous time signal into the frequency domain. It describes the continuous spectrum of a nonperiodic time signal. The Fourier transform *X(f)* of a continuous time function *x(t)* can be expressed as

$$X(f) = \int_{-\infty}^{\infty} x(t)e^{-j2\pi ft}dt \tag{2.1}$$

The inverse transform is

$$x(t) = \int_{-\infty}^{\infty} X(f)e^{j2\pi ft}df \tag{2.2}$$

2.1.1 Sampling and Aliasing

In many common situations in engineering a function *x(t)* is sampled. When a function is evaluated by numerical procedures, it is always necessary to sample the function in some manner, because digital computers cannot deal with analogue, continuous functions (except by sampling them!). Often the function is not even explicitly defined, but only known as a series of values recorded on tape, data logger or computer.

A/D Converters

If the signal to be analyzed is analogue in nature then it must be converted into digital form, as it is sampled, by an analogue to digital (A/D) converter.

Sampling

If delta is the time interval between consecutive samples, then the sampled time data can be represented as

$$h_n = h(n\Delta) \qquad n = 0,\ \pm 1,\ \pm 2 \ldots$$

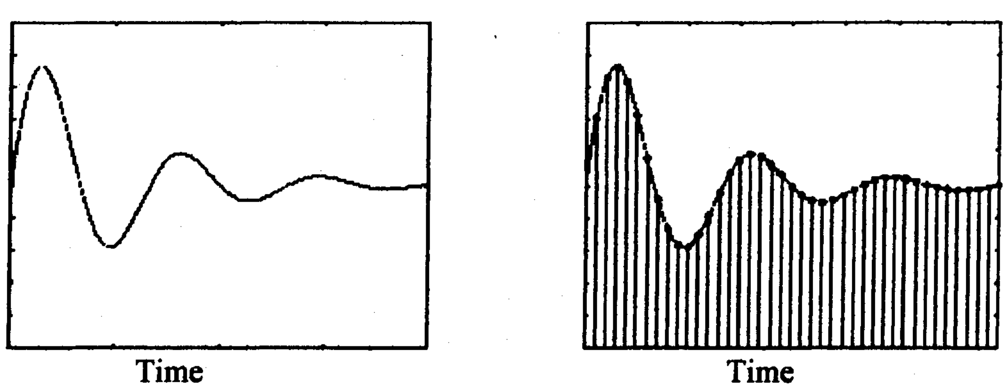

Figure 2.1: Continuous time signal and its corresponding sampled signal.

Consider an analogue signal $x(t)$ that can be viewed as a continuous function of time, as shown in Fig. 2.1. We can represent this signal as a discrete time signal by using values of $x(t)$ at intervals of nT_s to form $x(n)$ as shown. We are "grabbing" points from the function $x(t)$ at regular intervals of time, T_s, called the sampling period.

It is usual to specify a sampling rate or frequency f_s rather than the sampling period. The frequency is given by $f_s = 1/T_s$, where f_s is in Hertz. If the sampling rate were high enough, then the signal $x(t)$ could be constructed from $x(n)$ by simply joining the points by small linear portions. This approximates the analogue signal.

Aliasing and the Nyquist Theorem

One would expect that if the signal has significant variation then T_s must be small enough to provide an accurate approximation of the signal $x(t)$. Significant signal variation usually implies that high frequency components are present in the signal. It could therefore be inferred that the higher the frequency of the components present in the signal, the higher the sampling rate should be. If the sampling rate is not high enough to sample the signal correctly then a phenomenon called aliasing occurs.

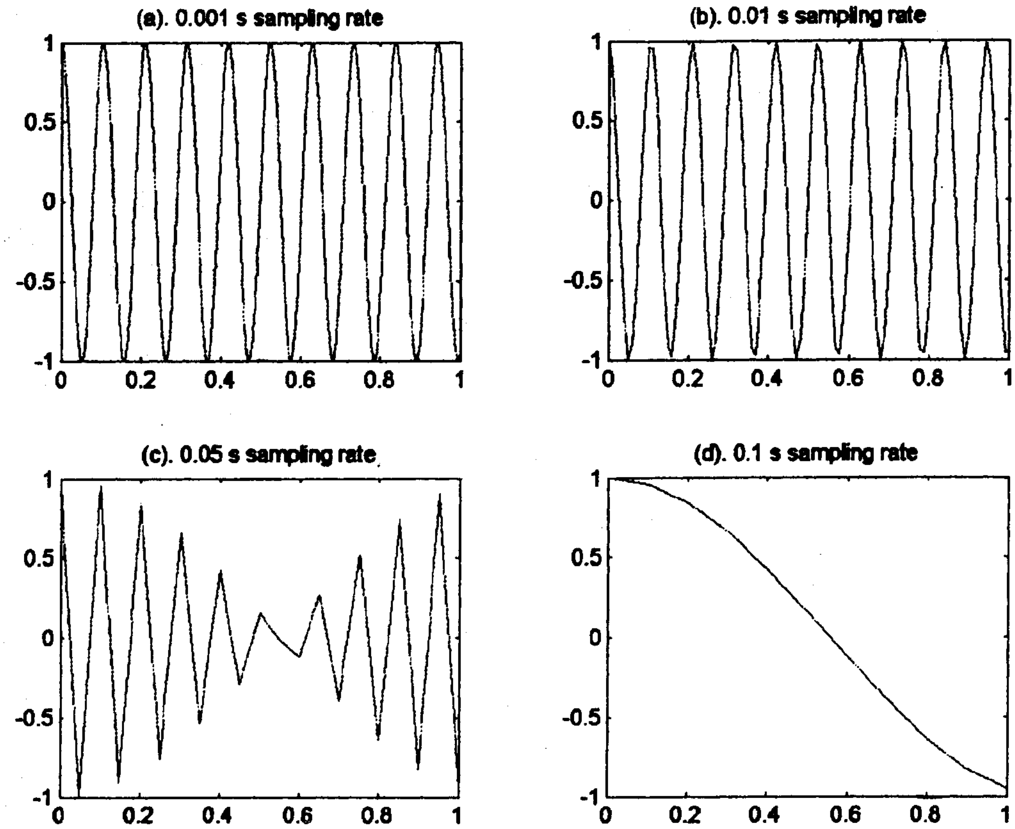

Figure 2.2: Effect of different sampling rates.

The Fig. 2.2 shows the effect of different sampling rates when sampling the function *cos(60t)*. The term aliasing refers to the distortion that occurs when a continuous time signal has frequencies larger than half of the sampling rate. The process of aliasing describes the phenomenon in which components of the signal at high frequencies are mistaken for components at lower frequencies.

The *Nyquist Sampling Theorem* states that to avoid aliasing occurring in the sampling of a signal the sampling rate should be greater than or equal to twice the highest frequency present in the signal. This is referred to as *the Nyquist Sampling Rate.*

Frequency Domain View of Sampling

When a continuous time signal is sampled, its spectrum will show the aliasing effect if aliasing occurs because regions of the frequency domain will be shifted by an amount equal to the sampling frequency.

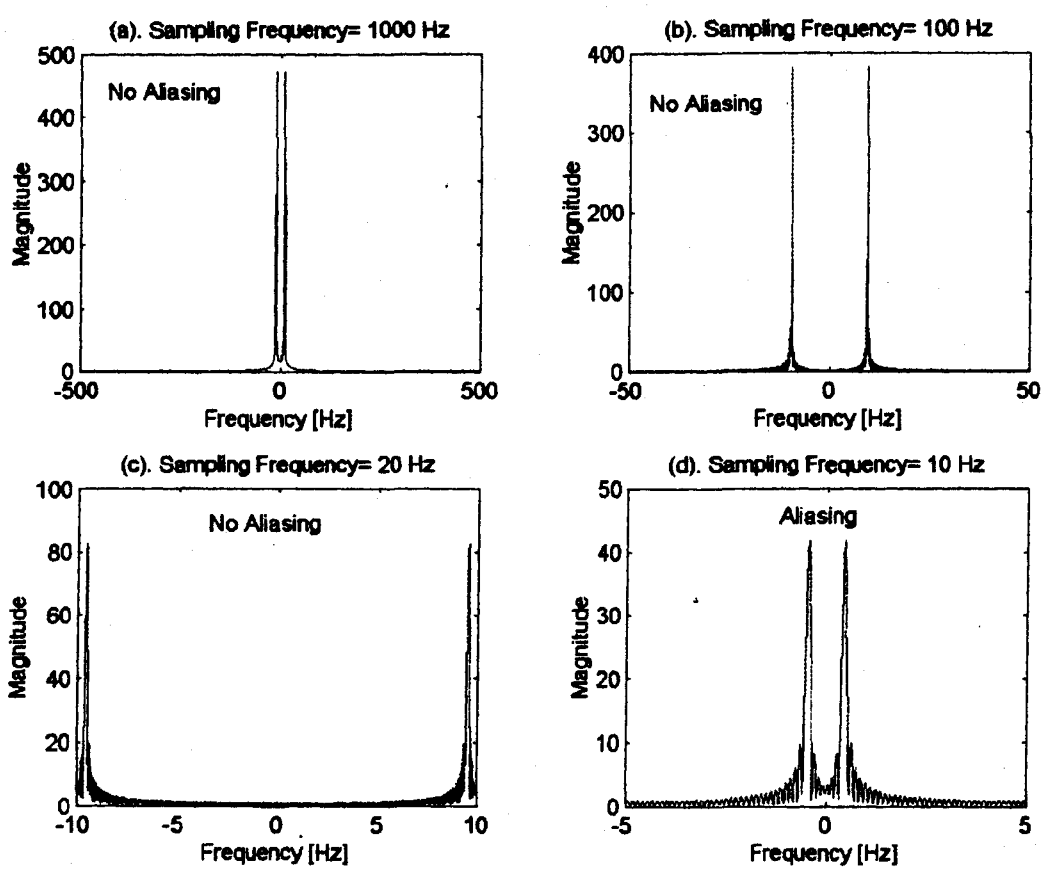

Figure 2.3: Magnitude spectra of sampled waveforms shown in Fig. 2.2.

The magnitude spectra of the signals in Fig. 2.2 that were sampled at different sampling frequencies of 1000 Hz, 100 Hz, 20 Hz and 10 Hz, respectively are shown in Fig. 2.3. From these figures it is clearly observed that if the sampling frequency is less than the Nyquist frequency, aliasing occurs.

2.2 Discrete Fourier Transform (DFT)

The Discrete Time Fourier Transform (DTFT) or simply Fourier Transform $X(e^{j\omega})$ of a discrete-time sequence *x(n)* is defined by

$$X(e^{j\omega}) = \sum_{n=-\infty}^{\infty} x(n)e^{-j\omega n} \tag{2.3}$$

In case of finite length sequence *x(n)*, $0 \le n \le N-1$, there is a simple relation between the sequence and its DTFT $X(e^{j\omega})$.In fact for a length-N sequence, only N values of $X(e^{j\omega})$, called the *frequency samples,* at N distinct points, $\omega = \omega_k$, $0 \le k \le N-1$, are sufficient to determine *x(n)* and hence, $X(e^{j\omega})$, uniquely. This leads to the concept of the Discrete Fourier Transform (DFT), a transform-domain representation that is applicable only to a finite-length sequence.

The simplest relation between a finite-length sequence *x(n)*, defined for $0 \le n \le N-1$, and its DTFT $X(e^{j\omega})$ is obtained by uniformly sampling $X(e^{j\omega})$ on the ω -axis between $0 \le \omega \le 2\pi$ at $\omega_k = 2\pi k/N$, $0 \le k \le N-1$. From Eq. (2.3),

$$X(k) = X(e^{j\omega})\Big|_{\omega = 2\pi k/N} = \sum_{n=0}^{N-1} x(n)e^{-j2\pi kn/N}, \qquad 0 \le k \le N-1 \tag{2.4}$$

Note that *X(k)* is also a finite-length sequence in the frequency domain and is of length *N*. The sequence *X(k)* is called the Discrete Fourier transform (DFT) of the sequence *x(n)*.

The Inverse discrete Fourier Transform (IDFT) is given by

$$x(n) = \frac{1}{N}\sum_{k=0}^{N-1} X(k)e^{j2\pi kn/N}, \qquad 0 \le n \le N-1 \tag{2.5}$$

Using the commonly used notation $W_N = e^{-j2\pi/N}$ we can rewrite Eq. (2.4) and (2.5) as

$$X(k)=\sum_{n=0}^{N-1}x(n)W_N{}^{kn}, \quad 0\le k\le N-1 \tag{2.6}$$

and

$$x(n)=\frac{1}{N}\sum_{k=0}^{N-1}X(k)W_N{}^{kn}, \quad 0\le n\le N-1 \tag{2.7}$$

The Fast Fourier Transform

The Fast Fourier Transform (FFT) is simply a class of special algorithms which implement the discrete Fourier transform with considerable savings in computational time. It must be pointed out that the FFT is not a different transform from the DFT, but rather just a means of computing the DFT with a considerable reduction in the number of calculations required.

While it is possible to develop FFT algorithms that work with any number of points, maximum efficiency of computation is obtained by constraining the number of time points to be an integer power of two, e.g. 1024 or 2048.

Approximation of Continuous Time Transforms with the DFT

The approximations involved when using the DFT in the analysis of continuous time systems must be carefully understood. There are problems that arise in the process that may lead to erroneous results unless proper precautions are taken.

While the mathematical properties of the DFT are exact, the DFT is seldom of interest as the end goal. It is usually employed to transform data which may arise from either an actual continuous time process or perhaps a discrete time process which is being analyzed from a continuous time system approach. The DFT is usually used to approximate the Fourier

Transform of a continuous time process, and it is necessary to understand some of the limitations inherent in this approach.

There are two possible phenomena that result in errors between the computed and the desired transform [8, 9]. These two phenomena are (a) picket-fence effect, and (b) leakage.

(a) Picket-Fence Effect: This effect is produced by the inability of the DFT to observe the spectrum as a continuous function, since computation of the spectrum is limited to integer multiples of the fundamental frequency $2\pi / N$ (reciprocal of the sample length N). Observation of the spectrum with the DFT is analogous to looking at it through a sort of "picket-fence," since we can observe the exact behavior only at discrete points. The major peak of a particular component could lie between two of the discrete transform lines, and the peak of this component might not be detected without some addition processing.

One procedure for reducing the picket-fence effect is to vary the number of points in a time period by adding zeros at the end of the original record, while maintaining the original record intact. This process artificially changes the period, which in turn changes the locations of the spectral lines without altering the continuous form of the original spectrum. In this manner, spectral components originally hidden from view can be shifted to points where they can be observed.

(b) Leakage: This problem arises because of the practical requirement that we must limit observation of the signal to a finite interval. The process of terminating the signal after a finite number of terms is equivalent to multiplying the signal by a window function. The net effect is a distortion of the spectrum. There is a spreading or leakage of the spectral components away from the correct frequency, resulting in an undesirable modification of the total spectrum.

The leakage effect cannot always be isolated from the aliasing effect because leakage may also lead to aliasing. Since leakage results in a spreading of the spectrum, the upper frequency may move beyond the Nyquist frequency, and aliasing may then result. The best approach for alleviating the leakage effect is to choose a suitable window function that minimizes the spreading.

To summarize this section, the DFT algorithm can be used to approximate the transform of a continuous time function, subject to the following limitations and difficulties.

1. The signal must be band limited, and the sampling rate must be sufficiently high to avoid aliasing.
2. If it necessary to limit the length of the signal for computational purposes, the spectrum will be degraded somewhat by the leakage effect. Leakage is most severe when the simple rectangular window function is used.
3. Components lying between discrete frequency lines are subject to error in magnitude due to the "picket-fence" effect.
4. The magnitude level may be different from that of the continuous-time transform due to the variation in definitions.

2.2.1 Discrete Fourier Transform Properties

There are a number of important properties of the DFT which are useful in digital signal processing applications [10]. These are tabulated in Table 2.1.

Table 2.1: General properties of the DFT.

Type of Property	Length-N Sequence	N-point DFT
	$g(n)$ $h(n)$	$G(k)$ $H(k)$
Linearity	$\alpha g(n)+\beta h(n)$	$\alpha G(k)+\beta H(k)$
Circular time-shifting	$g\left(\langle n-n_0\rangle_N\right)$	$W_N^{k_0 n}G(k)$
Circular frequency-shifting	$W_N^{-k_0 n}g(n)$	$G\left(\langle n-n_0\rangle_N\right)$
Duality	$G(n)$	$Ng\left(\langle -k\rangle_N\right)$
N-point circular convolution	$\sum_{m=0}^{N-1} g(m)h\left(\langle n-m\rangle_N\right)$	$G(k)H(k)$
Modulation	$g(n)h(n)$	$\frac{1}{N}\sum_{m=0}^{N-1} G(m)H\left(\langle k-m\rangle_N\right)$
Parseval's relation	$\sum_{n=0}^{N-1}\lvert x(n)\rvert^2=\frac{1}{N}\sum_{k=0}^{N-1}\lvert X(k)\rvert^2$	

2.3 Short Term Fourier Transform (STFT)

A description of a non-stationary signal in the frequency domain using a simple DFT of the complete signal will provide misleading results [10]. To get around the time-varying nature of the signal parameters, an alternative approach would be to segment the sequence into a set of subsequences of short lengths, with each subsequence centered at uniform intervals of time and its DFT computed separately. If the subsequence length is reasonably small, the signal can be safely assumed to be stationary for practical purposes. As a result, the frequency-domain description of a long sequence is given by a set of short–length DFTs, i.e., a time-dependent DFT that is called STFT.

DFT based analysis/synthesis methods are very prevalent in signal processing literatures, primarily due to the existence of Fast Fourier Transform (FFT) algorithms, which allow the computation of the DFT to be performed in $O(N \log N)$, rather than $O(N^2)$ computations.

In this section we present a particular Fourier based analysis method called the Short Term Fourier Transform (STFT) [11, 12]. The DFT operates on finite length (Length N) sequences. The STFT is a formulation that can represent sequences of any length by breaking them into shorter blocks, or *frames*, and applying the DFT to each block. Since we are using length N DFTs, we must take the frames length $M \leq N$. A frame is constructed by multiplying the (possibly) infinite length sequence $x(n)$ by a length M window $w(n)$. The resulting sequences of length M can now be represented completely by length M DFTs.

The Short Term Fourier transform operates by windowing a signal. Let us define a length M windowed frame of data by:

$$x_m(n) \equiv x(n)w(n-mS) \tag{2.8}$$

Where m is the frame number and S is the "frame spacing" or "frame skip" number of samples advanced between frames. The windowing operation for a given frame is illustrated in the Fig. 2.4.

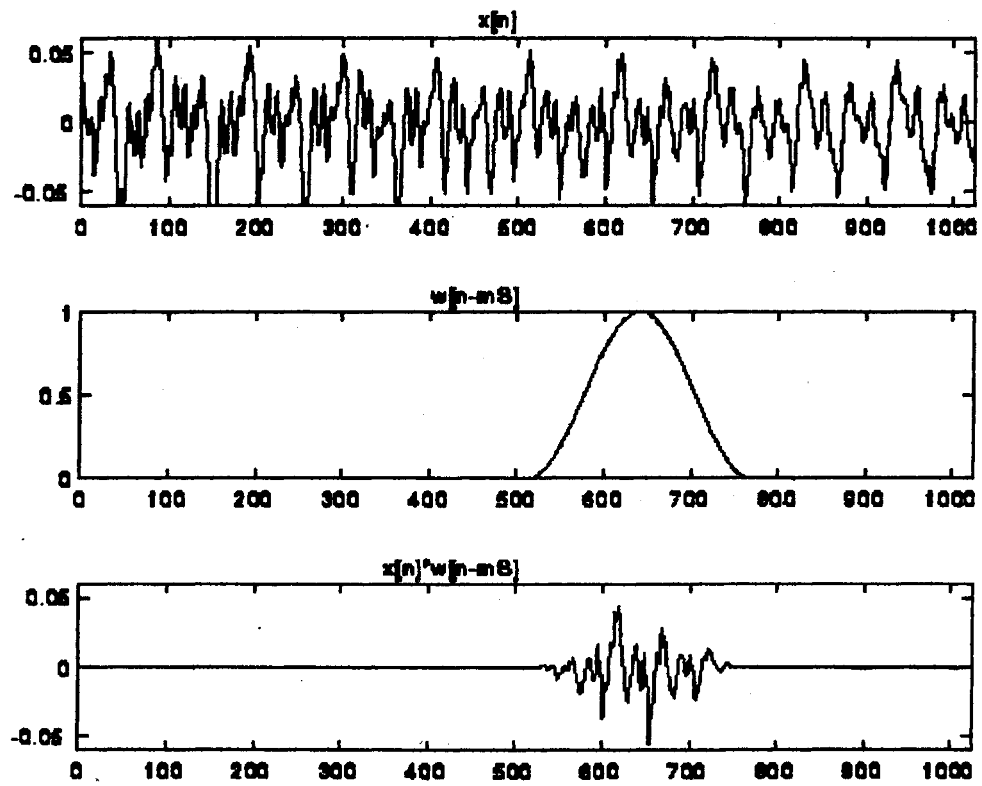

Figure 2.4: Windowing operation (Hanning window).

Now define the fixed-time-origin sequence

$$\overline{x_m}(n) \equiv x(n+mS)w(n) \tag{2.9}$$

where,

$$w(n)=0;\ n<0,\ n \geq M \tag{2.10}$$

Then we can define the DFT of $\overline{x_m}(n)$:

$$\overline{X_m}(k) = \sum_{n=0}^{N-1} \overline{x_m}(n) e^{-j\omega_k n} \tag{2.11}$$

This expression, a function of discrete frequency index *k*, and a frame index *m*, is the STFT of *x(n)*. Thus the STFT expresses a signal *x(n)* as a series of DFTs of windowed frames of *x(n)*.

Any time that $S \leq N$, it is possible to resynthesize *x(n)* from its STFT. In order to STFT synthesis using Overlap Add method, the windows and frame skip parameter *(S)* must be designed to meet the "Overlap Add (OLA) condition:"

$$\sum_{m=-\infty}^{\infty} w(n - mS) = 1 \tag{2.12}$$

If the Overlap Add condition is met, then

$$x(n) = x(n) \sum_{m=-\infty}^{\infty} w(n - mS) = \sum_{m=-\infty}^{\infty} \overline{x_m}(n - mS) \tag{2.13}$$

It is always best to design *w(n)* and *S* so that the STFT can be inverted using Overlap Add method.

The problem with STFT is the fact that its roots go back to what is known as the **Heisenberg Uncertainty Principle**. This principle originally applied to the momentum and location of moving particles, can be applied to time-frequency information of a signal. Simply, this principle states that one cannot know the exact time-frequency representation of a signal, i.e., one cannot know what spectral components exist at what instances of times. What one can know are the time intervals in which certain band of frequencies exist, which is a resolution problem [13].

2.3.1 Window Selection

In the STFT analysis of non-stationary signals, the window plays an important role. Both the length and shape of the window are critical issues that need to be examined carefully.

The function of the window *w(n)* is to extract a portion of the signal for analysis and ensure that the extracted section of *x(n)* is approximately stationary. To this end the window length *M* should be small, in particular for widely varying spectral parameters. A decrease in the window length increases the time-resolution property of the STFT, whereas the frequency-resolution property of the STFT increases with an increase in the window length. A shorter window thus provides a *wideband spectrogram* while a longer window results in a *narrowband spectrogram*. The two frequency-domain parameters characterizing the DTFT of a window are its main lobe width Δ_{ML} and the relative sidelobe amplitude A_{sl}. The former parameter determines the ability of the window to resolve two signal components in the vicinity of each other, while the latter controls the degree of leakage of one component into a nearby signal component. It thus follows that in order to obtain a reasonably good estimate of the frequency spectrum of a time-varying signal, the window should be chosen to have a very small relative sidelobe amplitude with a length chosen based on the acceptable accuracy of the frequency and time resolutions.

The considerations of narrow main lobe and very low amplitude sidelobes to avoid the "smearing" of the spectrum must be balanced against the OLA condition. The windows with the very best frequency selectivity, including the Hamming window, the Kaiser window doesn't satisfy the OLA condition.

The three most common windows that meet the OLA condition are the rectangular window, the triangular window and Hanning window.

The various window functions of length $2M+1$ are listed below:

Rectangular window is given by:

$$w_R(n) = \begin{cases} 1, 0 \le |n| \le M \\ 0, otherwise \end{cases} \tag{2.14}$$

Hanning window is given by:

$$w(n) = \frac{1}{2}\left[1 + \cos\left(\frac{2\pi n}{2M+1}\right)\right], \qquad -M \le n \le M, \tag{2.15}$$

Hamming window is given by

$$w(n) = 0.54 + 0.46\cos\left(\frac{2\pi n}{2M+1}\right), \qquad -M \le n \le M \tag{2.16}$$

Table 2.2 summarizes the essential properties of the above window functions.

Table 2.2 Properties of some fixed window functions.

Type of window	**Main lobe width Δ_{ML}**	**Relative sidelobe level A_{sl}**
Rectangular	$4\pi/(2M+1)$	13.3 dB
Hanning	$8\pi/(2M+1)$	31.5 dB
Hamming	$8\pi/(2M+1)$	42.7 dB

Magnitude Spectra of Different Window Functions

To get the magnitude spectra of most commonly used window functions like Rectangular, Hamming and Hanning window a sinusoidal signal of frequency 25 Hz is windowed using different windows and their magnitude spectra is shown in Fig. 2.5.

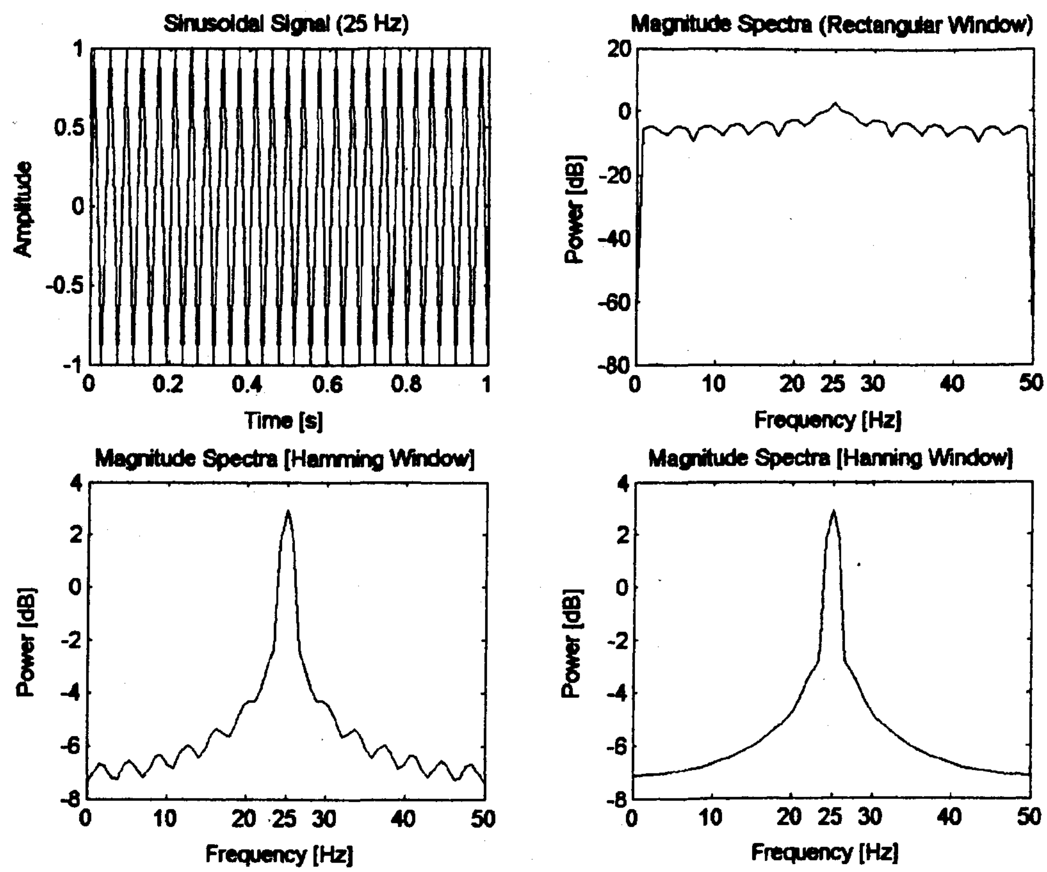

Figure 2.5: Magnitude spectra of different window functions

Lightning current derivative *(di/dt)* is segmented and windowed such that in the absence of spectral modifications, if the synthesis segments are added together, the resulting overall system reduces to an identity that is the Overlap Add (OLA) condition to reconstruct a signal. To improve the frequency resolution, one must use a window with a very small main lobe width, and to reduce the leakage, the window must have a very small relative sidelobe level

[10]. The main lobe width can be reduced by increasing the length of the window. Considering these parameters for window selection, Hanning window of length 2048 with number of overlapping points 1024 is chosen for this application [9].

2.3.2 Choice of FFT Length

Once we have decided the window function w and a length M, we can compute the DFT of this frame. The size, N, of this DFT must be at least M with additional samples being produced via "zero-padding". There are several issues involved in choosing a good value for N. First, in order to take advantage of the computational efficiency of the FFT algorithm, it is recommended to take N to be a power of 2. Secondly, the visual display produced by the analysis will be represented by N samples of DFT. The last issue to be considered in choosing the FFT length is based on the fact that we may modify the STFT before performing the re-synthesis [14].

2.3.3 Number of Overlapping Points

The decision for choosing overlap points is very application dependent. If the signal under analysis has rapid transients, then the analysis frame may require overlapping so that the overlapped portion contains the transients for better results. However, if the analysis is being performed with the ultimate goal of performing re-synthesis (with possible modifications), then there are more specific requirements. Usually, the length of overlapped points is half of the window width that is $M/2$. The Fig. 2.6 shows the overlapped frames.

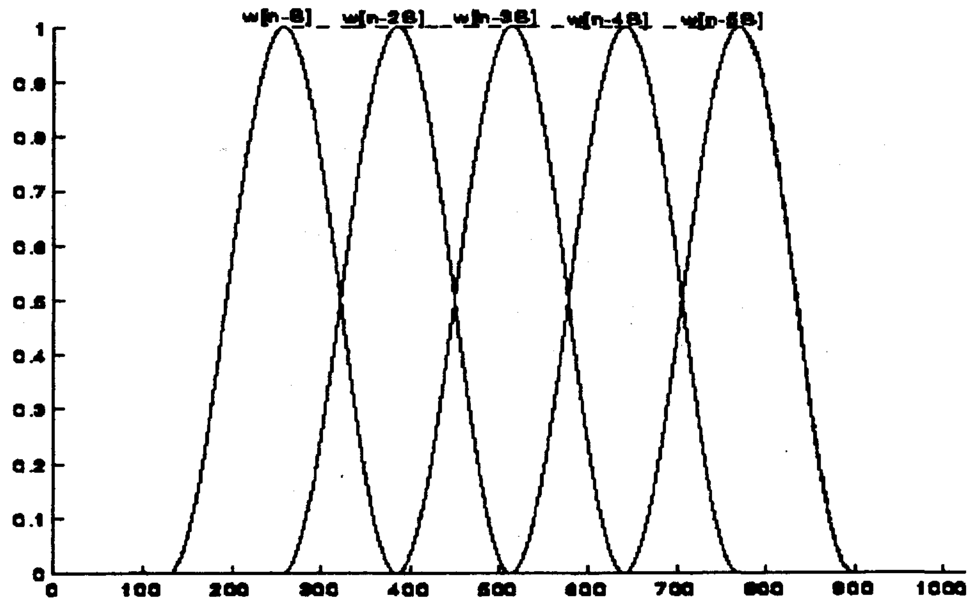

Figure 2.6: Overlapped frames using Hanning window.

2.3.4 Signal Reconstruction

In STFT, the method that is used for reconstructing the signal is called Overlap Add Method.

The overlap-add procedure showing the sum of three overlapping frames is shown is Fig. 2.7.

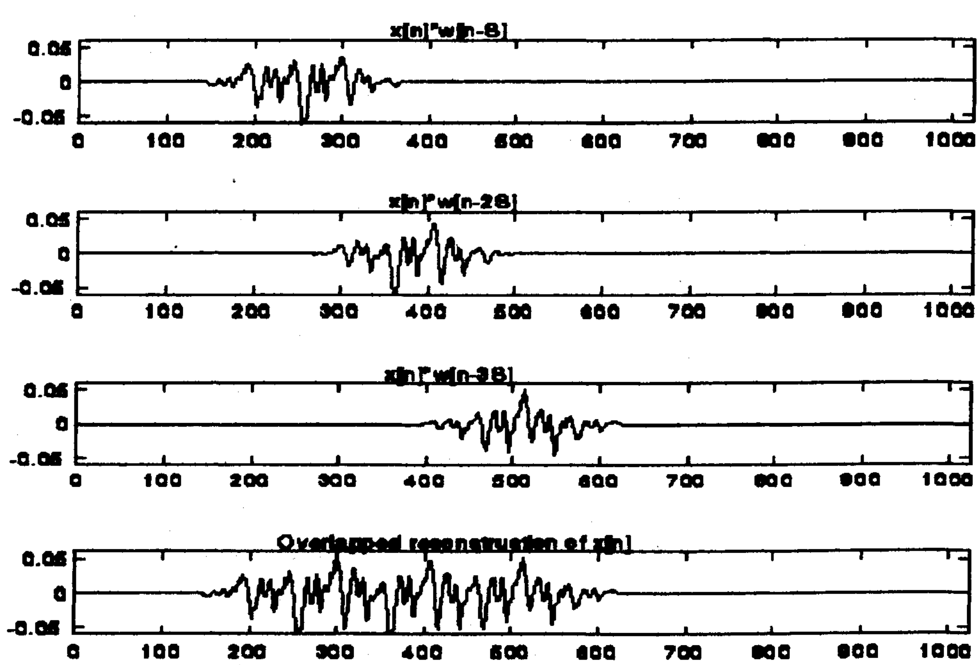

Figure 2.7: Overlap Add procedure to reconstruct the signal.

2.2.5 Overall System

In STFT, window type and size, length of FFT, length of overlapping points, etc. are basically application dependent. Once all parameters are selected for windowing and FFT, the next procedure is frequency domain modifications (problem dependent). Then using Overlap Add procedure, the signal can be reconstructed. The overall system block diagram is shown in Fig. 2.8.

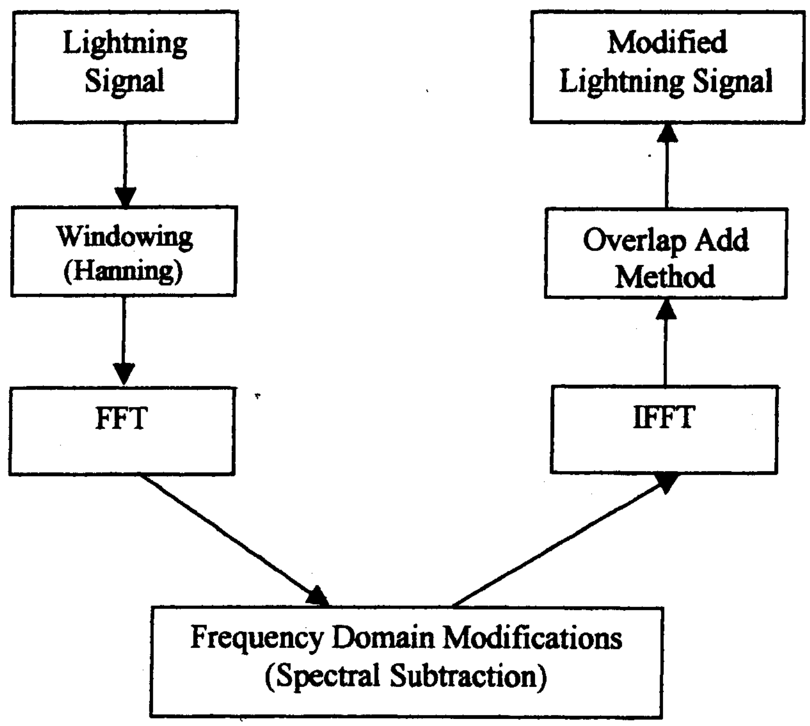

Figure 2.8: Block diagram of STFT analysis/ synthesis system.

Chapter 3

Formulation of the Algorithm

Formulation of the algorithm for reducing noise from the CN Tower lightning current signal is presented in this chapter. Development of the algorithm is presented after a brief review of the Spectral Subtraction method and Heidler function which is used to simulate the lightning current waveform. After reviewing all the relevant works, the final method/ algorithm is proposed and implemented in this chapter.

3.1 Spectral Subtraction Method

A stand-alone noise suppression algorithm is discussed in this section. This method is basically developed for reducing the spectral effects of additive noise from noisy signal. Spectral subtraction offers a computationally efficient, processor independent approach to digital signal analysis [15]. In this thesis, the STFT-based spectral subtraction is used to de-noise the CN Tower lightning current signal as well as electric field *(E)* and magnetic field *(H)*.

3.1.1 Assumptions

The following assumptions were used in developing the analysis:

1) The background noise is added to the pure signal.
2) The background noise environment remains locally stationary to the degree that the expected value of spectral magnitude prior to pure signal activity equals its expected value during pure signal activity.

3) Significant noise reduction is possible by removing the effect of noise spectrum.

3.1.2 Additive Noise Model

It is assumed that a windowed noise signal *u(n)* has been added to a windowed pure signal *s(n)*, with their sum denoted by *x(n)* [15]. Then

$$x(n) = s(n) + u(n) \tag{3.1}$$

Taking the Fourier transform gives,

$$X(e^{j\omega}) = S(e^{j\omega}) + U(e^{j\omega}) \tag{3.2}$$

Where

$$x(n) \leftrightarrow X(e^{j\omega}) \tag{3.3}$$

$$X(e^{j\omega}) = \sum_{n=0}^{N-1} x(n) e^{-j\omega n} \tag{3.4}$$

$$x(n) = \frac{1}{2\pi} \int_{-\pi}^{\pi} X(e^{j\omega}) e^{j\omega n} d\omega \tag{3.5}$$

3.1.3 Spectral Subtraction Estimator

At a given frequency bin, the estimated magnitude of the pure signal *s(n)* is the combined magnitude of the pure signal and noise *x(n)*, minus the estimated noise magnitude *u(n)*. Unfortunately we do not know the correct phase of the noise signal so we subtract the magnitude and leave the phase of $X(e^{j\omega})$ alone. The spectral subtraction filter $H(e^{j\omega})$ is calculated by replacing the noise spectrum $U(e^{j\omega})$ with spectra which can be readily measured. The magnitude $|U(e^{j\omega})|$ of $U(e^{j\omega})$ is replaced by its average value $\mu(e^{j\omega})$ taken during noise signal activity, and the phase $\theta_U(e^{j\omega})$ of $U(e^{j\omega})$ is replaced by the phase $\theta_x(e^{j\omega})$ of $X(e^{j\omega})$.

These substitutions result in the spectral subtraction estimator $\hat{S}(e^{j\omega})$:

$$\hat{S}(e^{j\omega}) = \left[\left|X(e^{j\omega})\right| - \mu(e^{j\omega})\right] e^{j\theta_x(e^{j\omega})} \tag{3.6}$$

or

$$\hat{S}(e^{j\omega}) = H(e^{j\omega}) X(e^{j\omega}) \tag{3.7}$$

with

$$H(e^{j\omega}) = 1 - \frac{\mu(e^{j\omega})}{\left|X(e^{j\omega})\right|} \tag{3.8}$$

$$\mu(e^{j\omega}) = E\left[\left|U(e^{j\omega})\right|\right] \tag{3.9}$$

The average noise magnitude $\mu(e^{j\omega})$ is calculated by taking the average of noise frames in each frequency bins.

Therefore the spectral error $e(e^{j\omega})$ resulting from this estimator is given by

$$e(e^{j\omega}) = \hat{S}(e^{j\omega}) - S(e^{j\omega}) = U(e^{j\omega}) - \mu(e^{j\omega}) e^{j\theta_x(e^{j\omega})} \tag{3.10}$$

This is the formulation behind spectral subtraction method, yet a number of simple modifications are available to reduce the effects of spectral error. These include:

1) Magnitude averaging
2) Half-wave rectification.

Magnitude Averaging

Since the spectral error equals the difference between the noise spectrum U and its mean μ, local averaging of spectral magnitudes can be used to reduce the error. Replacing $|X(e^{j\omega})|$ with $\overline{|X(e^{j\omega})|}$ where,

$$\overline{|X(e^{j\omega})|} = \frac{1}{M}\sum_{i=0}^{M-1}|X_i(e^{j\omega})| \tag{3.11}$$

$X_i(e^{j\omega}) = ith$ time-windowed transform of $x(k)$

gives

$$S_A(e^{j\omega}) = \left[\overline{|X(e^{j\omega})|} - \mu(e^{j\omega})\right]e^{j\theta_x(e^{j\omega})} \tag{3.12}$$

The rationale behind averaging is that the spectral error becomes approximately

$$e(e^{j\omega}) = S_A(e^{j\omega}) - S(e^{j\omega}) \cong \overline{|U|} - \mu \tag{3.13}$$

Where

$$\overline{|U(e^{j\omega})|} = \frac{1}{M}\sum_{i=0}^{M-1}|U_i(e^{j\omega})| \tag{3.14}$$

Thus, the sample mean of $|U(e^{j\omega})|$ will converge to $\mu(e^{j\omega})$ as a longer average is taken.

The obvious problem with this modification is that the signal is non-stationary, and therefore only limited time averaging is allowed.

Half-Wave Rectification

For each frequency bin ω where the noisy signal spectrum magnitude $|X(e^{j\omega})|$ is less than the average noise spectrum magnitude $\mu(e^{j\omega})$, the output will be negative after subtraction that doesn't have physical meaning. These negative outputs are set to zero. This modification can be simply implemented by half-wave rectification of $H(e^{j\omega})$. The estimator then becomes

$$\hat{S}(e^{j\omega}) = H_R(e^{j\omega})X(e^{j\omega}) \tag{3.15}$$

where

$$H_R(e^{j\omega}) = \frac{H(e^{j\omega}) + |H(e^{j\omega})|}{2} \tag{3.16}$$

Thus, the effect of half-wave rectification is to bias down the magnitude spectrum at each frequency ω by the noise bias determined at that frequency. The bias value can, of course, change from frequency to frequency as well as from analysis time window to time window. The advantage of half-wave rectification is that the noise floor is reduced by $\mu(e^{j\omega})$. The disadvantage of half-wave rectification can exhibit itself in the situation where the sum of the noise plus signal at a frequency ω is less than $\mu(e^{j\omega})$. Then the signal information at that frequency is incorrectly removed, implying a possible decrease in intelligibility.

Synthesis

After bias removal and half-wave rectification a time waveform is reconstructed from the modified magnitude. The overlapped data windows are added to form the output signal sequence. The overall system block diagram is shown in Fig. 3.1.

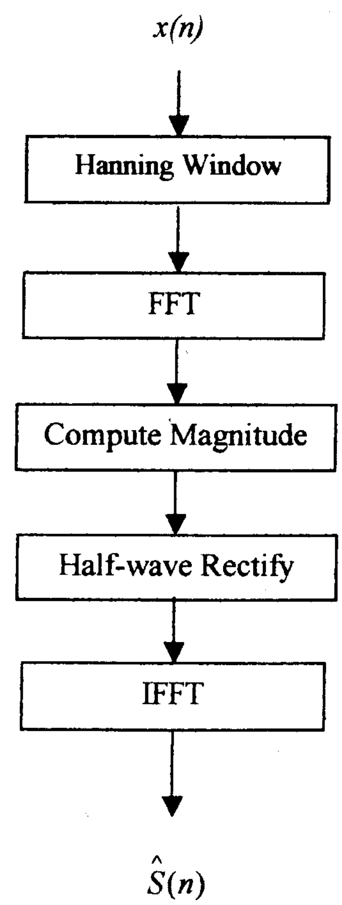

Figure 3.1: Block diagram of the overall Spectral Subtraction method.

3.2 Heidler Function Revisited

Heidler function [16,17] is a simulation of a lightning current stroke signal. Initially, a simulated Heidler function is considered to study the frequency components of the signal. Heidler function is given by,

$$i(t) = \frac{I_0}{2\alpha}\left[\frac{(t/\tau_1)^k}{1+(t/\tau_1)^k}e^{-t/\tau_2} + \frac{(t/\tau_3)^k}{1+(t/\tau_3)^k}e^{-t/\tau_4}\right] \tag{3.17}$$

Where

$\alpha = 0.92$ $\quad$ $\tau_4 = 5$ ms

$\tau_1 = \tau_3 = 0.23\ \mu s$ $\quad$ $k = 4$

$\tau_2 = 5\ \mu s$ $\quad$ $I_0 = 10$ kA (Current Peak)

The Heidler function (Fig. 3.2) is used to propose the STFT-based Spectral Subtraction as a technique for de-noising the CN Tower lightning current waveform. Initially, we artificially added frequency modulated signal to Heidler function and tried to remove the noise from the distorted Heilder function using manually de-noised method. Then this method is applied to the CN Tower current data and the de-noised signal is obtained. But it is always appreciated to develop an automated method that will take measured di/dt as its input and outputs the de-noised waveform. STFT-based Spectral Subtraction is one of the recommended methods. This method is applied to the derivative of the Heidler function, distorted by noise measured at the CN Tower during the absence of lightning.

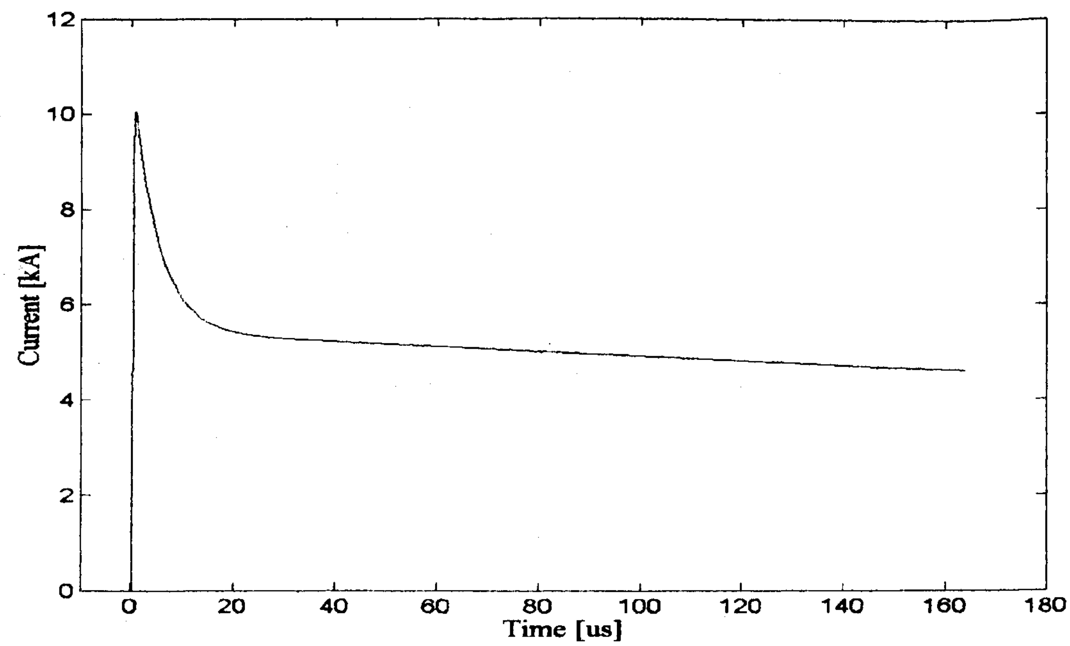

Figure 3.2: Heidler function.

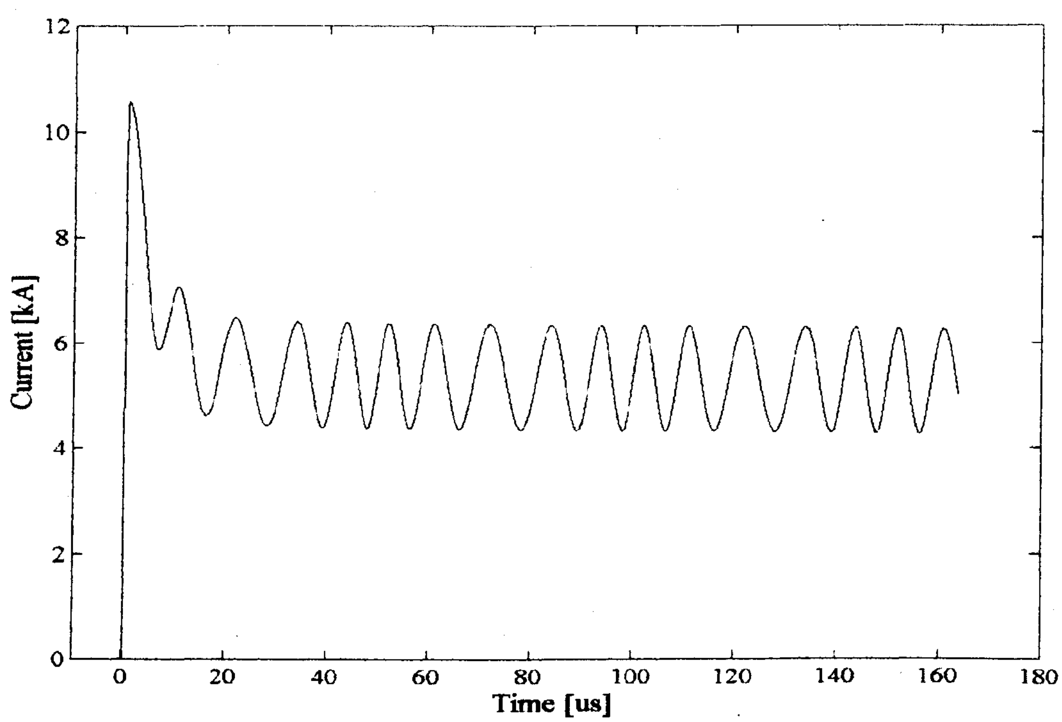

Figure 3.3: Distorted Heidler function.

As shown in Fig. 3.3, the Heidler function is distorted artificially by a frequency modulated signal (i_{noise}) of carrier frequency (f_c) 100 kHz and modulating frequency (f_m) 20 kHz.

$$i_{noise} = \sin(2\pi f_c t + \sin(2\pi f_m t)) \text{ [kA]} \tag{3.18}$$

The idea behind taking the carrier frequency 100 kHz and modulating frequency 20 kHz is because the mentioned dominant low frequency noise is around 100 kHz. When the FFT of the distorted Heidler function and that of the original Heidler function are compared, a local peak around 100 kHz is observed (see Fig. 3.4).

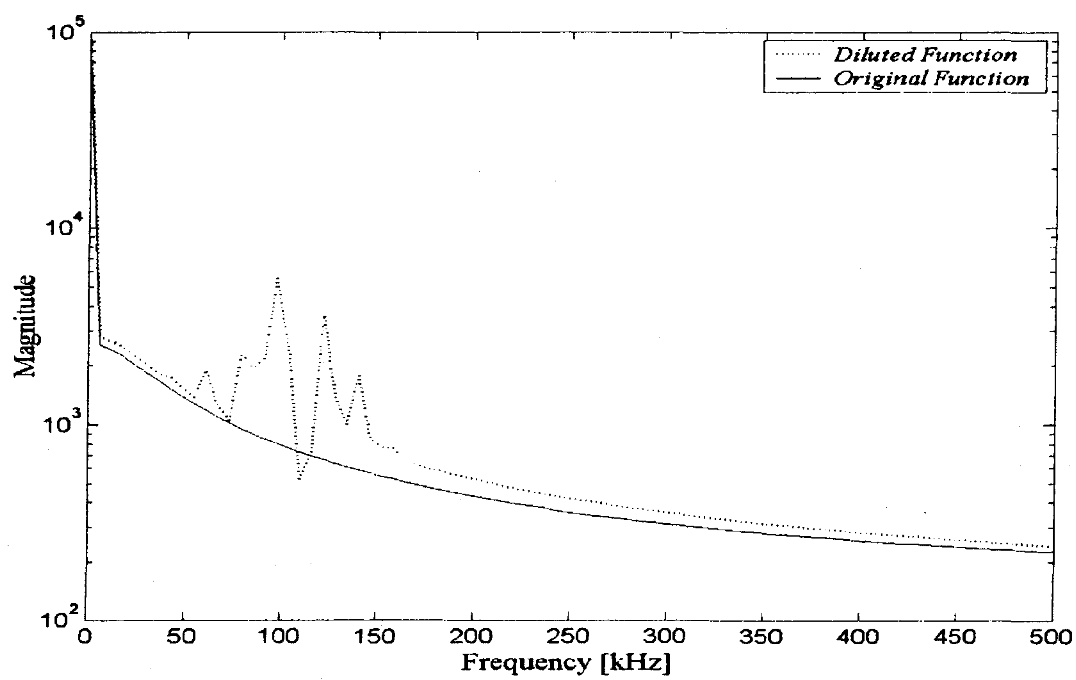

Figure 3.4: FFT of distorted and original Heidler function.

We then tried to de-noise the distorted Heidler function. In order to remove such a noise signal, the real and imaginary parts of the FFT of the distorted Heidler function are separated and a best fit with different order polynomial was used to replace a number of points in the vicinity of 100 kHz (see Figs. 3.5 and 3.6).

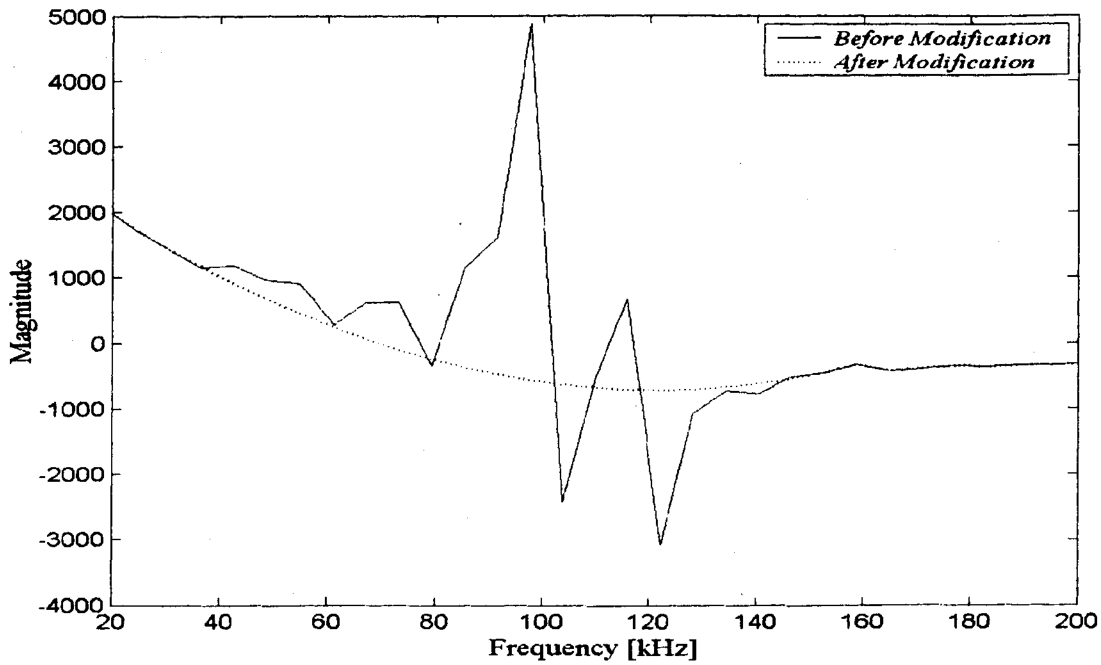

Figure 3.5: Real part of the FFT.

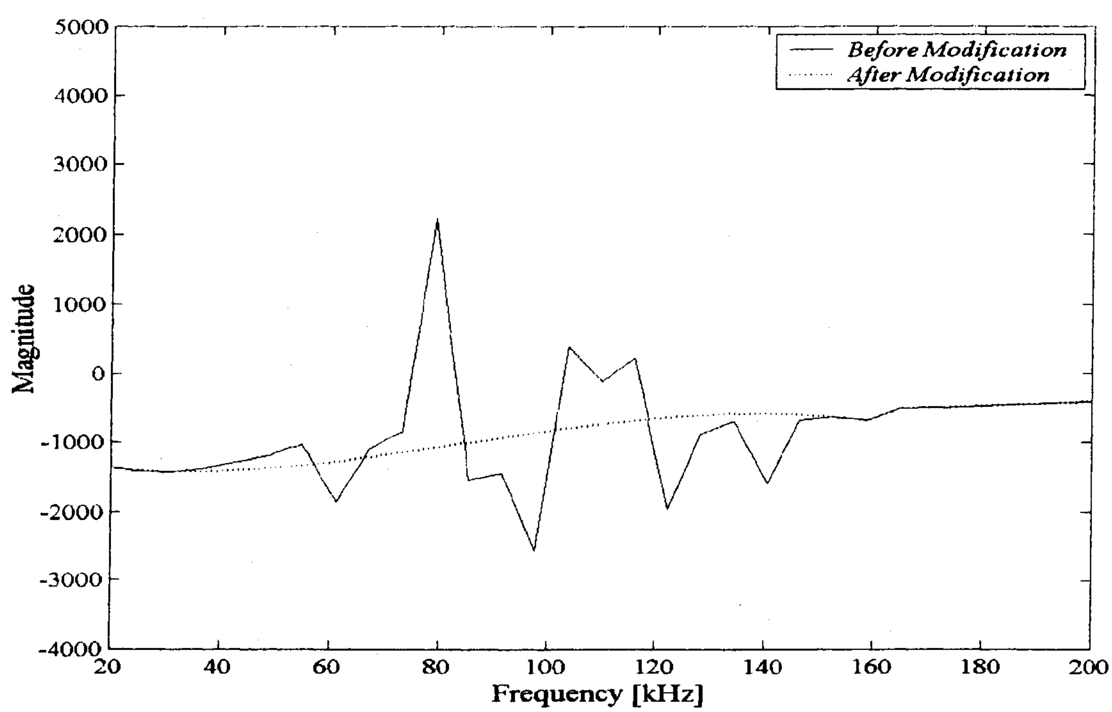

Figure 3.6: Imaginary part of the FFT.

Then the modified real and imaginary parts were combined together to form the modified FFT of the distorted Heidler function (Fig. 3.7). In Fig. 3.8, the modified FFT is compared with the FFT of the original Heidler function.

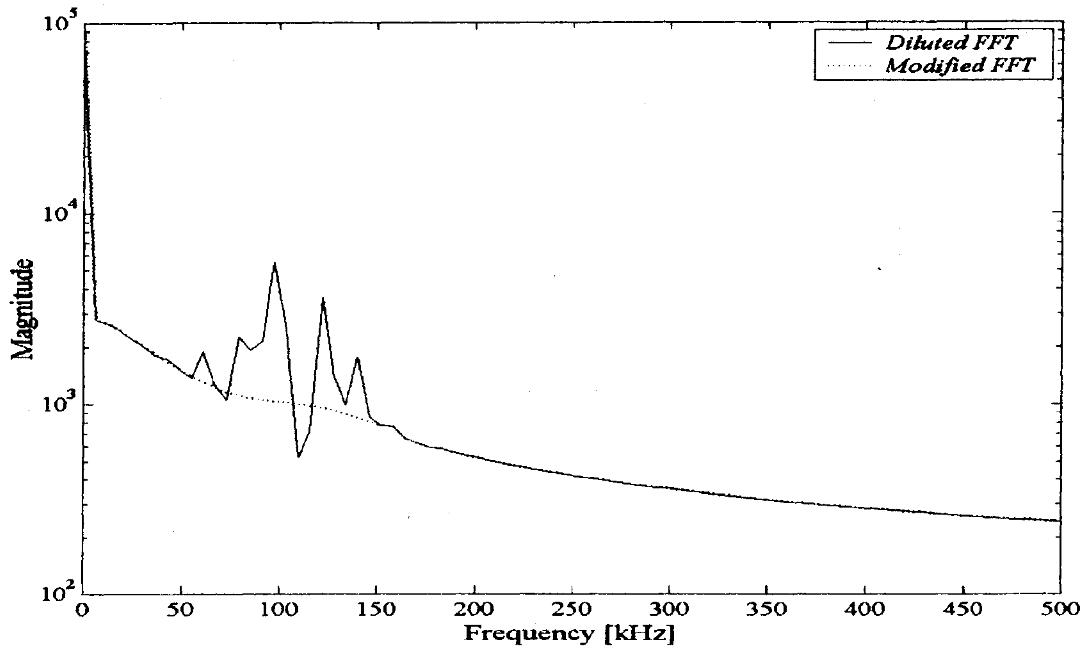

Figure 3.7: Modified and distorted FFT.

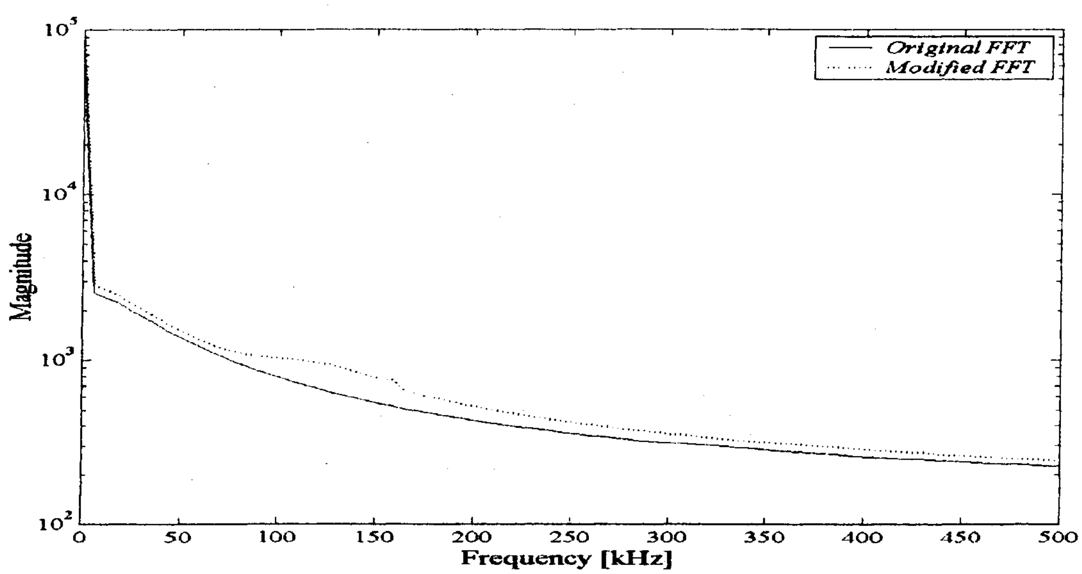

Figure 3.8: Modified and original FFT.

Then the modified FFT is converted back to time-domain using Inverse Fast Fourier Transform (IFFT). The time-domain signal after de-noising as shown in Fig 3.9 and Fig. 3.10, are compared to distorted and original Heidler function, respectively.

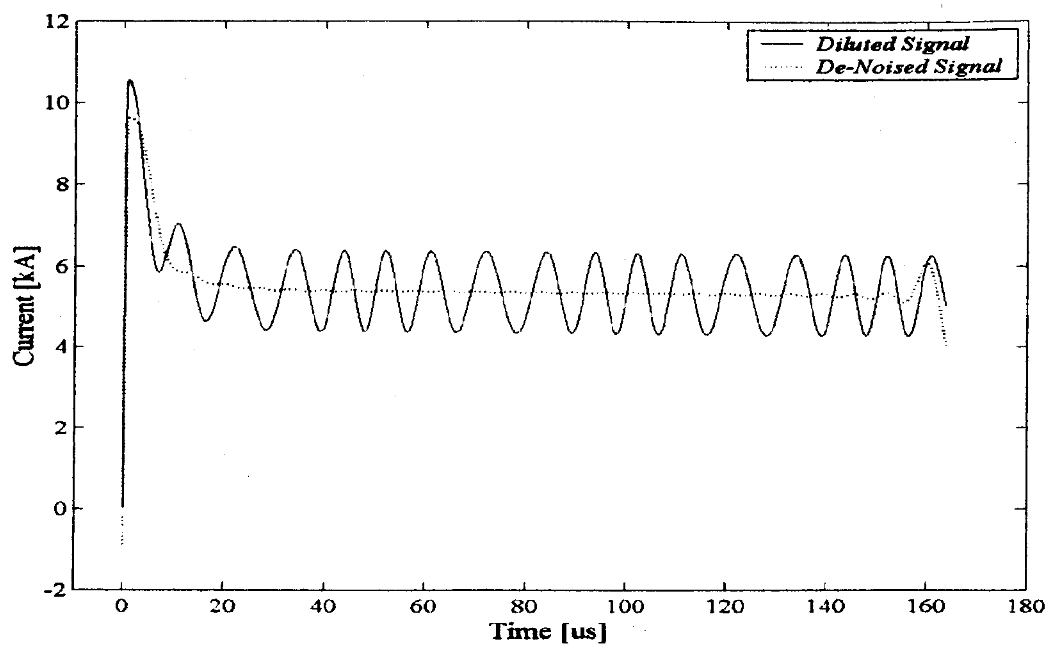

Figure 3.9: De-noised and distorted Heidler function.

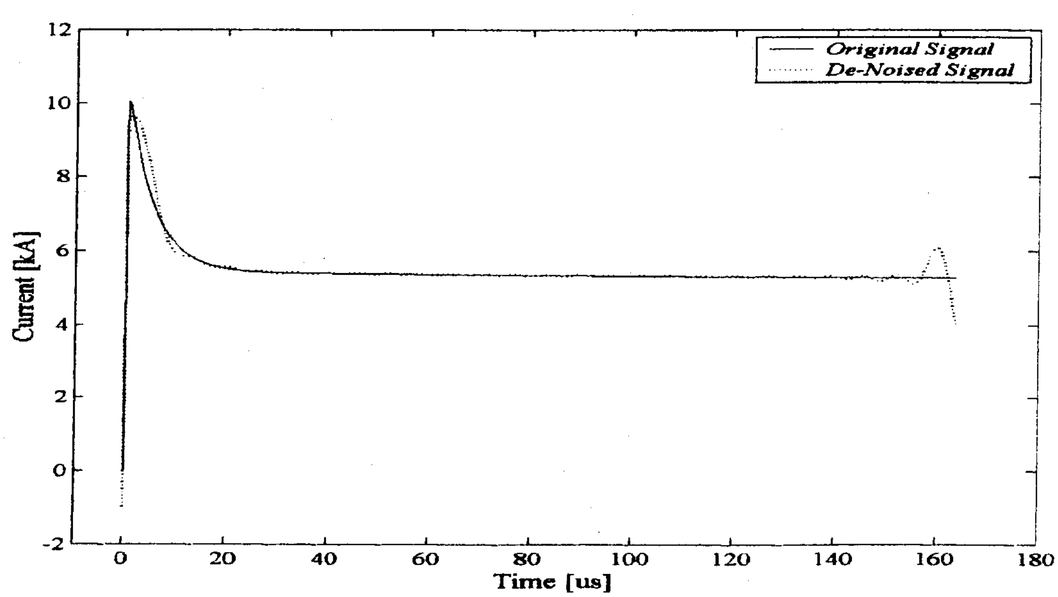

Figure 3.10: De-noised and original Heidler function.

The same procedure that is discussed above was applied to an actual CN Tower lightning current signal. The real and imaginary parts were separated from the FFT of the CN Tower lightning current signal and a best fit 1st order polynomial (straight line) was applied to the points surrounding 100 kHz frequency to modify. The real and imaginary parts of the FFT of the CN Tower lightning current signal (File name: F2050091.997) before and after modification are shown in the Fig. 3.11 and Fig. 3.12, respectively.

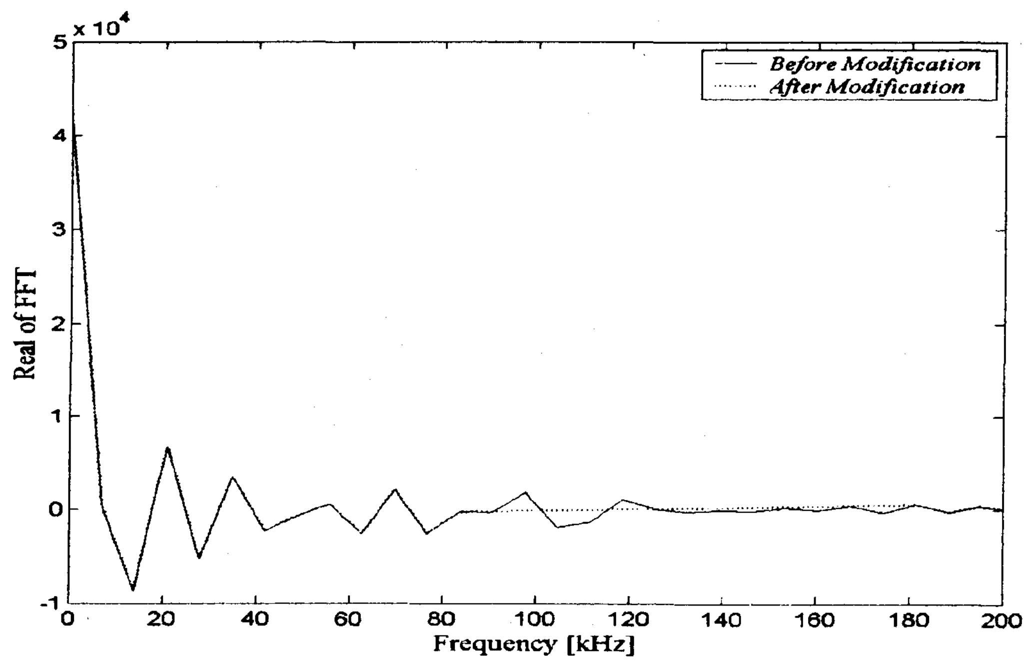

Figure 3.11: Modified and distorted real part of the FFT.

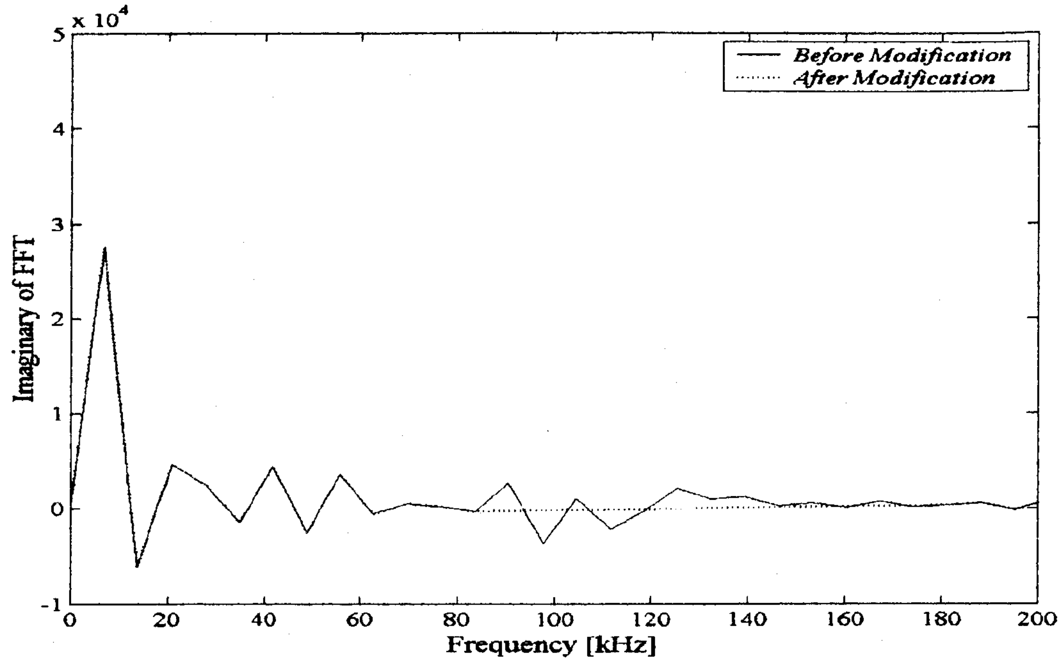

Figure 3.12: Modified and distorted imaginary part of the FFT.

The modified real and imaginary parts are combined together to form a complex vector that is the modified FFT. The modified FFT is then converted back to the time domain using IFFT. The frequency response (FFT) of the measured and de-noised CN Tower lightning current signal and their time-domain signals are shown in the Fig. 3.13 and Fig. 3.14, respectively.

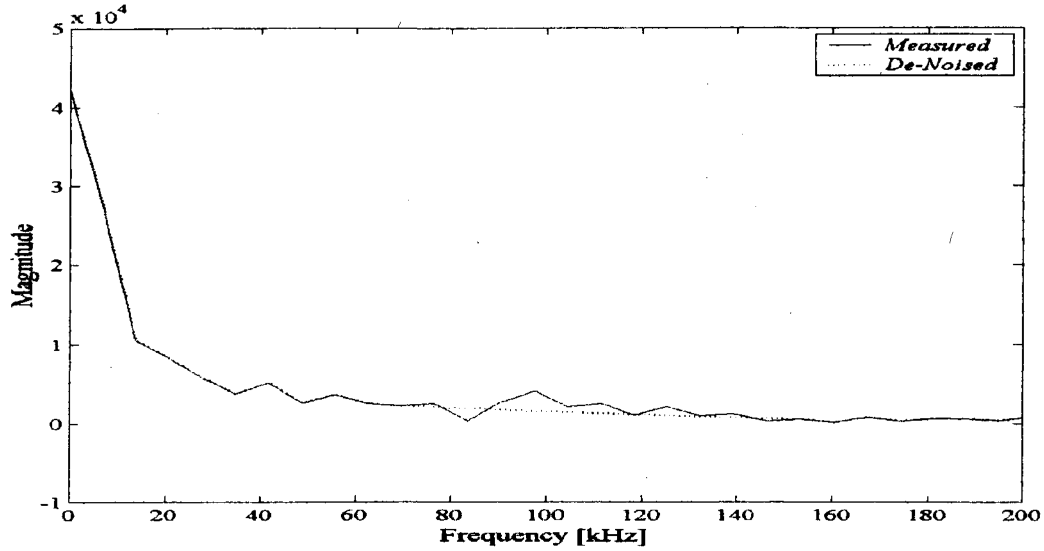

Figure 3.13: FFT of measured and de-noised CN Tower lightning current waveform.

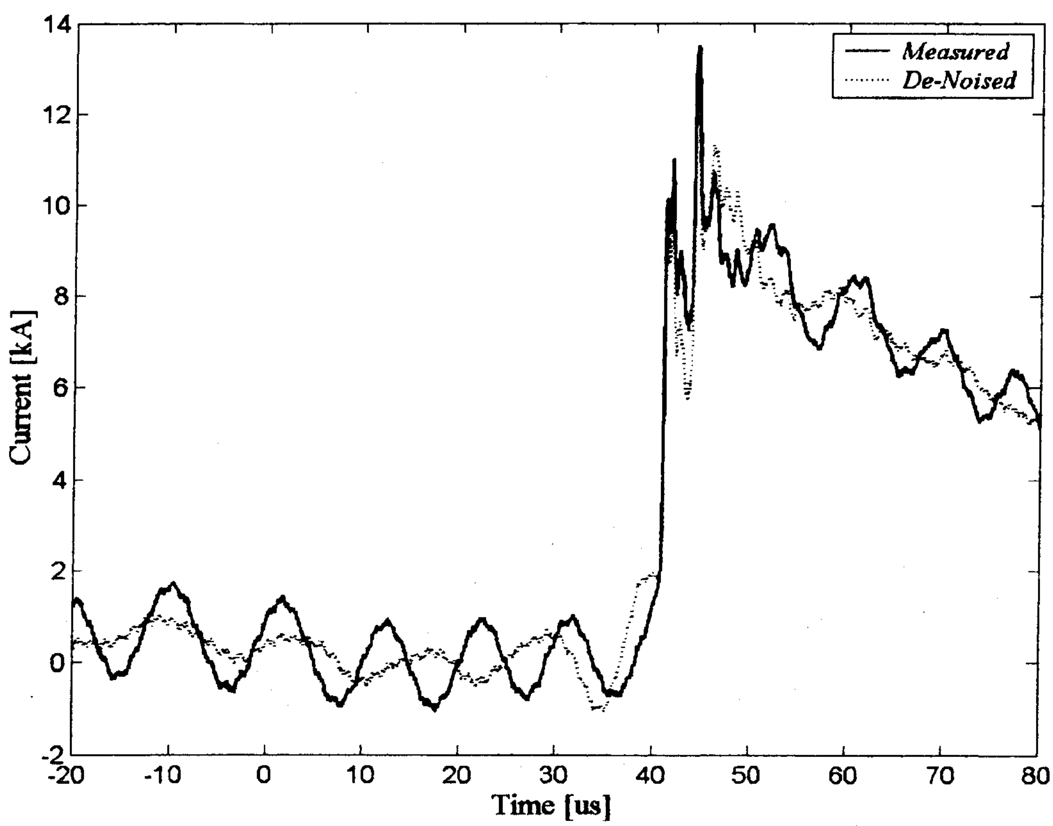

Figure 3.14: Measured and de-noised CN Tower lightning current waveform. (File name: F2050091.997).

For the purpose of our studies a **signal-peak to noise-peak ratio (SPNPR)** is proposed. It is defined as the signal peak divided by 50% of the peak-to-peak noise during the time before the arrival of lightning current return stroke. This ratio reaches to ∞ in the absence of noise.

For the case discussed above,

SPNPR before de-noising = 10.56

SPNPR after de-noising = 23.58

So, SPNPR is increased by more than 2 times in comparison to that before de-noising.

We can also represent the method using a flow chart that is shown Fig. 3.15. For de-noising a CN Tower lightning current signal by manually modifying its FFT, the same flow chart is used only the Heidler function is replaced by the CN Tower lightning current signal [17].

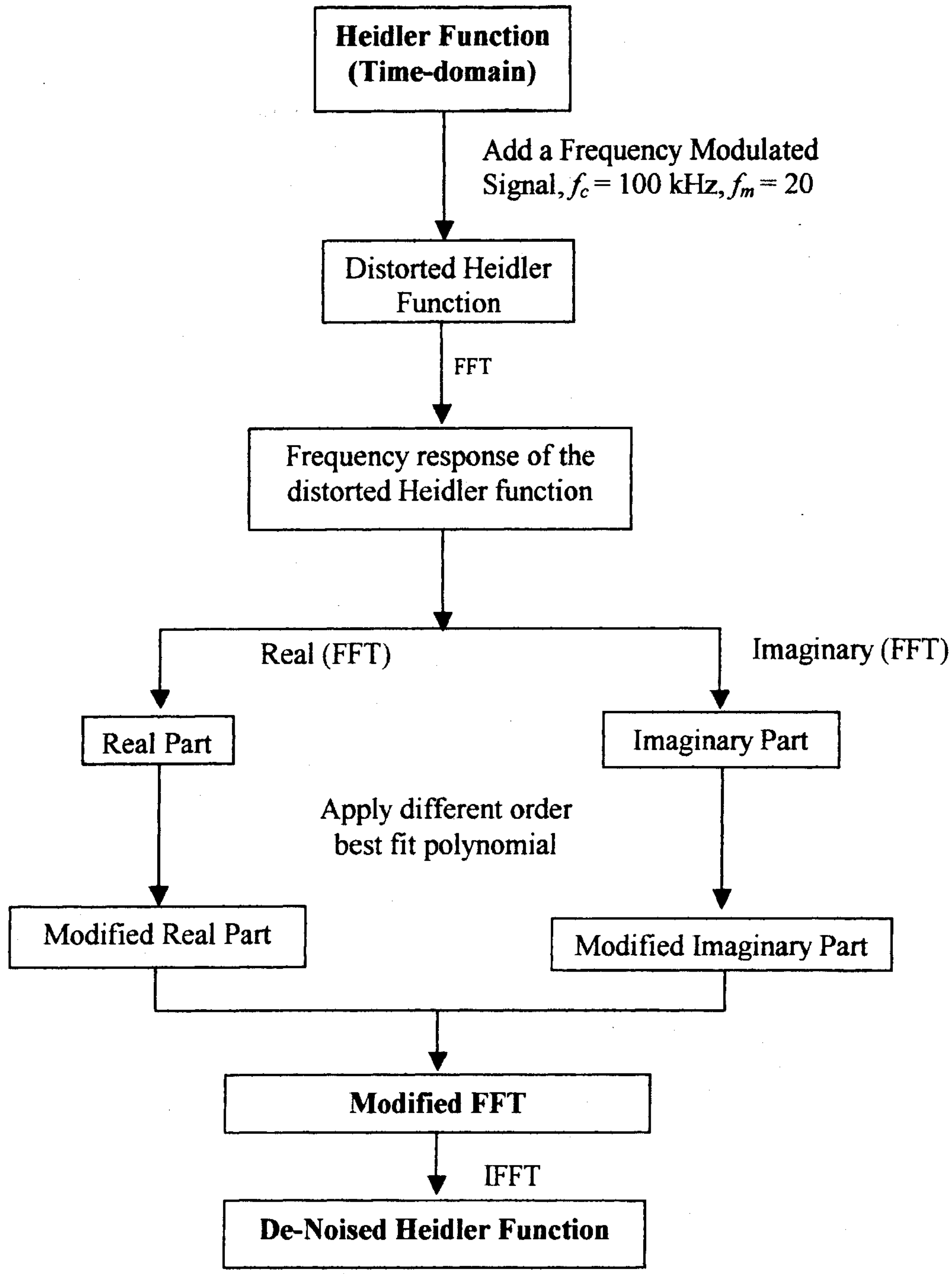

Figure 3.15: The proposed manual de-noising method.

From the calculated values of the SPNPR, before and after the de-noising procedure, it is shown that applying the manual proposed method to the CN Tower lightning current signal improves the SPNPR but the success is still limited. The reason for not getting more satisfactory success in case of CN Tower lightning current signal is its frequency modulated nature. But in case of using Heidler function, only a narrow band frequency modulated noise is added, this particular band of frequency is easily removed by applying the manually de-noised technique. Since the CN Tower lightning current signal is composed of a frequency modulated noise, it is not easy to remove it in the frequency domain while keeping the original signal unchanged.

3.2.1 Assessment of Spectral Subtraction Method Using Distorted Heidler Function

In order to simulate a current derivative waveform the Heidler function is differentiated numerically and artificially distorted by the noise signal measured at CN Tower that is assumed the same noise embedded in CN Tower lightning current derivative signal. The Spectral Subtraction method is applied to the distorted Heidler current derivative for de-noising it. The noise signal measured at CN Tower in the absence of lightning and its numerically integrated waveform is shown in Fig. 3.16. The Heidler function and its derivative is shown in Fig. 3.17. The distorted Heidler current derivative and the current waveform obtained by integration are shown in Fig. 3.18. The de-noised Heidler current derivative and its current waveforms are compared with the distorted Heidler current derivative and current waveforms that in Fig. 3.19.

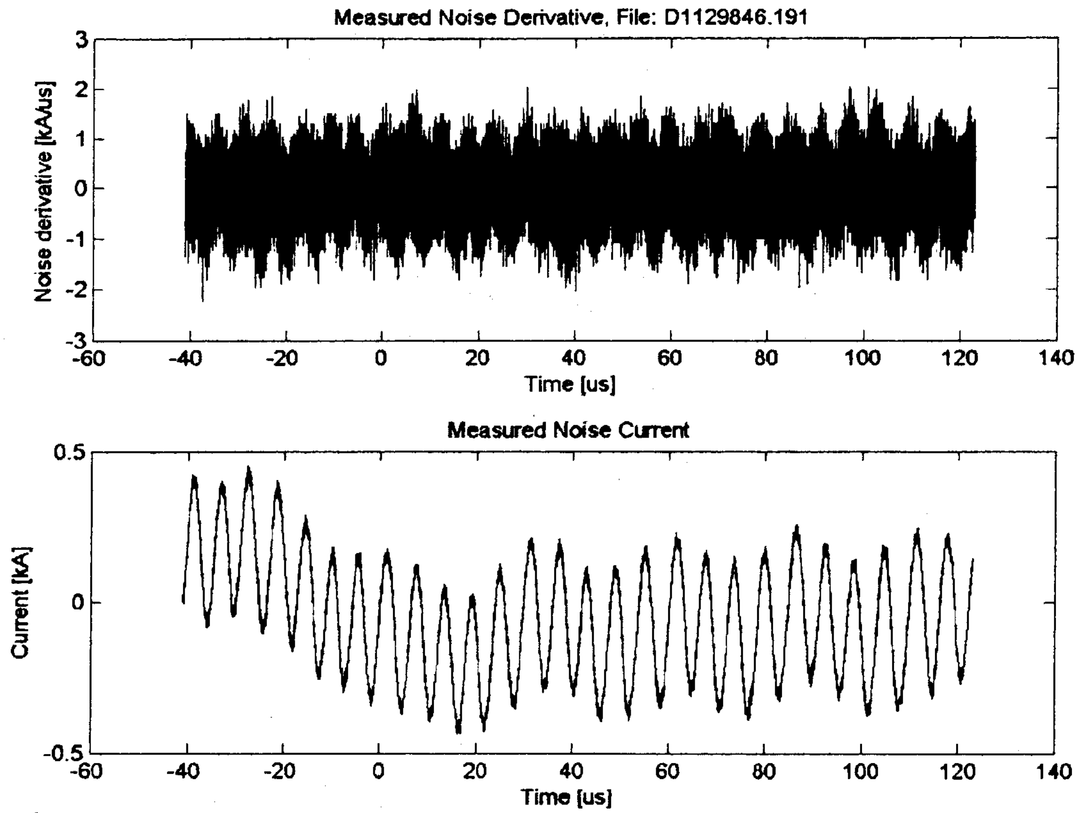

Figure 3.16: Measured noise derivative and noise waveform.

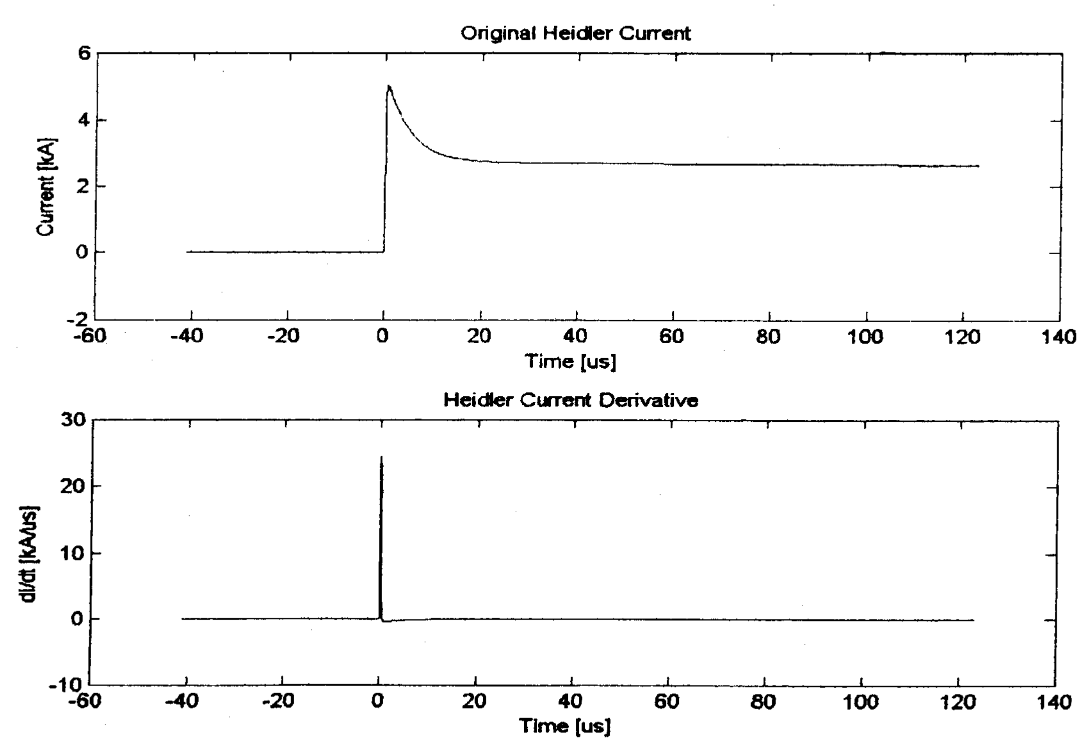

Figure 3.17: Heidler Current and its derivative.

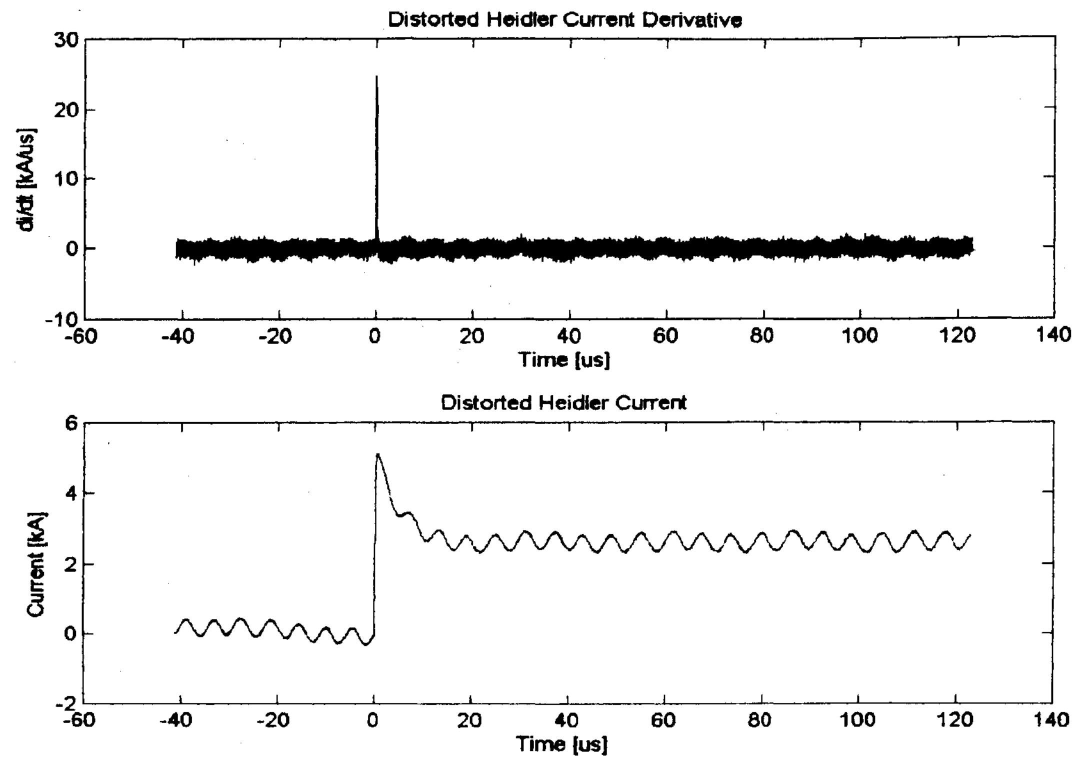

Figure 3.18: Distorted Heidler Current derivative and Heidler Current.

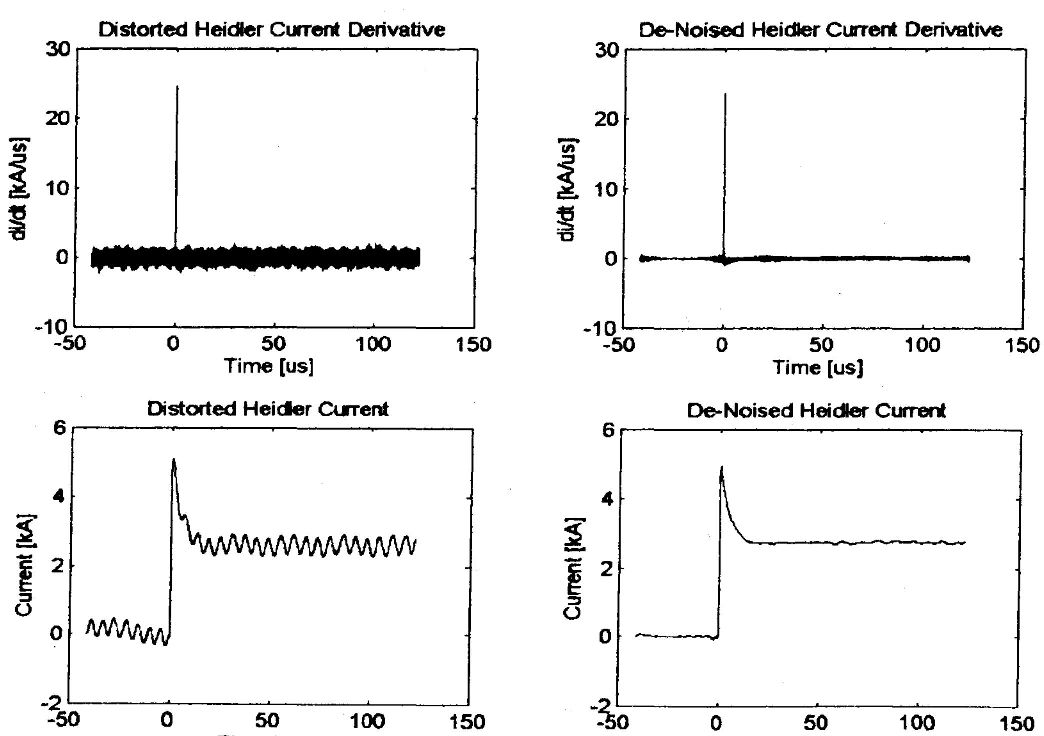

Figure 3.19: Comparison of distorted and de-noised (Using Spectral Subtraction) Heidler current derivative and Heidler current.

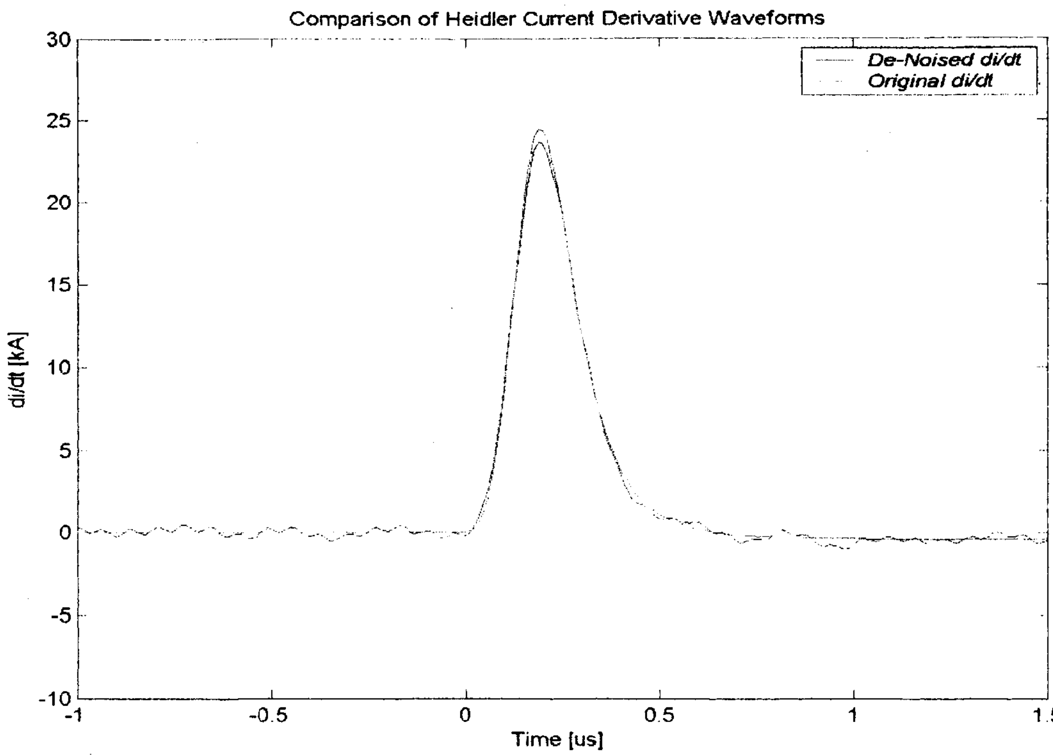

Figure 3.20: Comparison of de-noised and original Heidler current derivative.

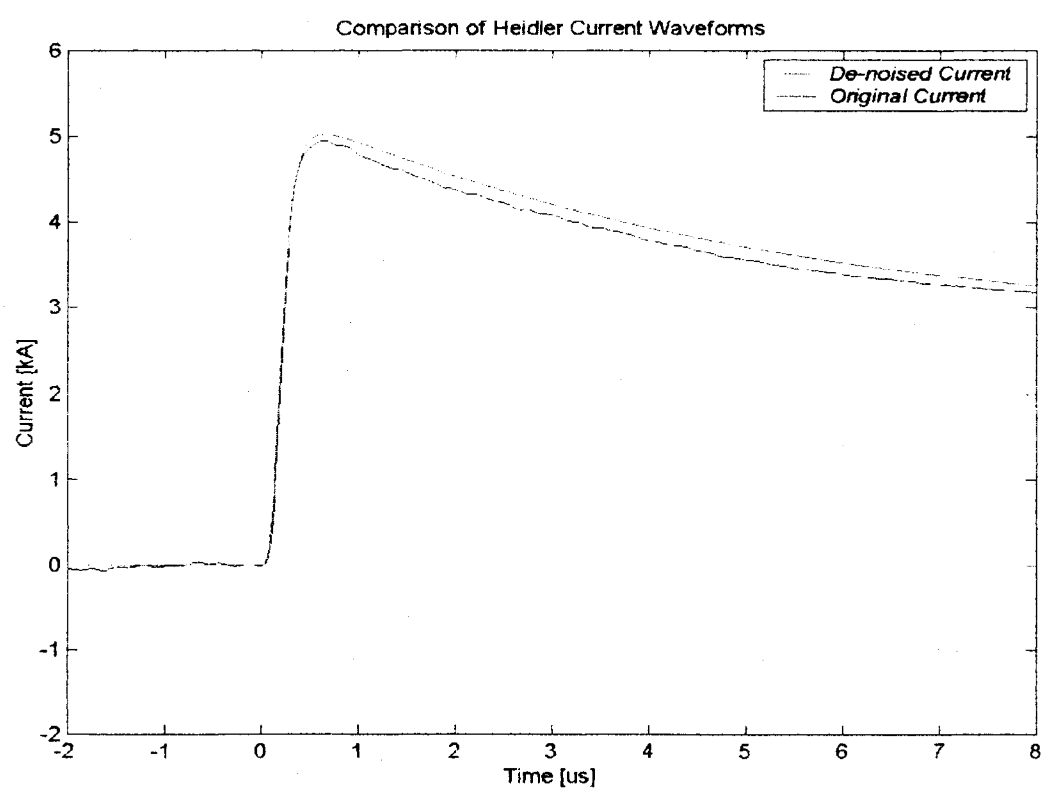

Figure 3.21: Comparison of de-noised and original Heidler currents.

From the analysis of Figs. 3.19- 3.21, it is clearly evident that the Spectral Subtraction method gives us de-noised signal that is very close to the original Heidler current derivative and Heidler current. Since Spectral Subtraction method works exceptionally well for simulated Heidler current derivative, it is expected to also work well for CN Tower lightning current derivative waveforms. Accordingly, the STFT-based Spectral Subtraction method is appropriate for de-noising CN Tower lightning current waveforms.

3.3 Formulation of the Proposed Algorithm

In section 3.1, STFT-based spectral subtraction is discussed which is basically the chosen method for de-noising the CN Tower lightning current signal. The manually proposed de-noising method is applied initially to an artificially distorted Heidler function as discussed in section 3.2. In section 3.2.1, to simulate a current derivative waveform, the Heidler function is differentiated numerically and distorted by the actual noise signal measured at CN Tower, and a de-noised signal is achieved by applying the Spectral Subtraction that is shown in section 3.2.1. From the successful recovery of original Heidler function from the distorted Heidler function motivated us to propose STFT-based Spectral Subtraction as our final method. In this section we will formulate the proposed method to de-noise the CN tower lightning current signals and the associated electric and magnetic fields.

Assumptions

The same assumptions that is discussed in spectral subtraction section of section 3.1 can be used making suitable for lightning current signal:

4) The noise is added to the lightning signal.
5) The noise remains locally stationary to the degree that the expected value of spectral magnitude prior to lightning (pre-stroke) activity equals its expected value during lightning activity. The rationale behind this assumption is that by observing the lightning current waveform even the magnitude response of lightning current it is found that noise is oscillating around 100 kHz during the pre-stroke portion and the lightning period.
6) Significant noise reduction is possible by removing the effects of noise spectrum.

The additive noise model, spectral subtraction estimator, magnitude averaging, half-wave rectification and so on that are discussed in section 3.1 are used to formulate the proposed method for this particular application. To formulate the method following subsections are used.

3.3.1 Input-Output Data Windowing

Lightning current derivative *(di/dt)* is segmented and windowed such that in the absence of spectral modifications, if the synthesis segments are added together, the resulting overall system reduces to an identity according to the OLA condition. The data is segmented and windowed in such a way that if a sequence is separated into half overlapped data segments and each segment is multiplied by a Hanning window, then the sum of the windowed sequences generates the original signal. The window length is chosen 2048 points and the overlapping points is 1024 which equals one half of the window length.

3.3.2 Frequency Analysis

The DFT of each data window is taken and the magnitude is computed. The FFT size is set equal to the window size of 2048. As correctly noted by Allen [12], spectral modification followed by inverse transforming can distort the time waveform due to temporal aliasing caused by circular convolution with the time response of the modification. Augmenting the input time waveform with zeros before spectral modification minimizes this aliasing. To take care of this temporal aliasing, 1024 zero points (half window) are added to a half of first and last segment of time domain signal [17]. The length of the lightning current derivative is 16 kB. Adding 2 kB, the total size is 18 kB (18432 sample points). If we divide the signal into its frame of length 2048 and overlapping points 1024 it looks like the Fig. 3.22.

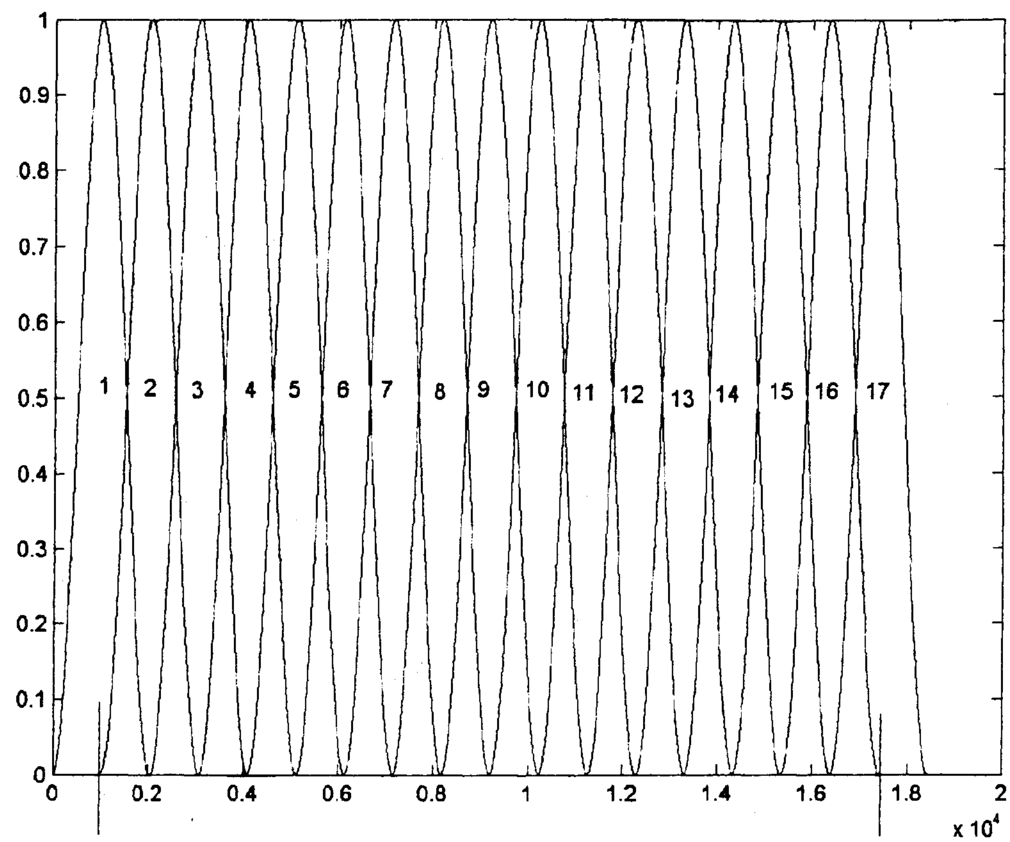

Figure 3.22: Segmented Signal into frames (1... 17).

First half (1:1024) of the first frame (frame 1) and second half (17409:18432) of the last frame (frame 17) is zero padded for the ease of signal reconstruction.

3.3.3 Bias Estimation

The spectral subtraction method requires an estimate at each frequency bin of the expected value of the noise spectrum:

$$\mu(e^{j\omega}) = E\{|U(e^{j\omega})|\} \tag{3.19}$$

This estimate is obtained by averaging the magnitude spectrum $|U(e^{j\omega})|$ of noise only measured during non-lightning activity.

3.3.4 Bias Removal and Half-Wave Rectification

The spectral subtraction estimator $\hat{S}$ is obtained by subtracting the average noise magnitude spectrum μ from the magnitude signal spectrum $|X|$. Thus

$$\left|\hat{S}(k)\right| = |X(k)| - \mu(k), \qquad k=0, \ldots, L-1 \tag{3.20}$$

or

$$\hat{S}(k) = H(k)X(k), \qquad k=0, \ldots, L-1 \tag{3.21}$$

$$H(k) = 1 - \frac{\mu(k)}{|X(k)|}, \qquad k=0, \ldots, L-1 \tag{3.22}$$

Where, L = DFT buffer length.

After subtracting, the differenced values having negative magnitudes are set to zero (half-wave rectification). These negative differences represent frequencies where the sum of lightning signal plus local noise is less than the expected noise.

3.3.5 Synthesis

After bias removal and half-wave rectification a time waveform is reconstructed from the modified magnitude. The data windows are overlap-added to form the output lightning sequence as discussed in chapter 2. The modified magnitude is combined with the unmodified phase angle to formulate the complex form of the DFT for each frame. Taking Inverse Fast Fourier Transform (IFFT) of these frames, the time domain modified signal is reconstructed.

3.4 Implementation of the Proposed Algorithm

The STFT-based spectral subtraction to de-noise the CN Tower lightning current signal is described by a set of simple mathematical equations. It can be easily implemented in software in the form of a code written in a programming language like C/C++ or computational software like Matlab. This section presents the implementation of the proposed algorithm in software form using Matlab computational software.

Window Selection

There are three most commonly used window functions for signal segmentation. They are Hamming, Hanning and Boxcar window and the selection of window is basically application dependent. The properties of different windows are discussed in chapter 2. From this analysis, it is obvious that Hanning window is the best for this application.

Window Size (Frame Length) Selection

In STFT, window size plays an important role. Shorter windows gives high time resolution and larger window gives high frequency resolution. So there is a trade off between time resolution and frequency resolution. Therefore, we need to optimize the window size that will result in good time and frequency resolution.

To solve the window size dilemma for the CN Tower lightning current derivative and lightning current signal application, we tried the STFT-based spectral subtraction for different window sizes calculated the resulting SPNPR values in each case. We compared these SPNPR values to select optimal window size. Window lengths of 512, 1024, 2048, and 3072 points were tried for the current derivative (*di dt)* and for the current signal (obtained by integration). A comparison of the resulting SPNPR values are shown in Table 3.1- 3.3 for different *di dt* files.

Table 3.1: SPNPR using different window sizes. File: G0363096.363.

Frame Size (Points)	Signal peak-to-noise peak ratio (SPNPR)		Comments
	di/dt	**Current (i)**	
Original (Full Length)	7.27	20.16	Measured Signal
512	383.25	347.45	3rd Highest SPNPR
1024	717.85	1057.17	Highest SPNPR
2048	151.30	361.39	2nd Highest SPNPR
3072	39.60	39.59	Lowest SPNPR

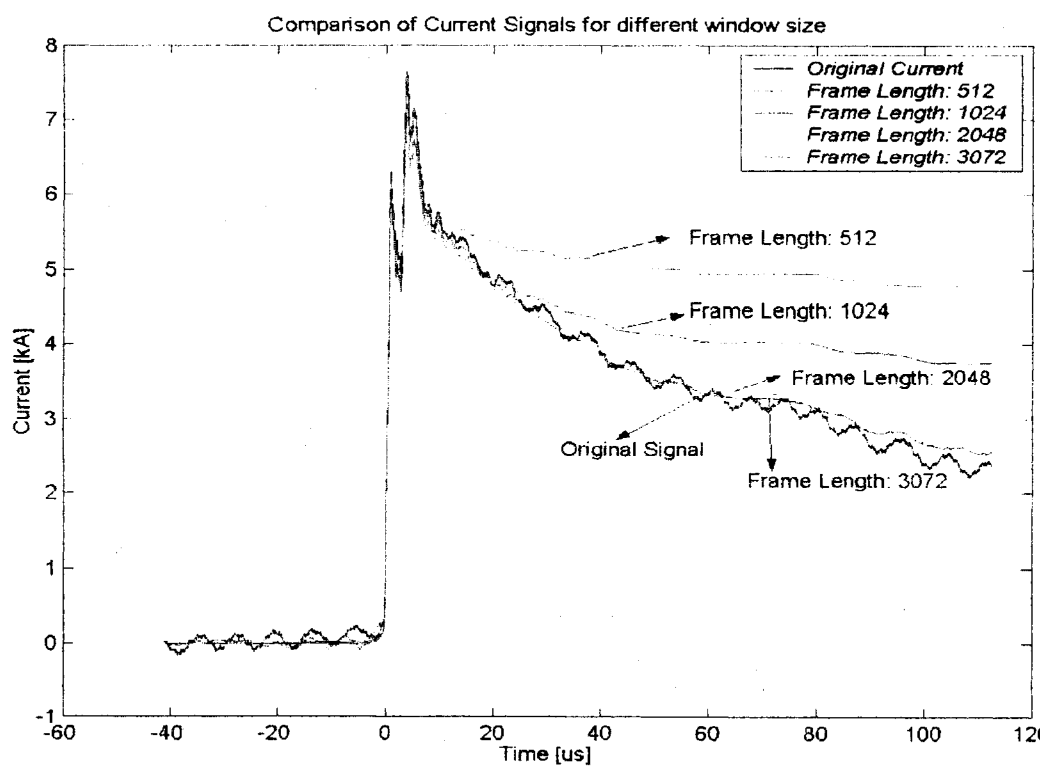

Figure 3.23: The current waveform after de-noising the current derivative signal using different window sizes. File: G0363096.363.

Table 3.2: SPNPR using different window sizes. File: G0363096.525.

Frame Size (Points)	SPNPR		Comments
	di/dt	Current (i)	
Original (Full Length)	5.75	10.38	Measured Signal
512	274.88	1530	Highest SPNPR
1024	179.20	409	2nd Highest SPNPR
2048	51.72	57.30	3rd Highest SPNPR
3072	22.72	18.04	Lowest SPNPR

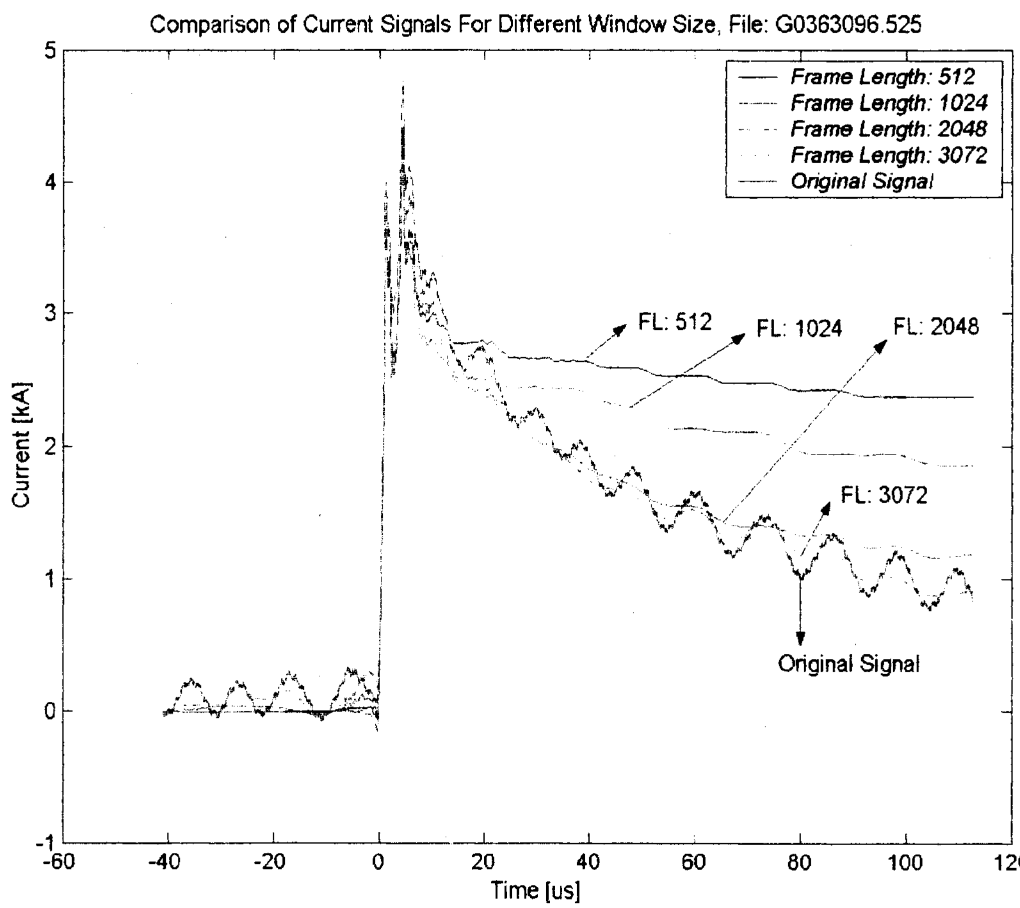

Figure 3.24: The current waveform after de-noising the current derivative signal using different window sizes. File: G0363096.525.

Table 3.3: SPNPR using different window sizes. File: G0363096.788.

Frame Size (Points)	SPNPR		Comments
	di/dt	Current (i)	
Original (Full Length)	9.48	15.64	Measured Signal
512	646.05	226.76	3rd Highest SPNPR
1024	246.68	522.59	2nd Highest SPNPR
2048	147.95	951.20	Highest SPNPR
3072	34.16	23.09	Lowest SPNPR

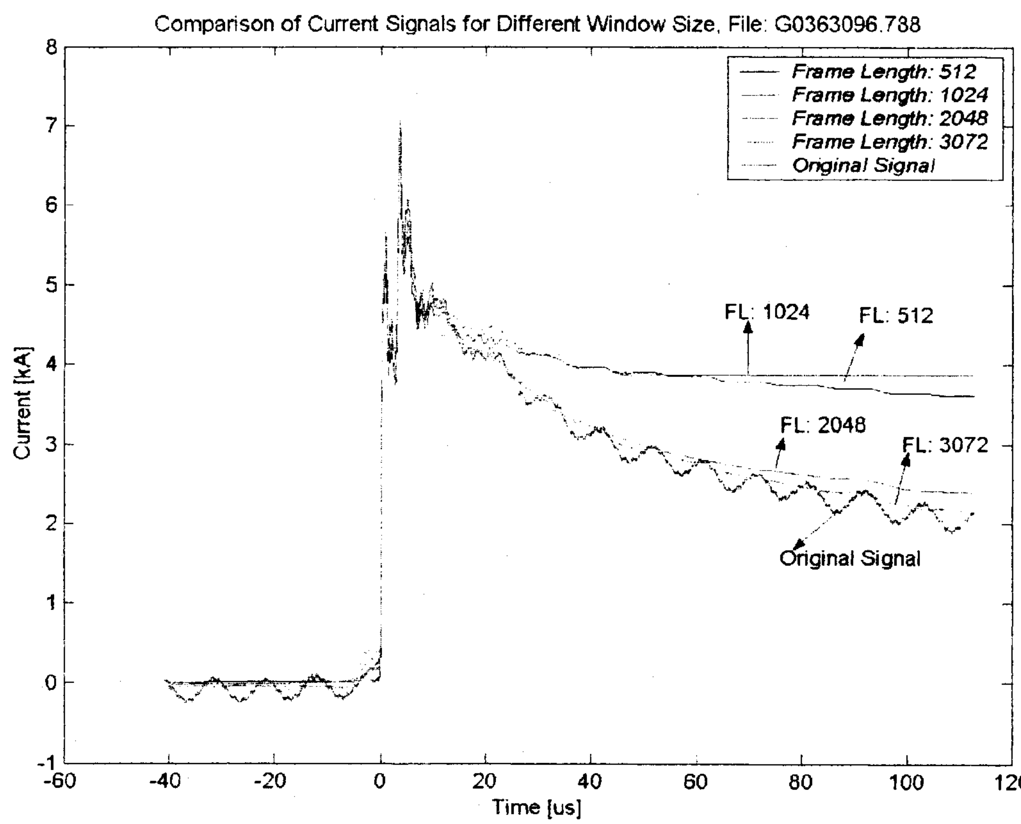

Figure 3.25: The current waveform after de-noising the current derivative signal using different window sizes. File: G0363096.788.

From Tables 3.1-3.3, it is observed that it is really difficult to say which size is the best. To solve this problem if we take a look at the de-noised current waveforms (Figs. 3.23-3.25), it is evident that the 2048 window size is the best in all aspects although sometimes its SPNPR is lower than the SPNPR values obtained with 512 or 1024-point window sizes. But this is the only window size for which the de-noised current signal follows the original signal tail and SPNPR is better in comparison with other cases. So, considering SPNPR and the shape of the signal, 2048 window size gives the best result in this particular application. It is also worth mentioning here that to determine the SPNPR the signal level is taken to be the absolute peak in case of di/dt and the first peak in case of current.

Spectral Subtraction on di/dt or Current

The current derivative (di/dt) is measured at the CN tower whereas the current waveform is derived from the di/dt through time integration. We can apply spectral subtraction to either di/dt signal or the current signal. In each case a different result is observed. So there is an optimization between these two options. To get the better result Spectral Subtraction was tried both in di/dt and current signal. It was found out that using Spectral subtraction process on the di/dt signal gives a better result than using it on the current. This is shown in Figs. 3.26- 3.28.

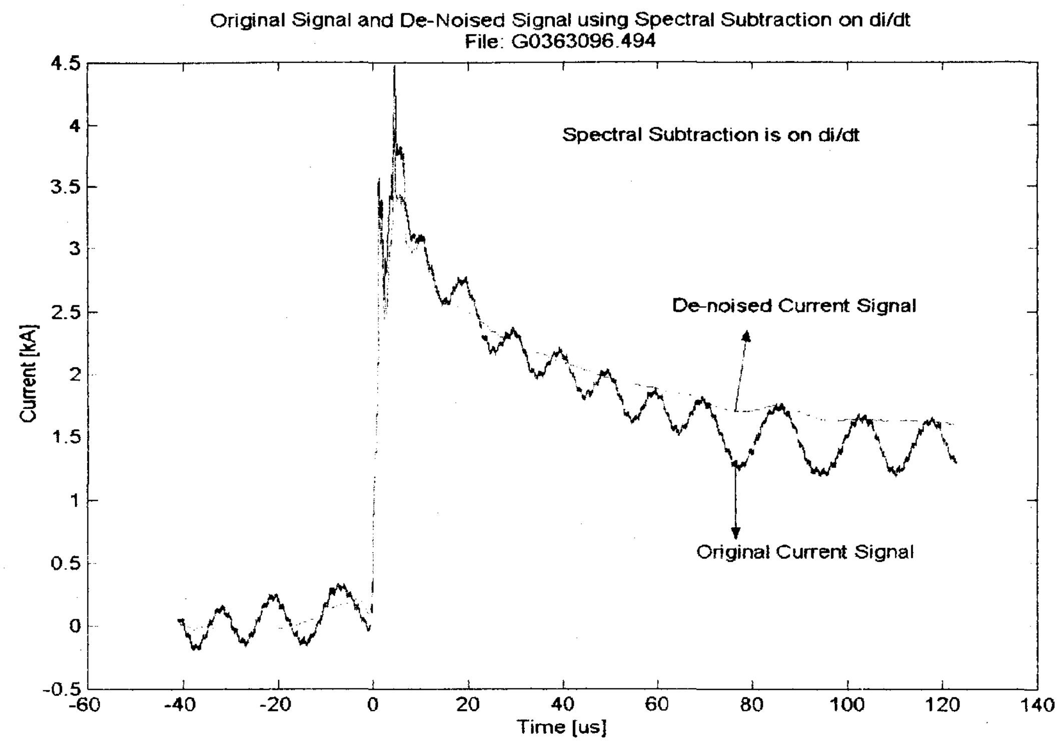

Figure 3.26: Spectral Subtraction is applied on current derivative and de-noised current signal.

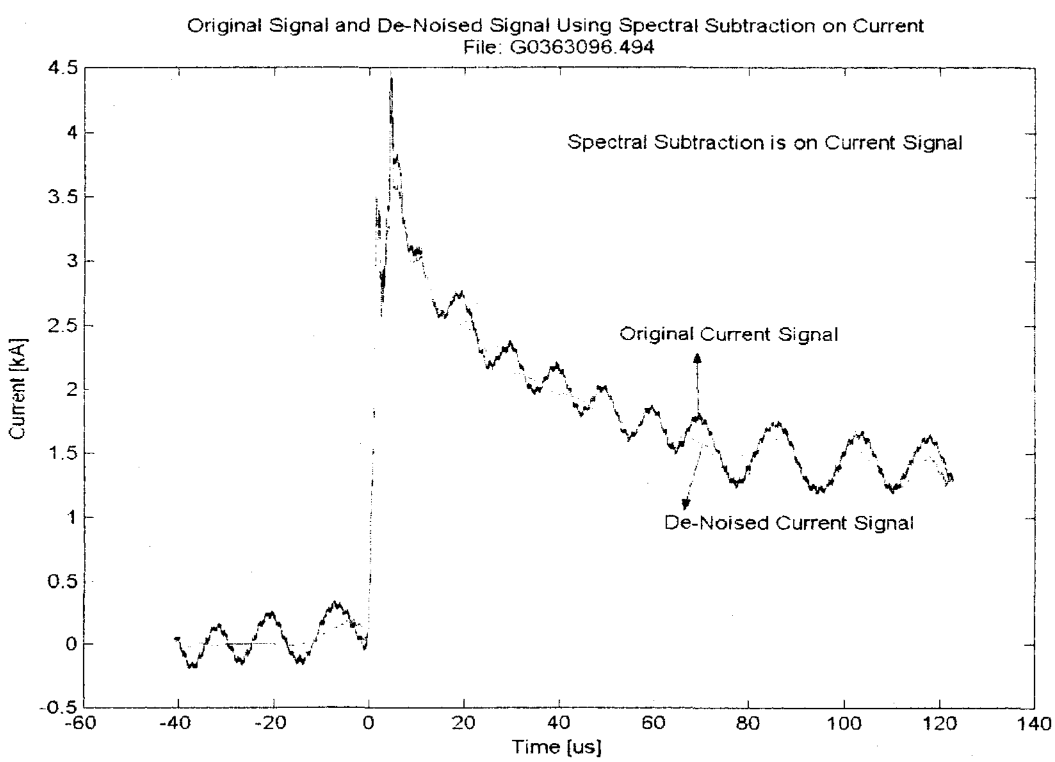

Figure 3.27: Spectral Subtraction is on current and de-noised current signal.

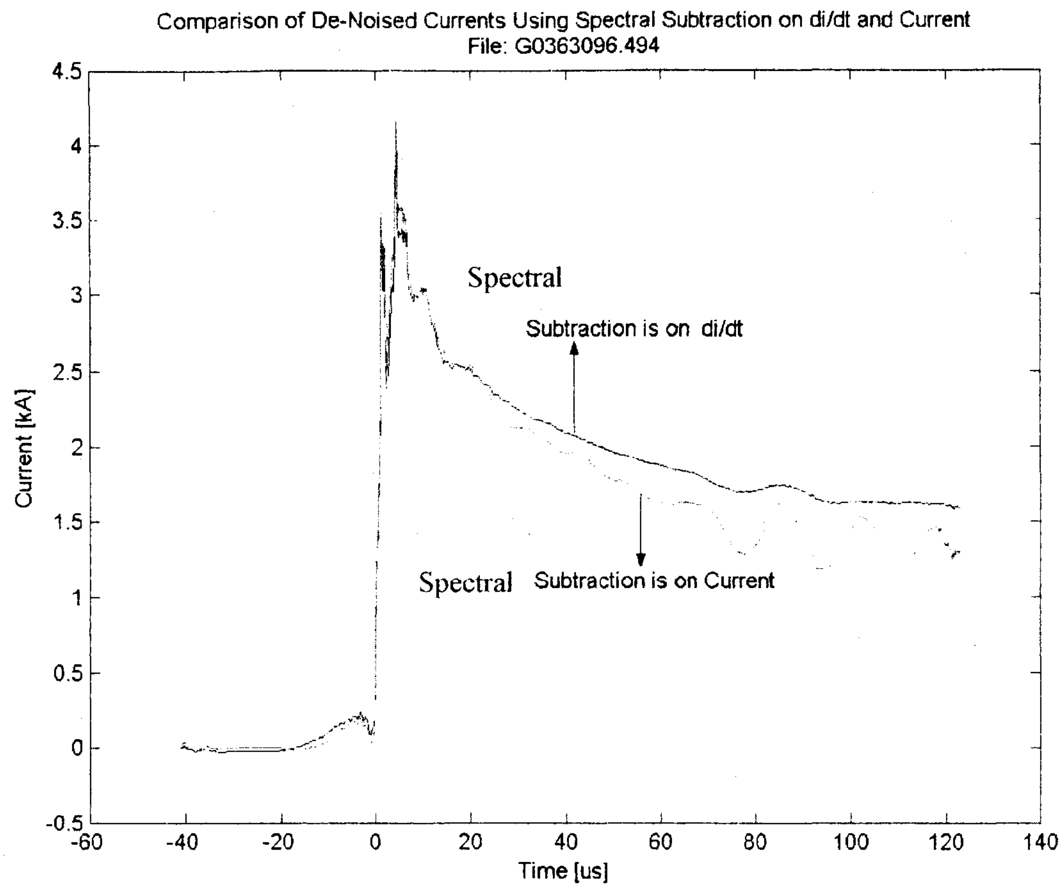

Figure 3.28: Comparison of de-noised current signals using Spectral Subtraction on current derivative and current.

From the figures (Fig. 3.26- 3.28), it is obvious that spectral subtraction on *di dt* gives better result than that on current in the point of wave shape and peaks.

3.4.1 Evaluation of the Proposed Method Based on Data from the Noise-Protected Current Measurement System

A current derivative signal (D0777188.213), simultaneously measured by both the new, noise-protected, coil and the old coil on April 07, 1999 is shown in Figs. 3.29 and 3.30, respectively. The corresponding currents obtained by numerical integration are also shown. The Spectral Subtraction method is applied on the *di/*dt signal measured by the old coil. The de-noised *di/dt* waveform is compared with the new coil *di/dt* waveform in Figs. 3.31 and 3.32, respectively. In Figs. 3.33 and 3.34 the corresponding currents are also compared. Waveform peaks measured by the two coils are slightly different because of calibration problems. Furthermore, for the new coil current waveform the ground reflection arrives a little later than for the old coil because the new coil is located 35 meters above the old coil.

The results shown in Figs. 3.31-3.34 points out to the success of the Spectral Subtraction method in de-noising the CN Tower lightning current signals.

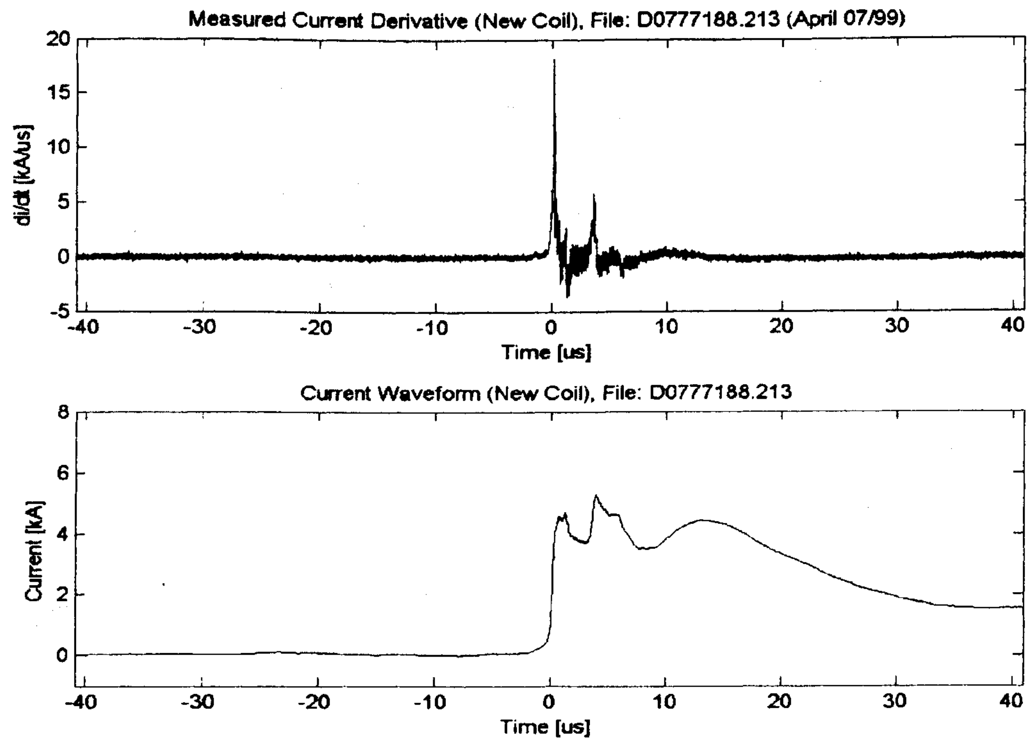

Figure 3.29: New coil measured current derivative and its current waveform.

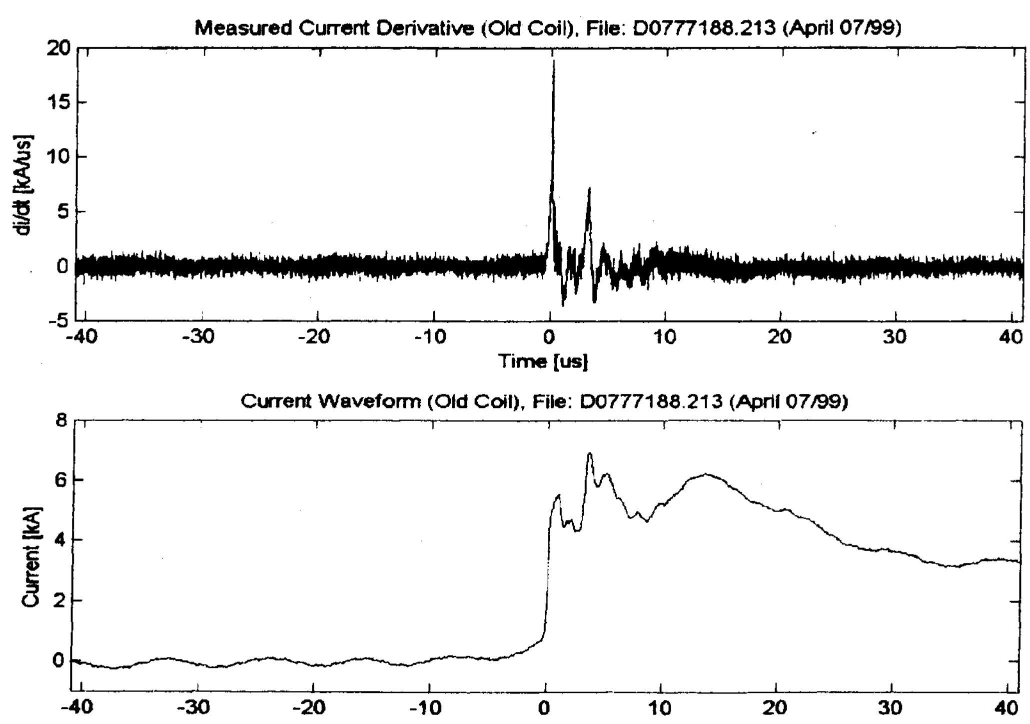

Figure 3.30: Old coil measured current derivative and its current waveform.

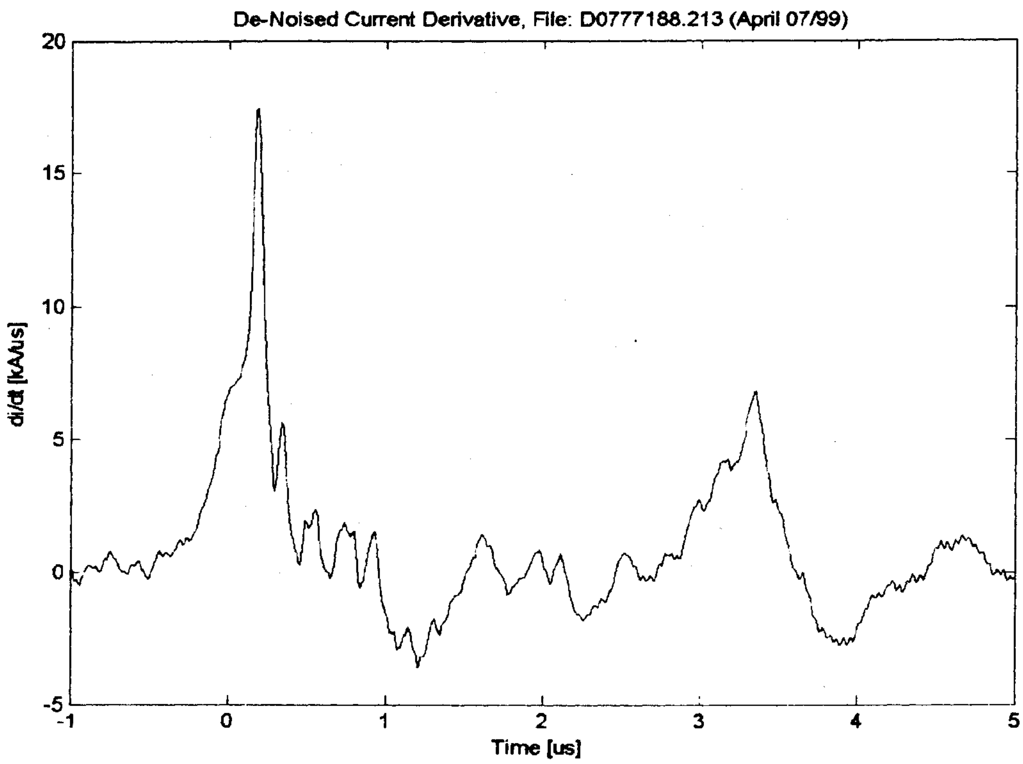

Figure 3.31: De-noised current derivatives.

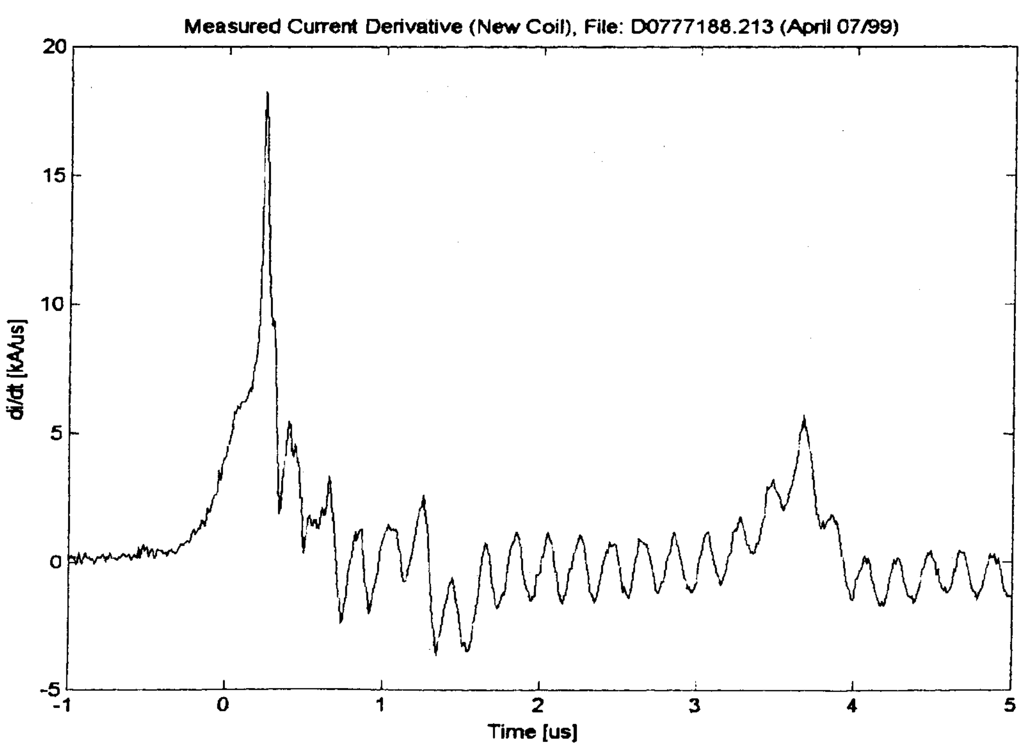

Figure 3.32: Measured current derivative (New coil).

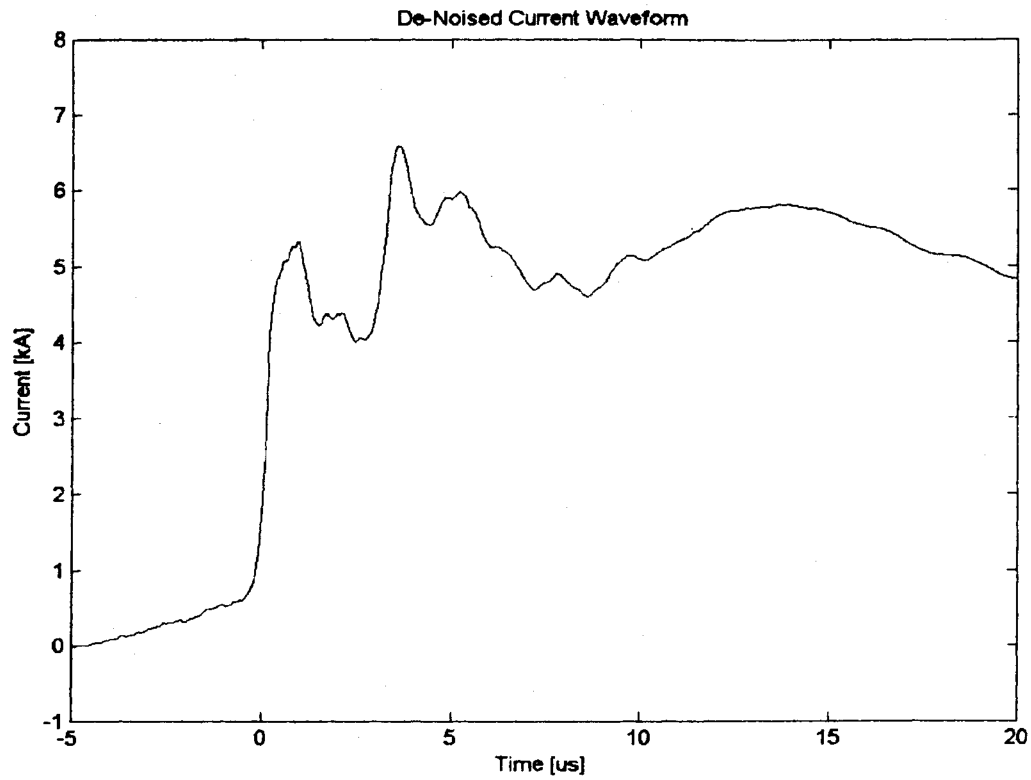

Figure 3.33: De-Noised current waveform

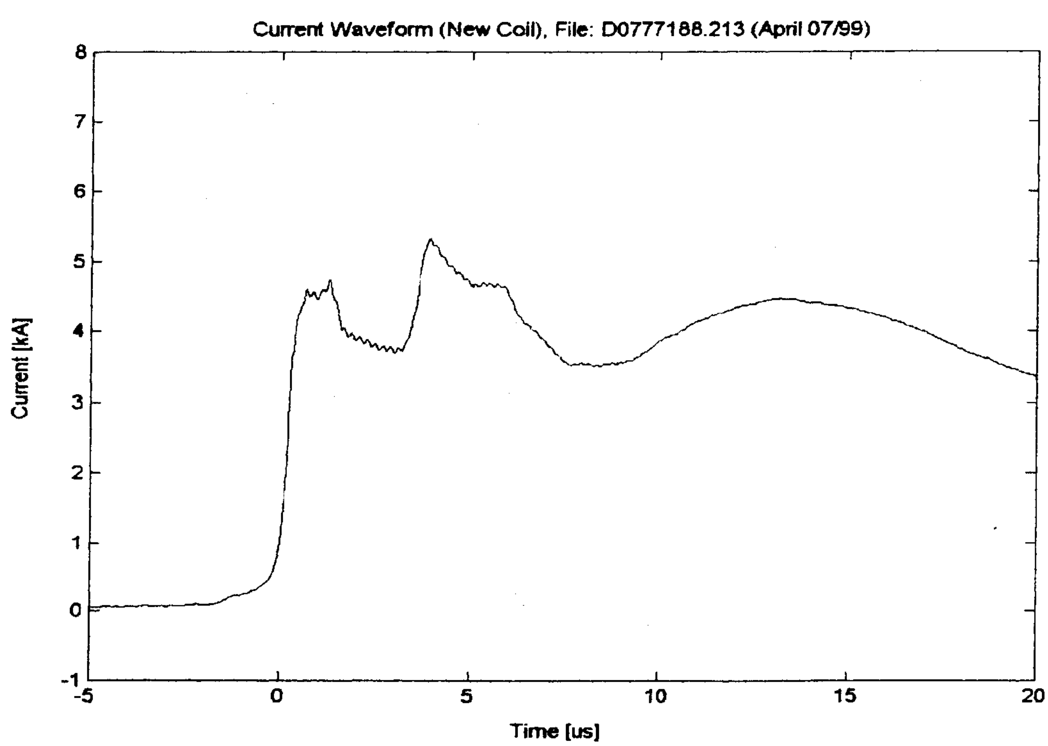

Figure 3.34: New coil current waveform.

3.6 Results of the Proposed Method

According to the success of the STFT-based Spectral Subtraction method with parameters Hanning window of size 2048 and 1024 overlap points, it is decided to applying it on the measured current derivative. Using these parameters, we applied the proposed method on measured *di/dt* and then integrate the de-noised *di/dt* to derive the current waveforms. The de-noised *di/dt* and current waveforms are shown in Figs. 3.35-3.40.

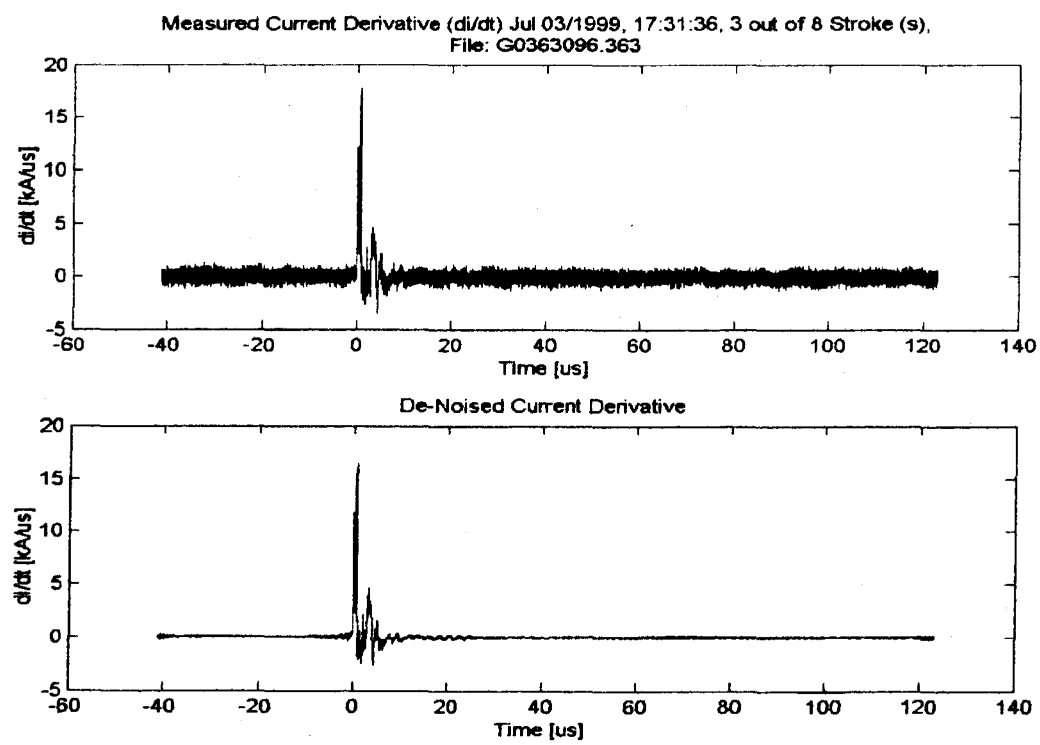

Figure 3.35: Measured and de-noised *di/dt* using the proposed method.

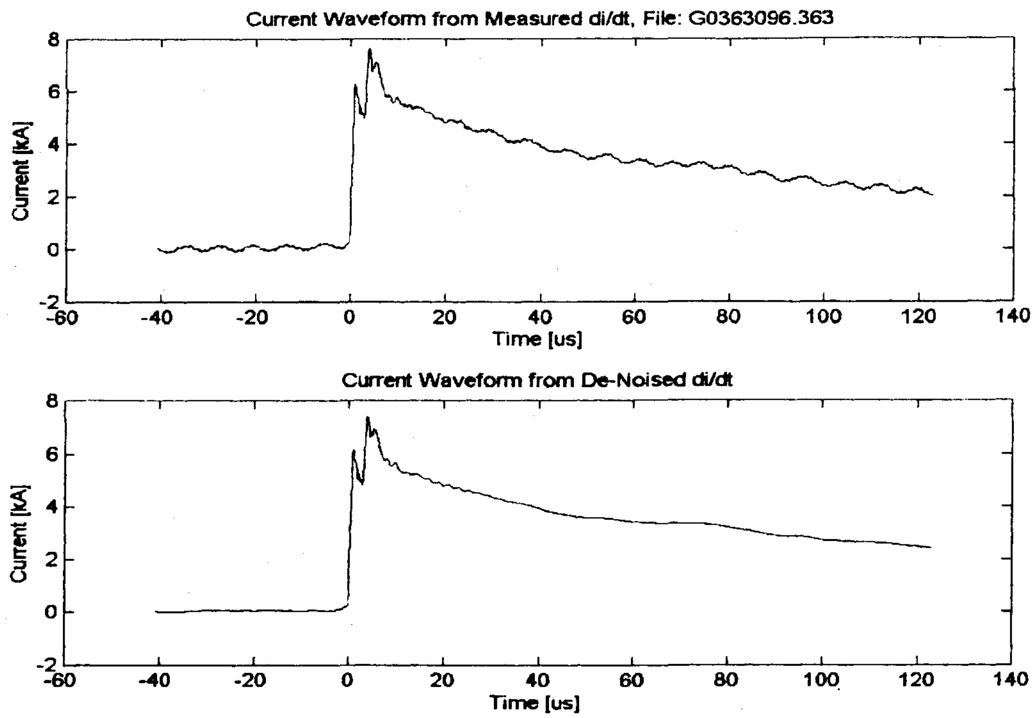

Figure 3.36: Current waveforms from measured and de-noised *di/dt*. File: G0363096.363.

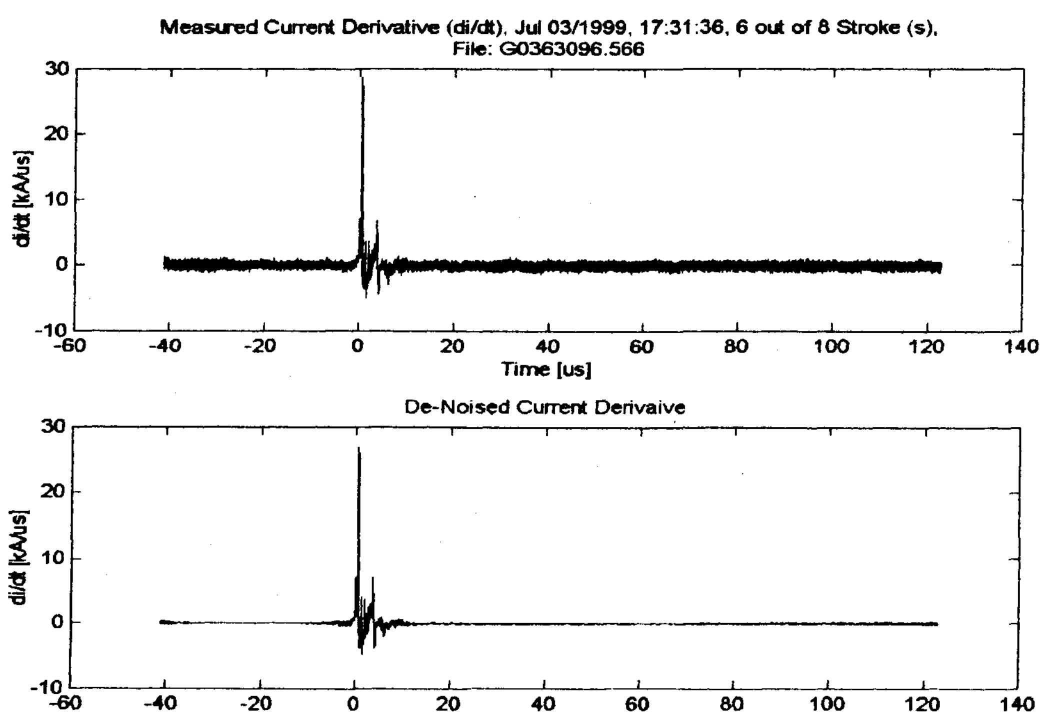

Figure 3.37: Measured and de-noised *di/dt* using the proposed method. File: G0363096.566.

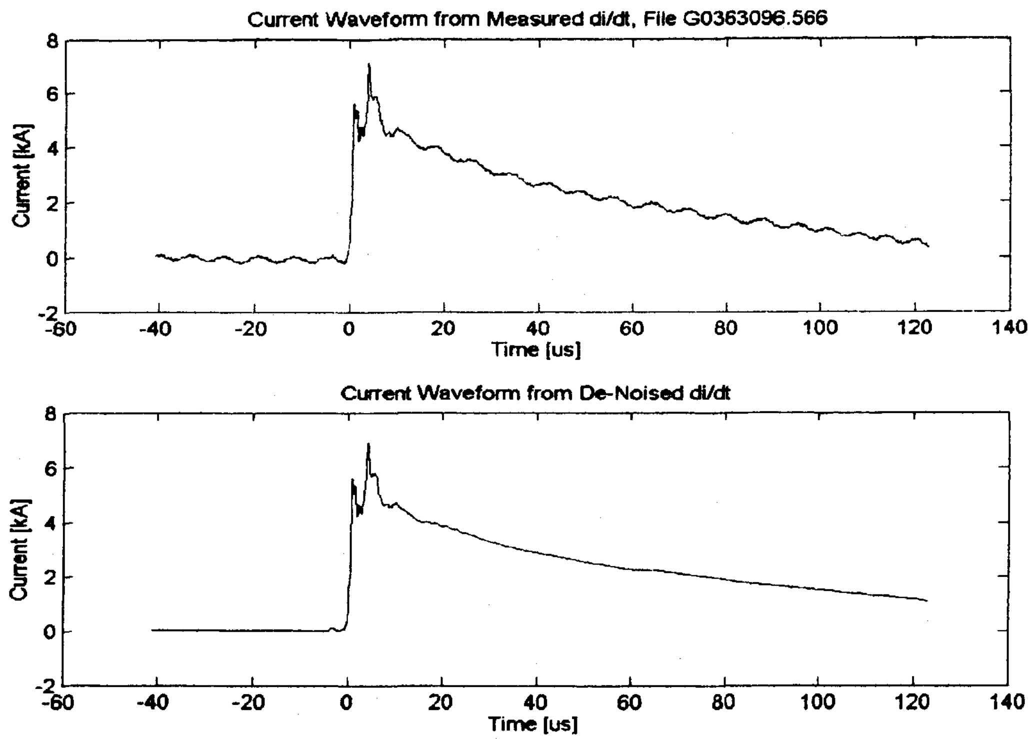

Figure 3.38: Current waveforms from measured and de-noised *di/dt.* File: G0363096.566.

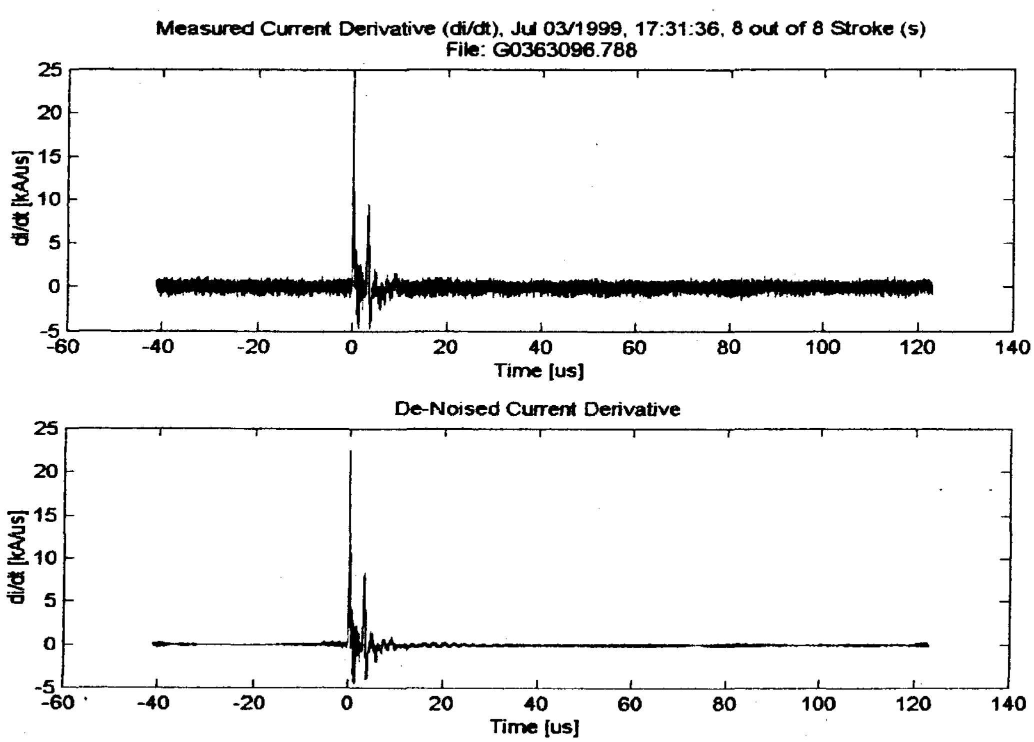

Figure 3.39: Measured and de-noised *di/dt* using the proposed method. File: G0363096.788.

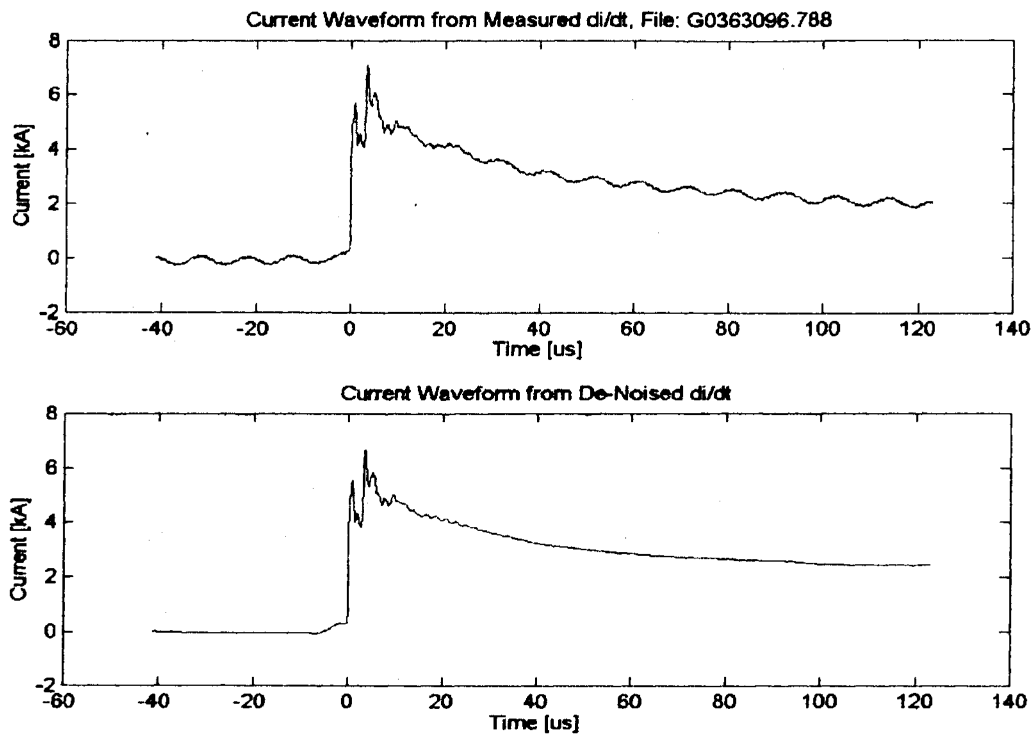

Figure 3.40: Current waveforms from measured and de-noised *di/dt.* File: G0363096.788.

Short Term Fourier Transform Response

3D mesh plot of time, frequency and amplitude responses were constructed from the measured current derivative and the de-noised current derivative which are shown in Fig. 3.41 and 3.42 From Figs. 3.41-3.42, the improvement of the signal *(di/dt)* after applying the proposed spectral subtraction method is clearly demonstrated.

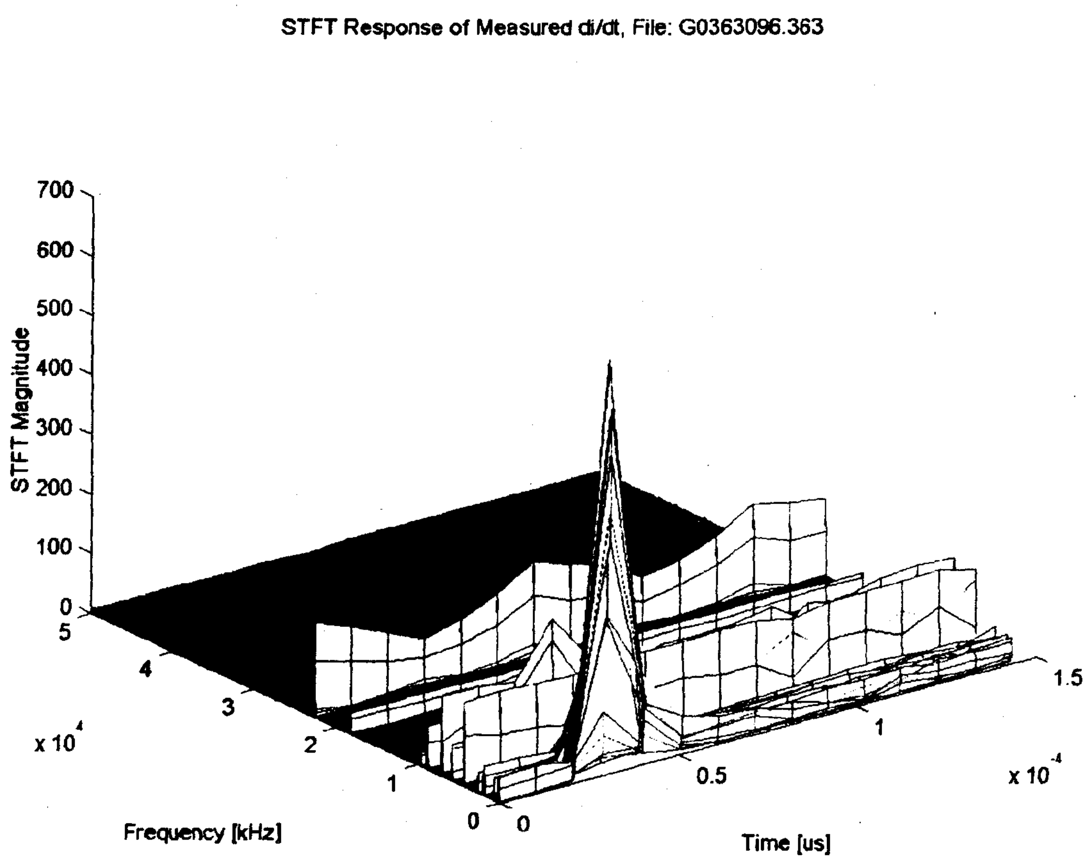

Figure 3.41: Spectrogram of measured *di/dt.* File: G0363096.363.

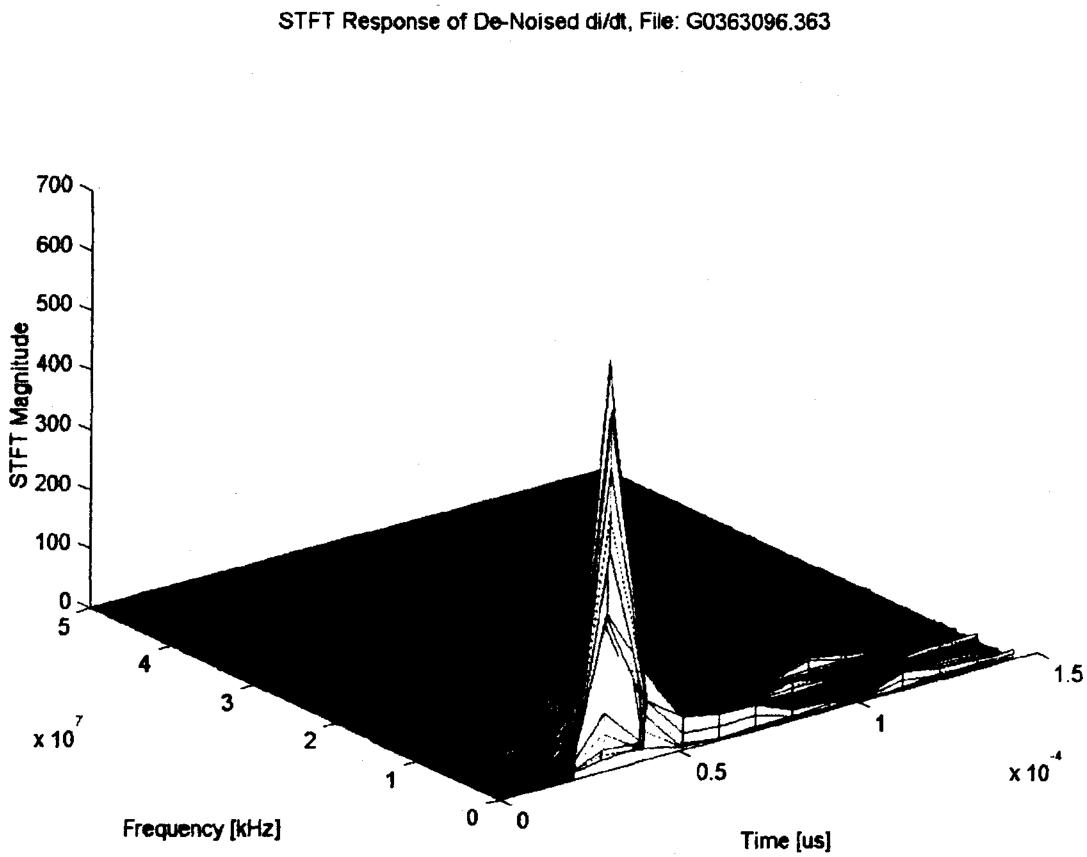

Figure 3.42: Spectrogram of de-noised *di/dt.* File: G0363096.363.

3.7 Proposed Pre-Stroke of Lightning Signal

The pre-stroke portion of the recorded lightning current derivative is 40.96 μs (-40.96 μs to 0 μs, 4 kB -4096 points). By analyzing the recorded noise signal at the CN Tower, it is found that the proposed method shows better result with respect to the SPNPR and signal shape in time domain if the pre-stroke portion is 81.92 μs *(-81.92 μs to 0 μs, 8 kB- 8192 Points)* rather than 40.96 μs. The following figures (Figs. 3.45-3.49) provides a comparison of de-noised signals taking only frame 2 and then mean of frames 2:3, 2:4, 2:5, . . . ,2:13, 2:14 and 2:15. The 1st half of the first frame (1:1024) and 2nd half of last frame (17409:18432) contain only zeros, that's why we didn't take the mean of first and last frame.

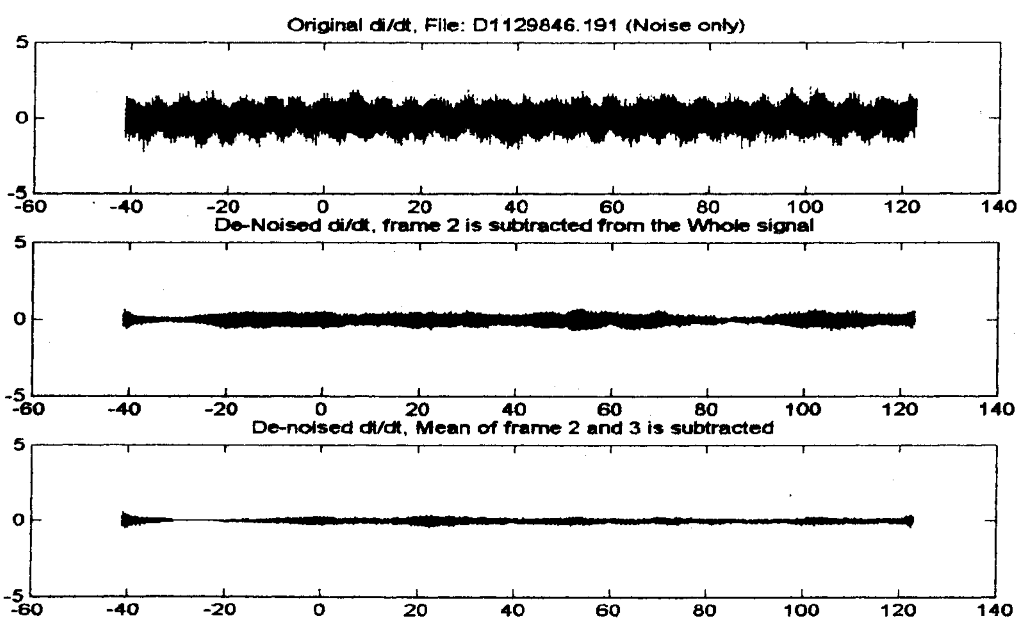

Figure 3.43: Original and de-noised signals subtracting frame 2 and mean of frames 2 and 3

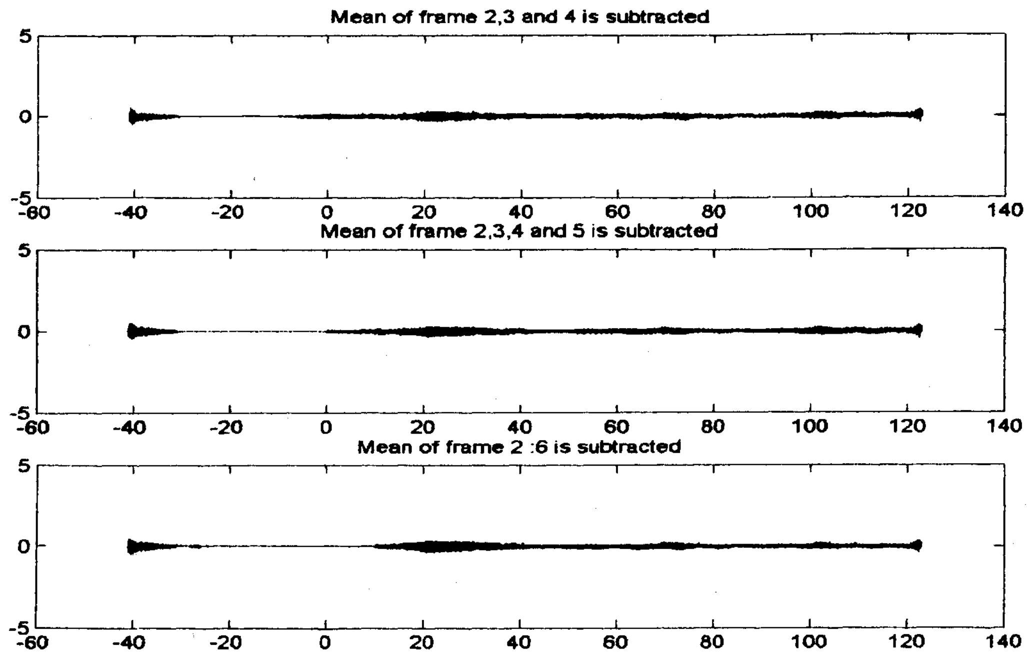

Figure 3.44: De-noised signals subtracting mean of frames 2:4, 2:5 and 2:6.

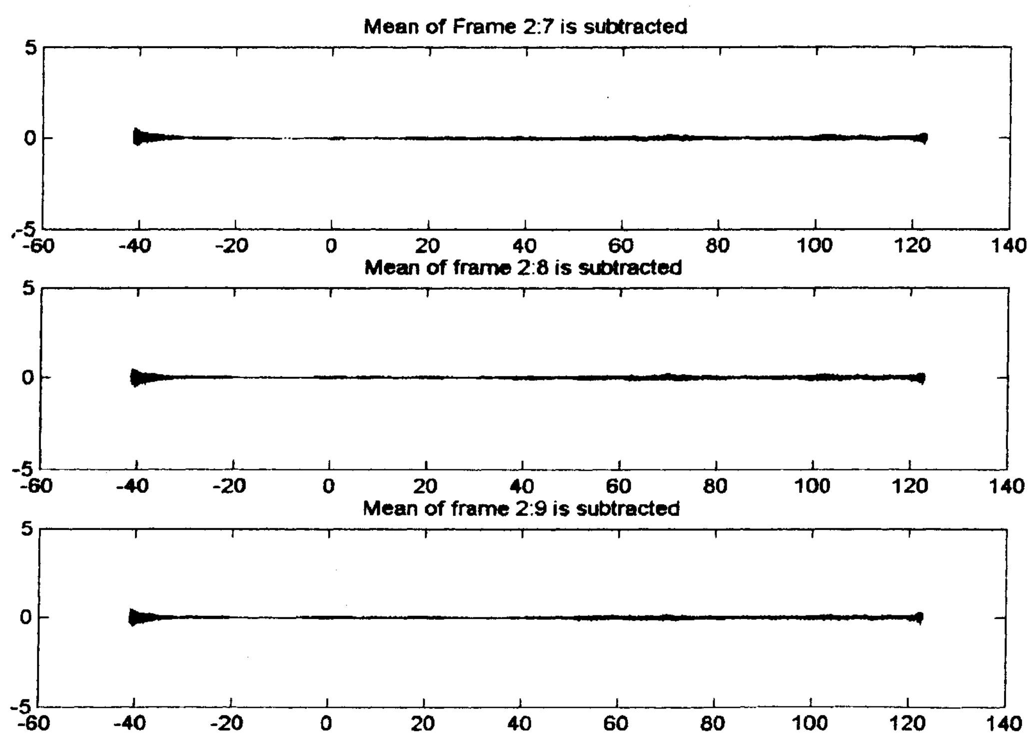

Figure 3.45: De-noised signals subtracting mean of frames 2:7, 2:8 and 2:9.

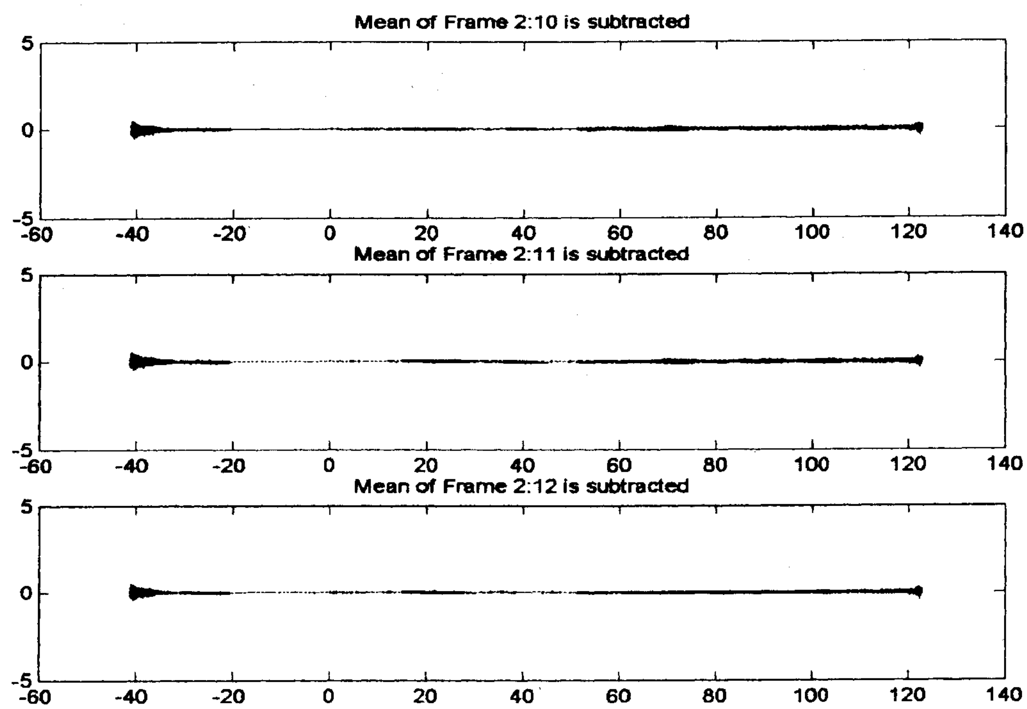

Figure 3.46: De-noised signals subtracting mean of frames 2:10, 2:11 and 2:12.

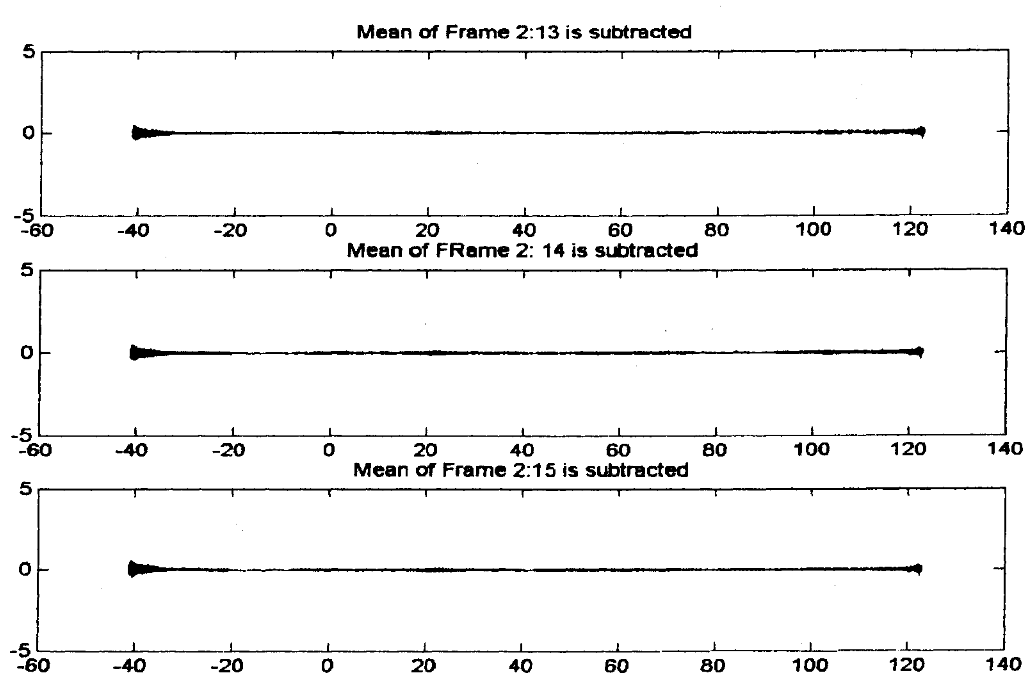

Figure 3.47: De-noised signals subtracting mean of frames 2:13, 2:14 and 2:15.

From the Figs. 3.43-3.47, it is obvious that the de-noised signal quality is improved when the mean of more frames of noise part is subtracted from the original signal. From the analysis, it is obvious that the mean of frames 2:7 and after, the improvement (de-noising) is very close to each other. So, we recommend to record at least 1/3 (6 kB for our case instead of 4 kB) of the whole record as pre-stroke portion.

Chapter 4

Obtaining Waveform Parameters

Statistical data of the current waveform parameters of CN Tower strokes is determined [18] from the measured *di/dt* waveforms that are contaminated by various kinds of noise. The obtained data inaccurately represents the injected current waveform parameters because instrumentation noise, environmental interference and structural discontinuities of the tower contaminate the measurements.

In order to study the characteristics of lightning impact on tall structures, analysis should represent the waveform parameters of the injected current to such structures. In this chapter, the waveform parameters both of current derivative *(di/dt)* and current are obtained from de-noised waveforms after applying the proposed de-noising method.

4.1 Definition of Waveform Parameters

In this thesis, the following waveform parameters are obtained from the de-noised waveforms using the proposed de-noising technique.

Parameters deduced from the current derivative (di/dt) waveforms:

1. *Maximum Steepness of the Current* $(di/dt|_{max})$

   This parameter is defined as the rise from the base level to the maximum peak in the *di/dt* waveform.

2. 10%- 90% Risetime to Maximum Current Derivative (T_d)

   This is the time for *di/dt* waveform to rise above base level from 10% to 90% of the peak value.

The definition of these parameters is shown in Fig. 4.1.

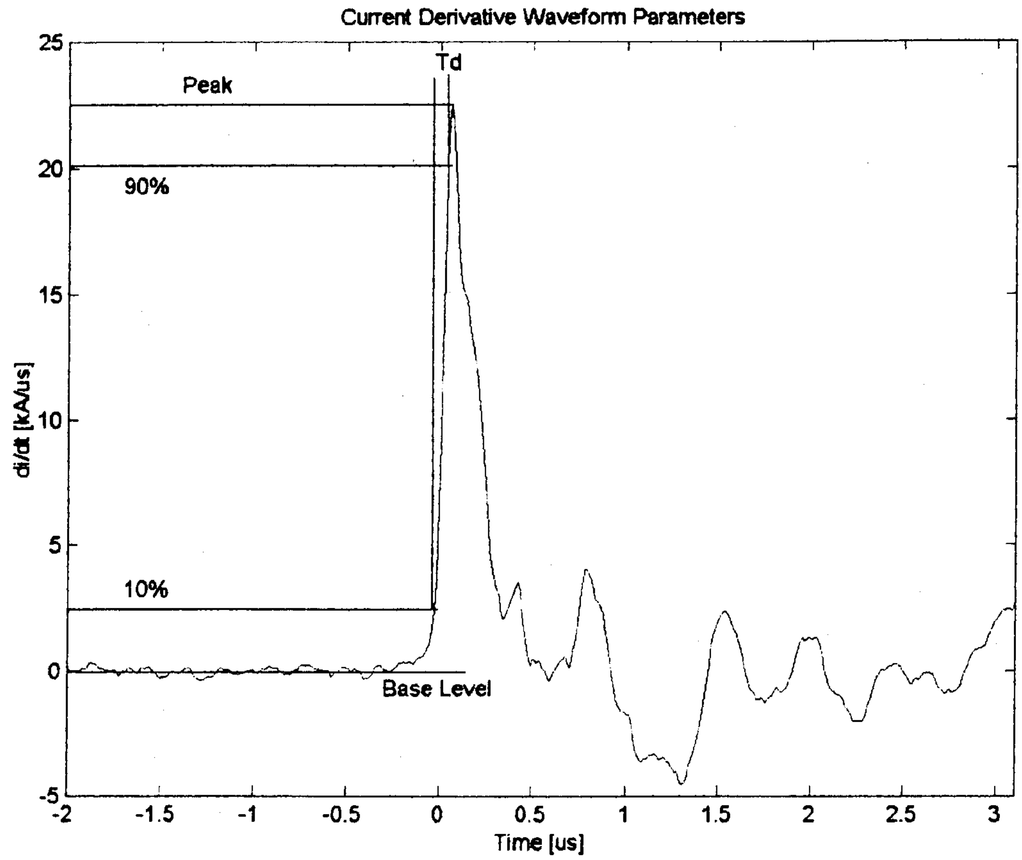

Figure 4.1: Definitions of current derivative waveform parameters.

Parameters deduced from the current waveforms:

1. Current Peak (I_{peak})

   This parameter is defined as the rise from the base level to the first peak value of the current waveform.

2. 10%- 90% Risetime of Current Waveforms (T)

   This is the time for current to rise above the base level from 10% to 90% of the peak value

The definition of these current waveform parameters is shown in Fig. 4.2.

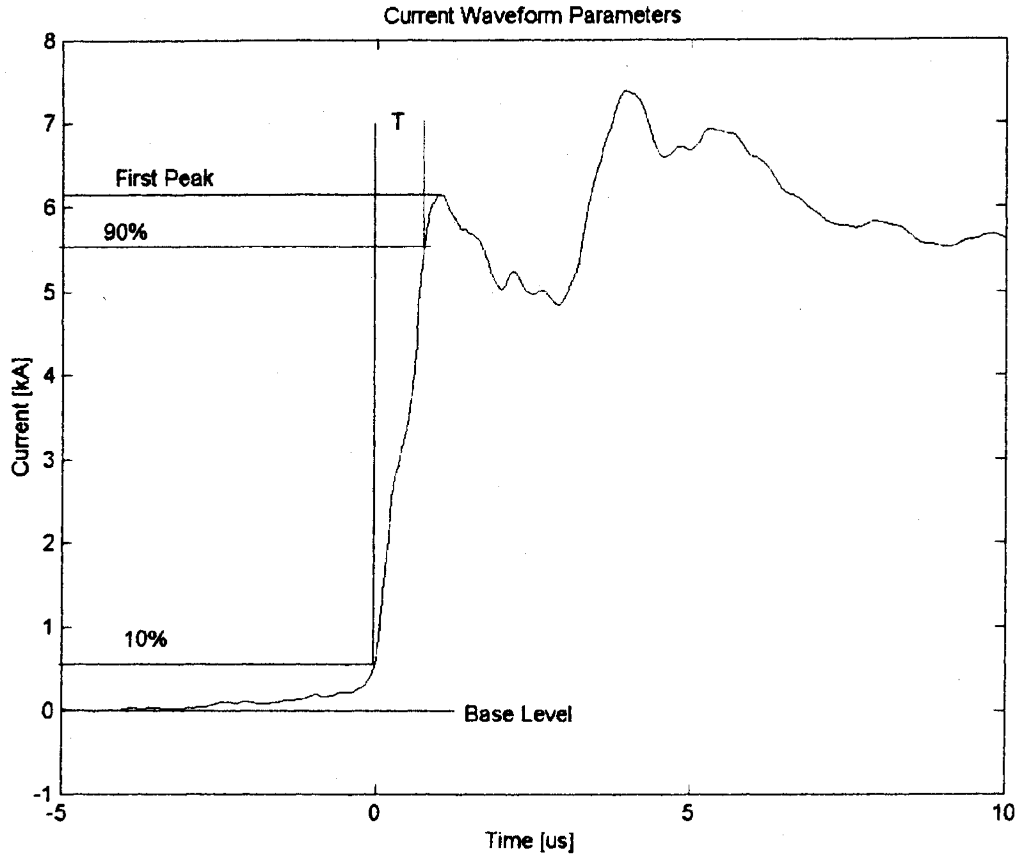

Figure 4.2: Definitions of current waveform parameters.

There are other waveform parameters that are also used to characterize a lightning current signal which are not indicated in the Figs. 4.1 and 4.2.

4. *Time to Half Value of Current*

It is defined as the time when the current decays to half value of the first peak.

5. *Impulse Charge*

It is defined as total charge calculated from the integration of the current waveform. Several researchers obtained the *di/dt* and current waveform parameters from noisy waveforms. But the measured *di/dt* records on May 09, 2002 were too much contaminated by noise and it became difficult to determine those parameters. The proposed de-noising method is applied on the May 09, 2002 data files. The obtained waveform parameters are shown in Figs. 4.3-4.30.

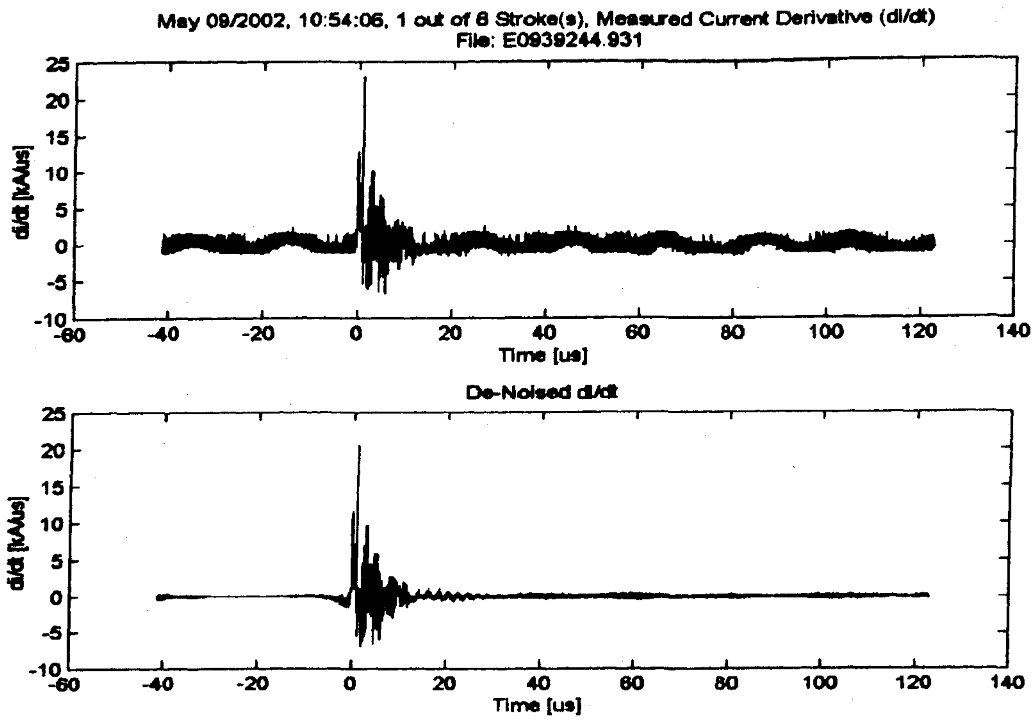

Figure 4.3: Measured and de-noised *di/dt.* File: E0939244.931.

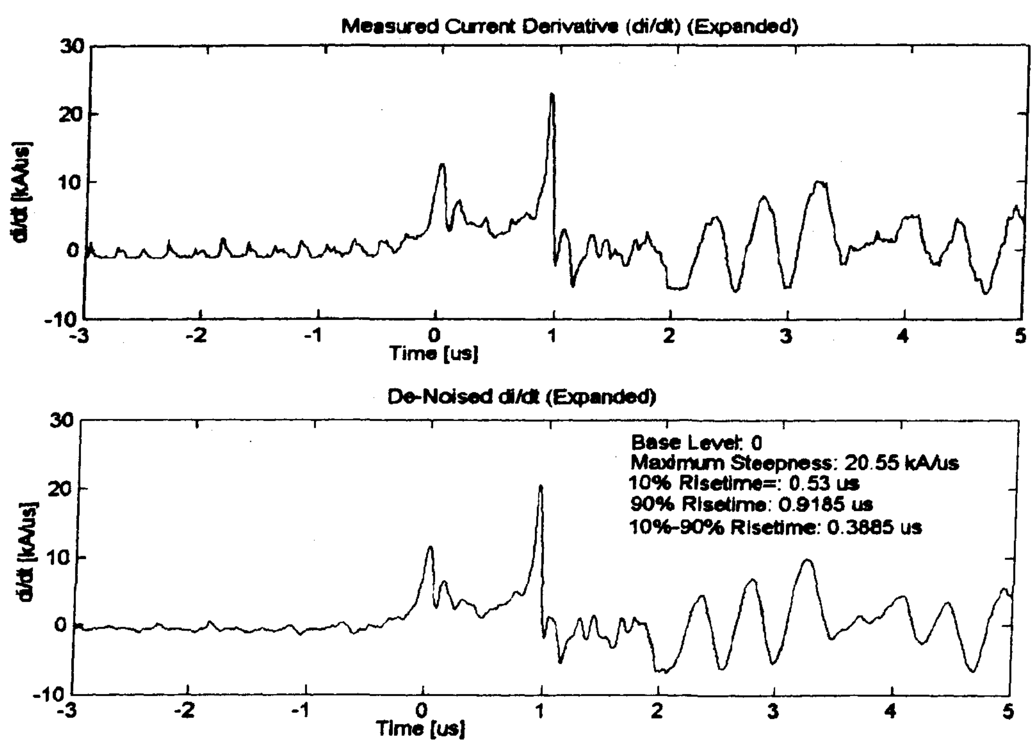

Figure 4.4: Expanded form of measured and de-noised *di/dt* and its parameters.

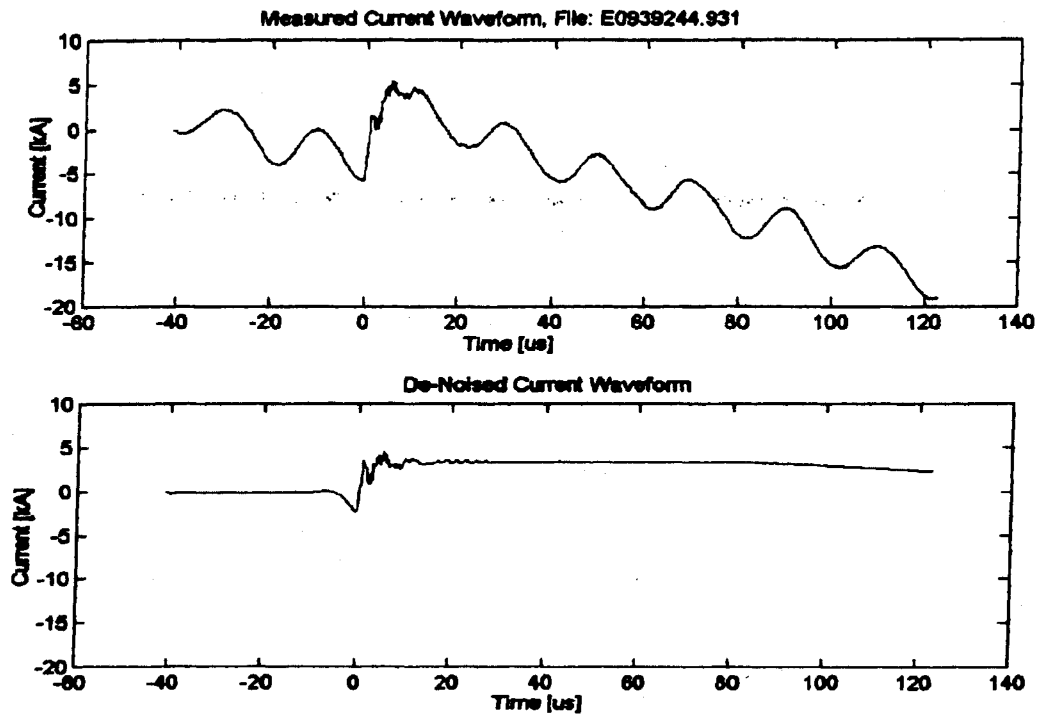

Figure 4.5: Current waveform from measured and de-noised *di/dt*. File: E0939244.931.

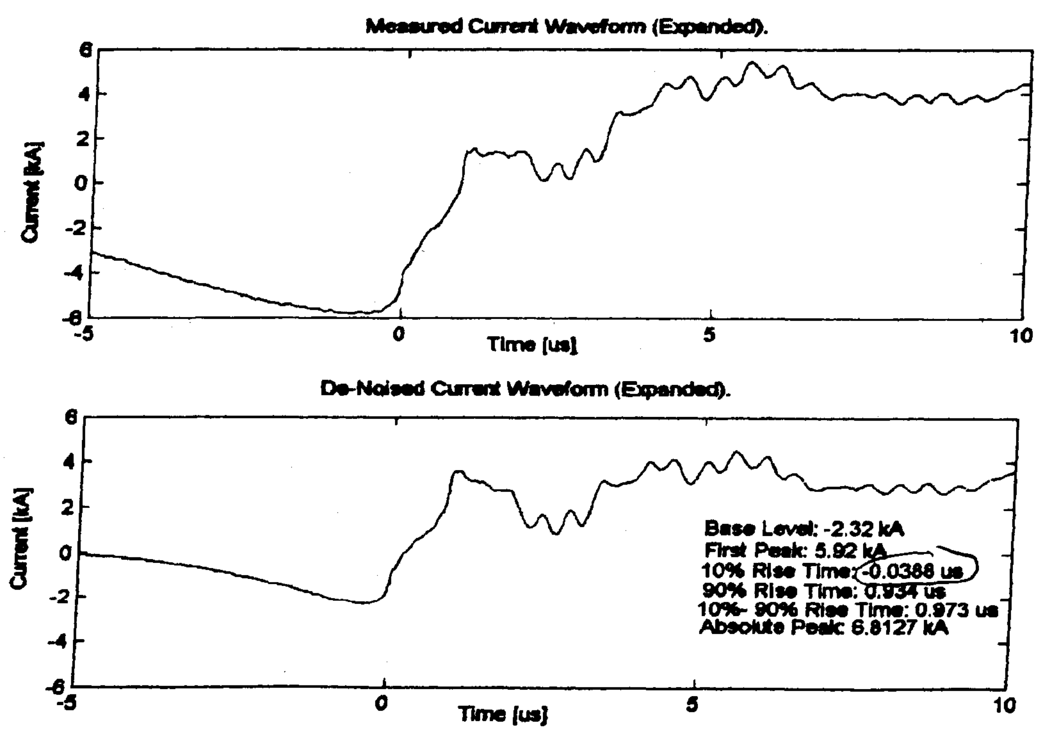

Figure 4.6: Expanded form of current waveform and its parameters.

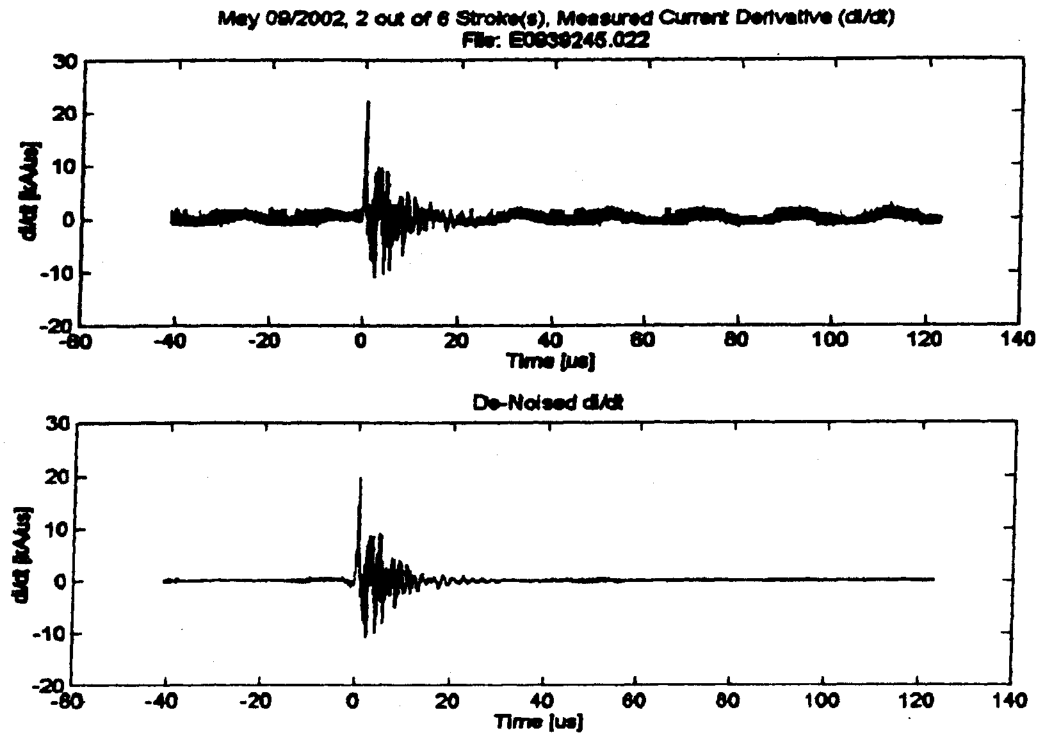

Figure 4.7: Measured and de-noised *di/dt*. File: E0939245.022.

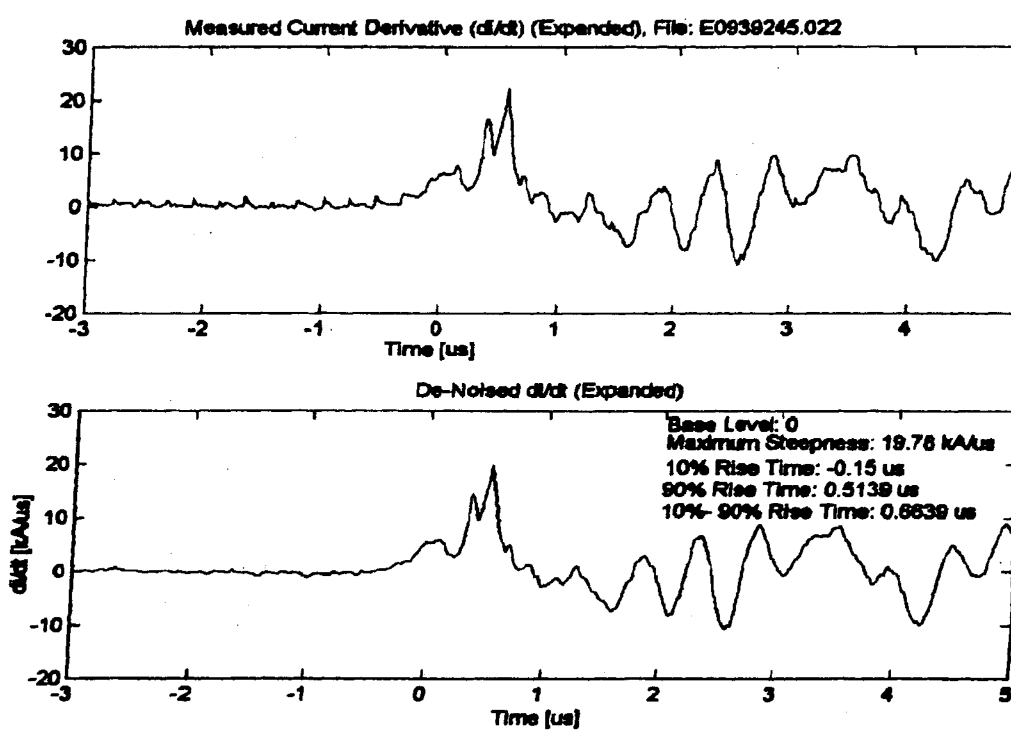

Figure 4.8: Expanded form of measured and de-noised *di/dt* and its parameters.

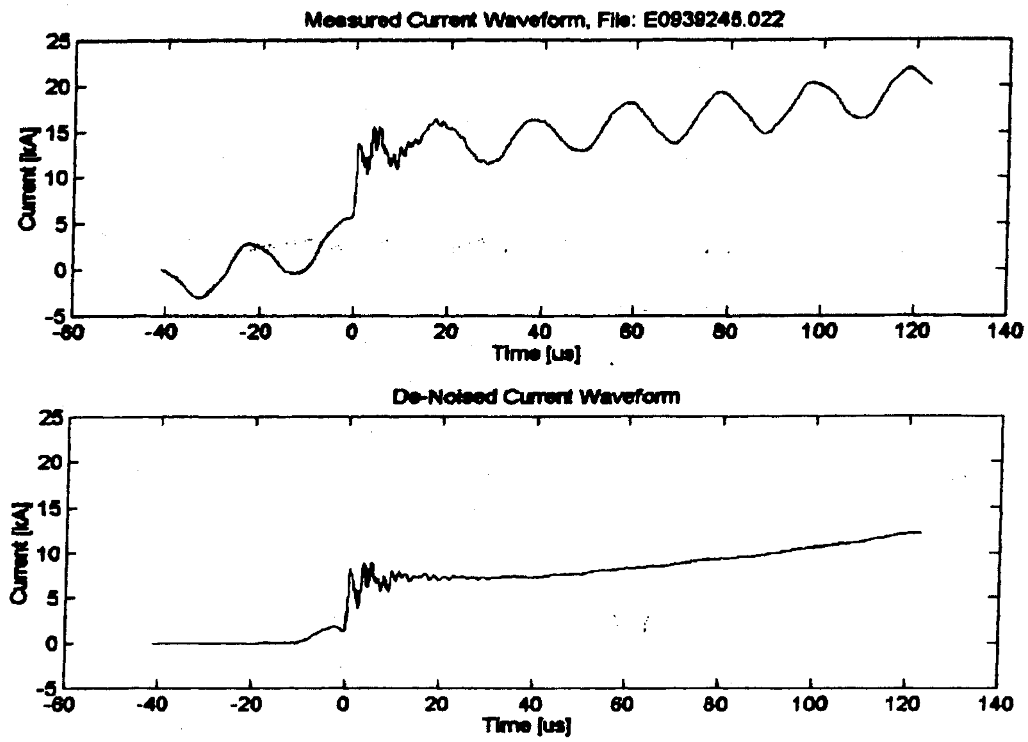

Figure 4.9: Current waveform from measured and de-noised *di/dt*. File: E0939245.022.

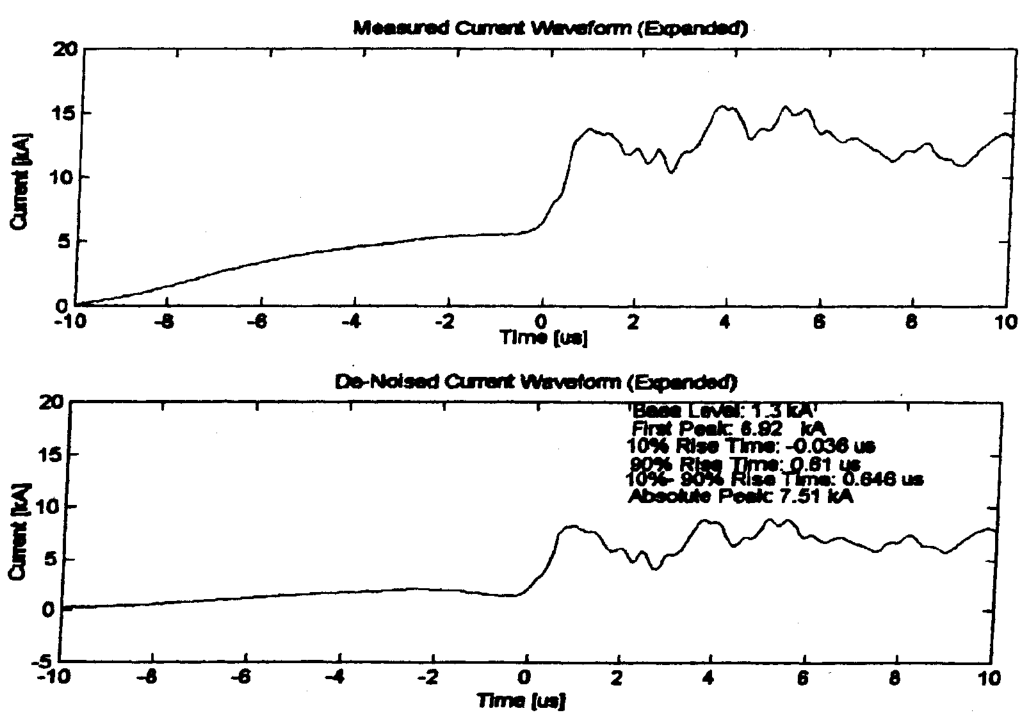

Figure 4.10: Expanded form of current waveform and its parameters.

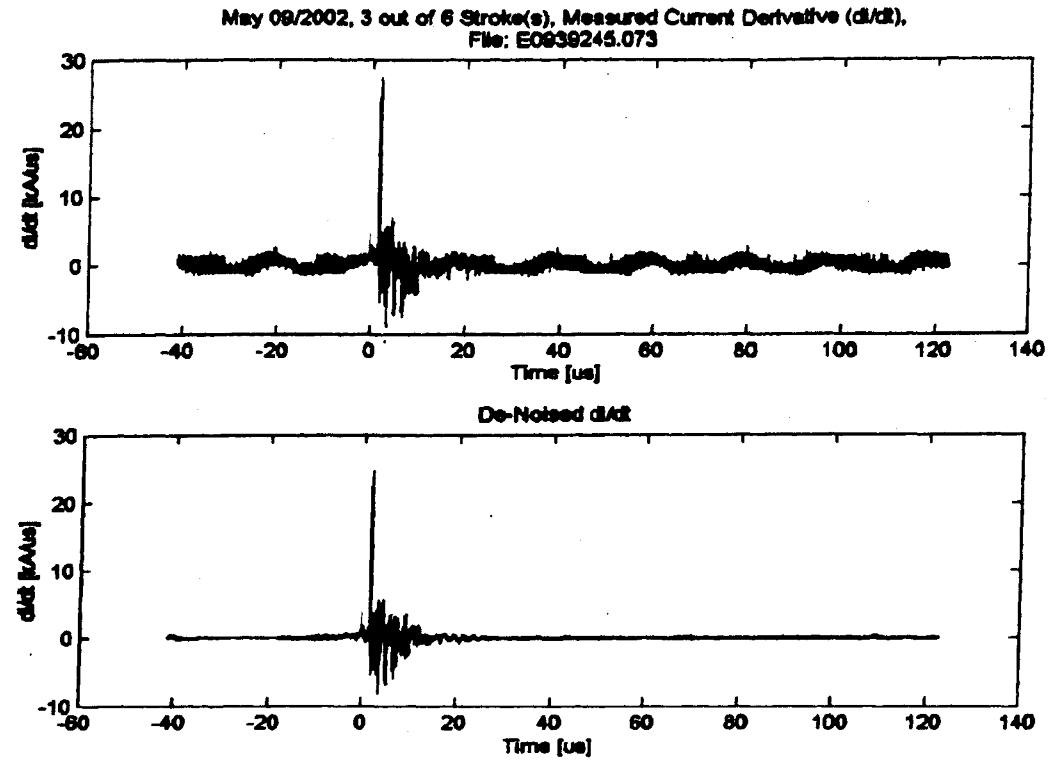

Figure 4.11: Measured and de-noised *di/dt*. File: E0939245.073.

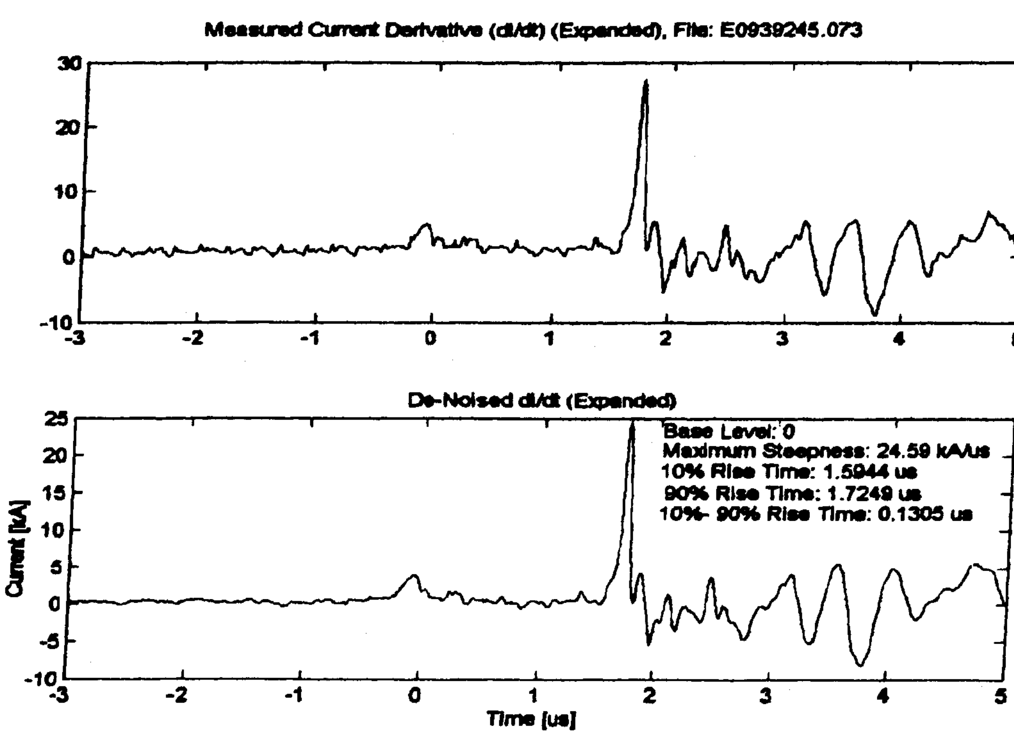

Figure 4.12: Expanded form of measured and de-noised *di/dt* and its parameters.

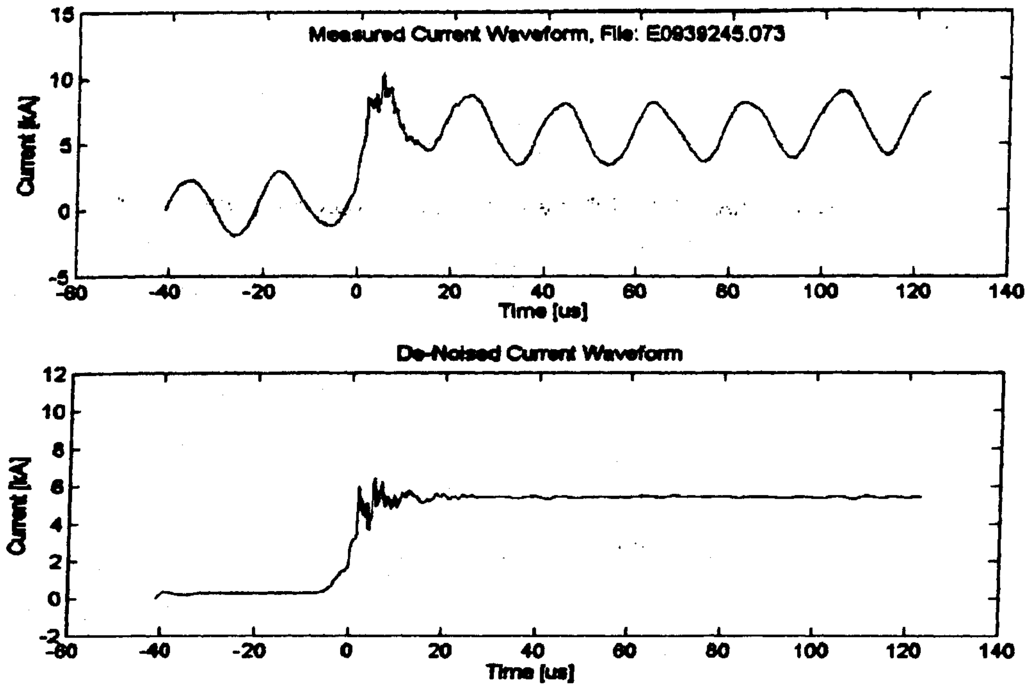

Figure 4.13: Current waveform from measured and de-noised *di/dt*. File: E0939245.073.

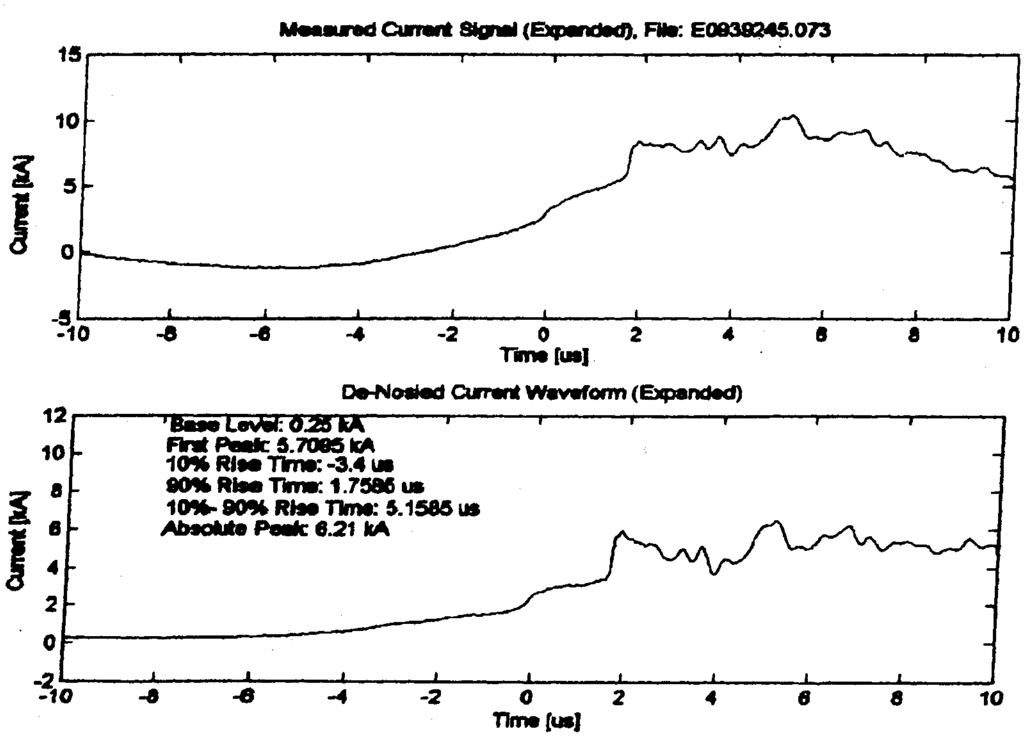

Figure 4.14: Expanded form of current waveform and its parameters.

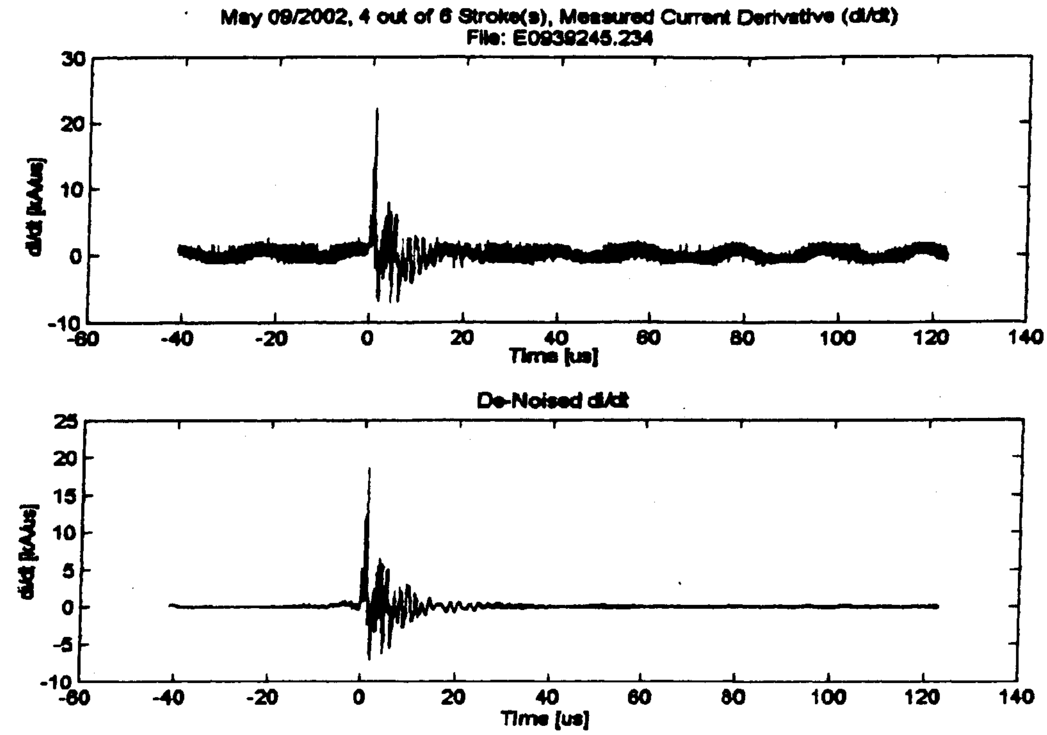

Figure 4.15: Measured and de-noised *di/dt*. File: E0939245.234.

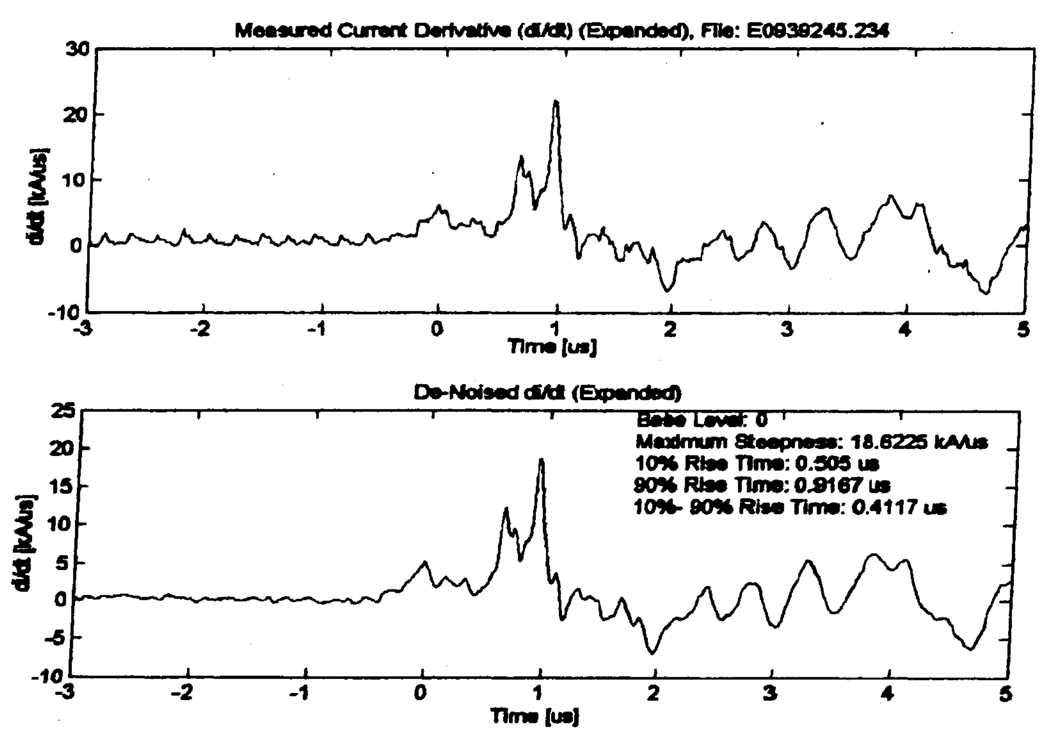

Figure 4.16: Expanded form of measured and de-noised *di/dt* and its parameters.

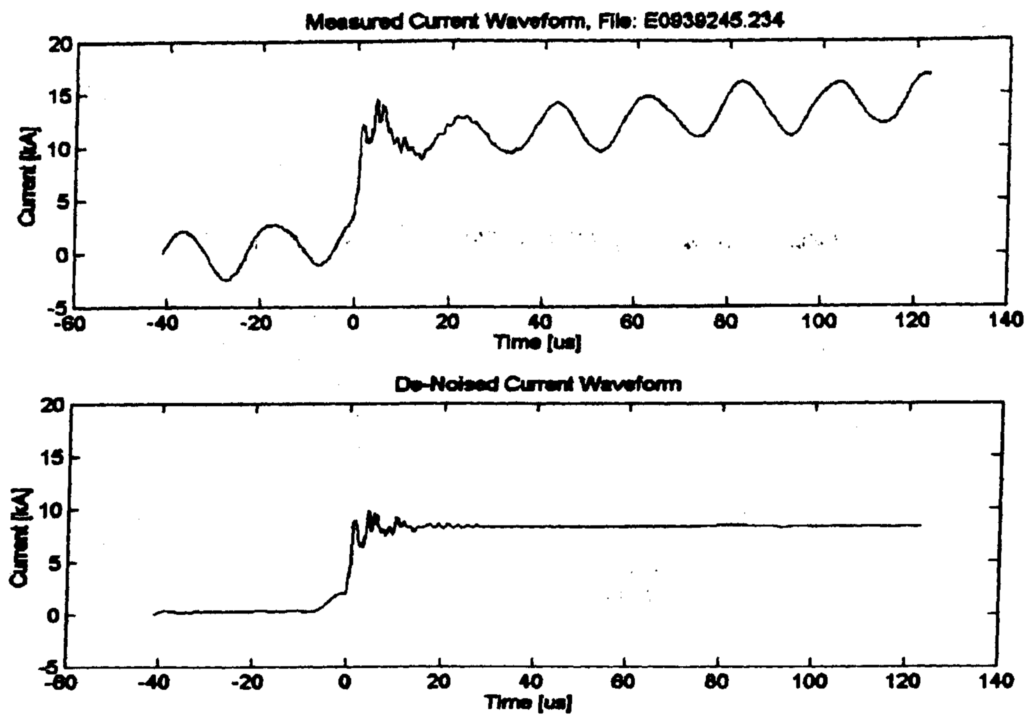

Figure 4.17: Current waveform from measured and de-noised *di/dt*. File: E0939245.234.

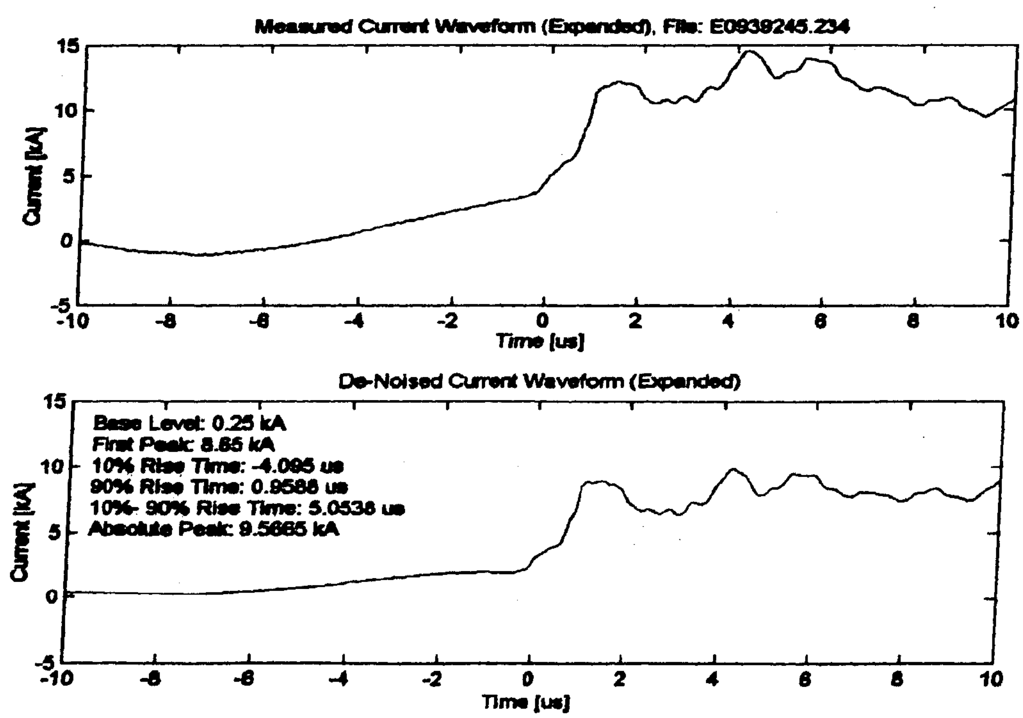

Figure 4.18: Expanded form of current waveform and its parameters.

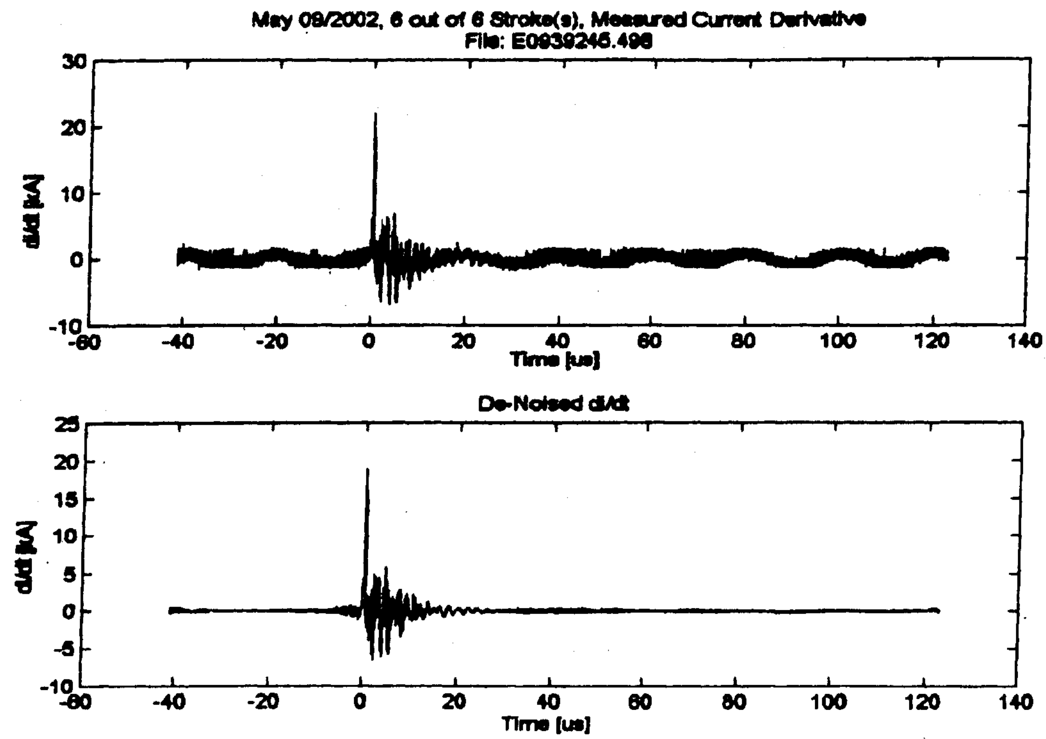

Figure 4.19: Measured and de-noised *di/dt*. File: E0939245.496.

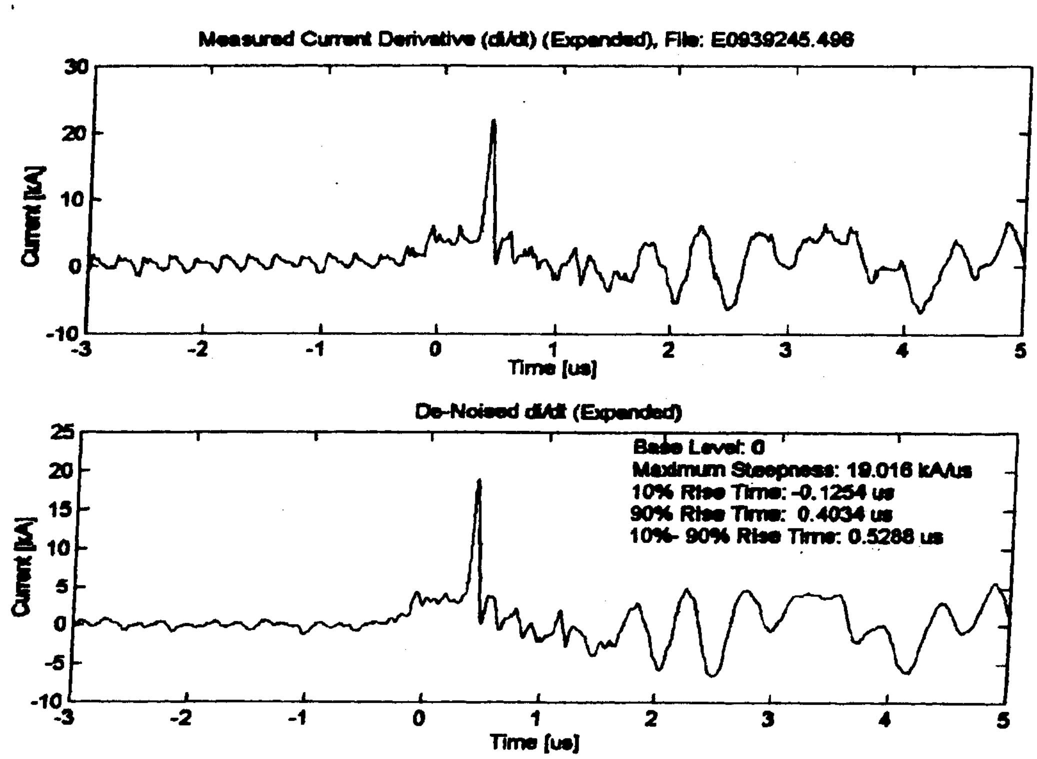

Figure 4.20: Expanded form of measured and de-noised *di/dt* and its parameters.

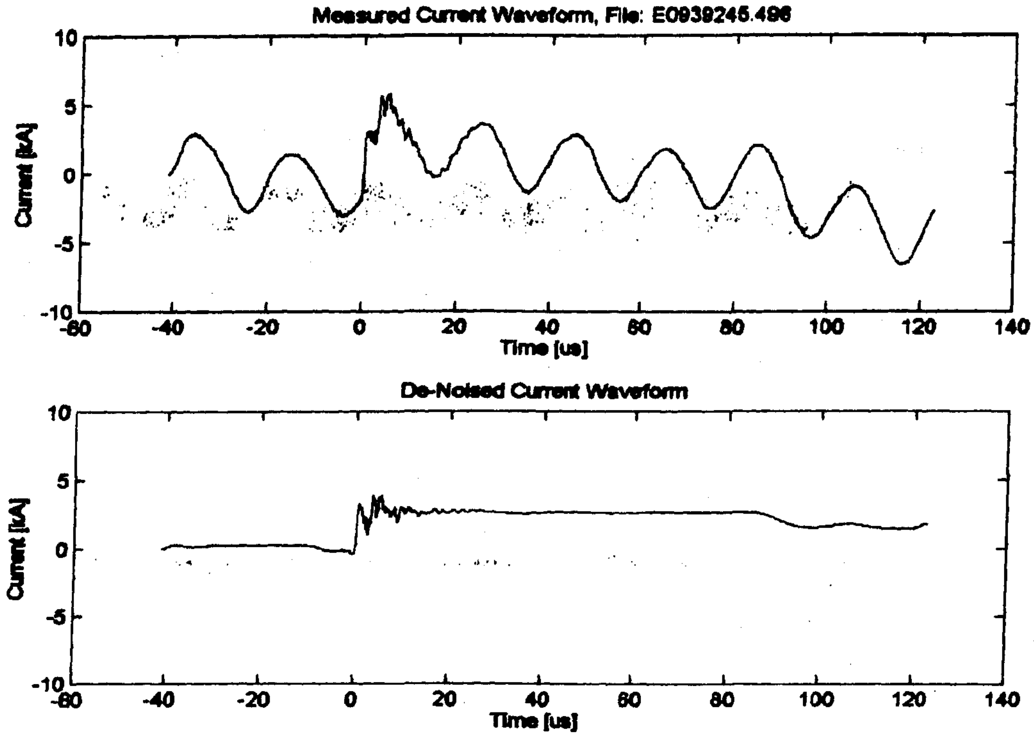

Figure 4.21: Current waveform from measured and de-noised *di/dt*. File: E0939245.496.

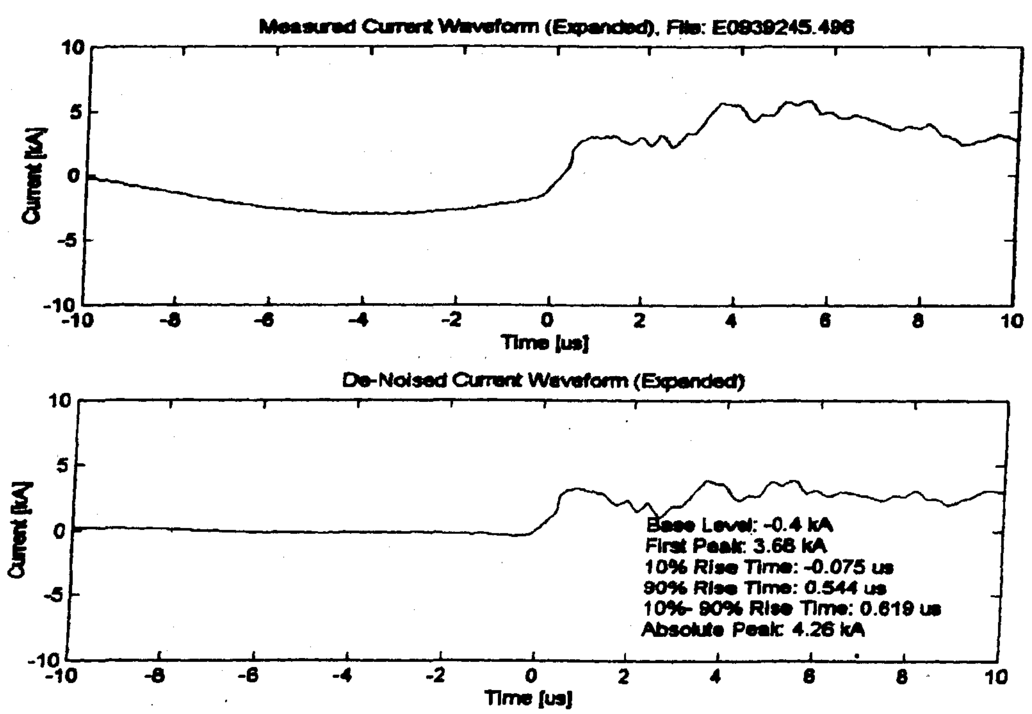

Figure 4.22: Expanded form of current waveform and its parameters.

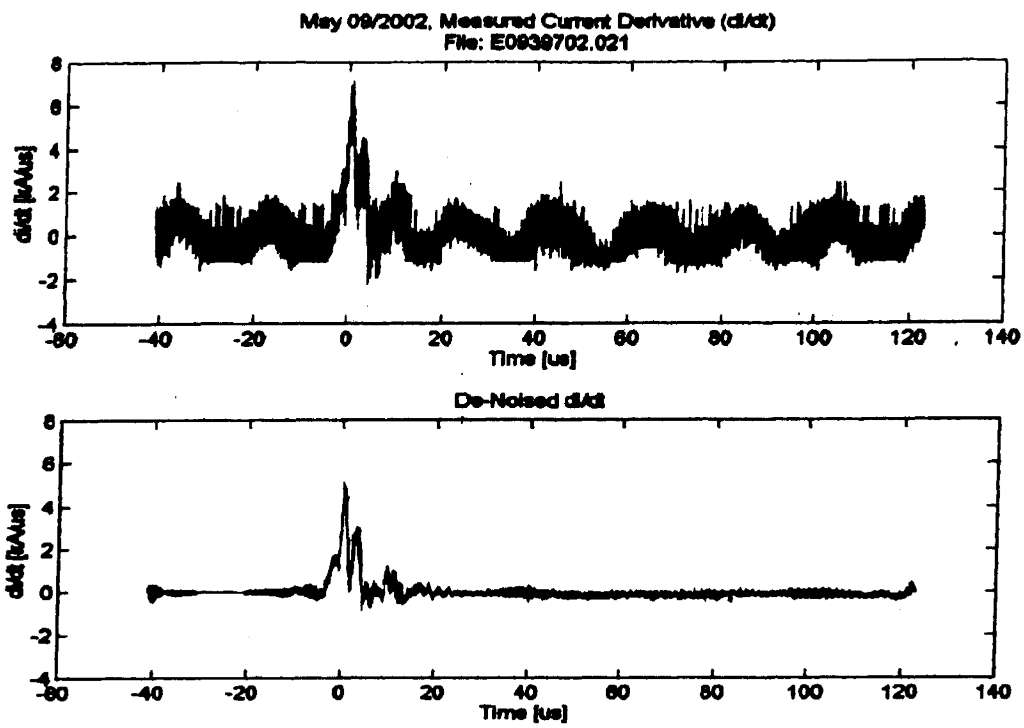

Figure 4.23: Measured and de-noised *di/dt*, File: E0939702.021.

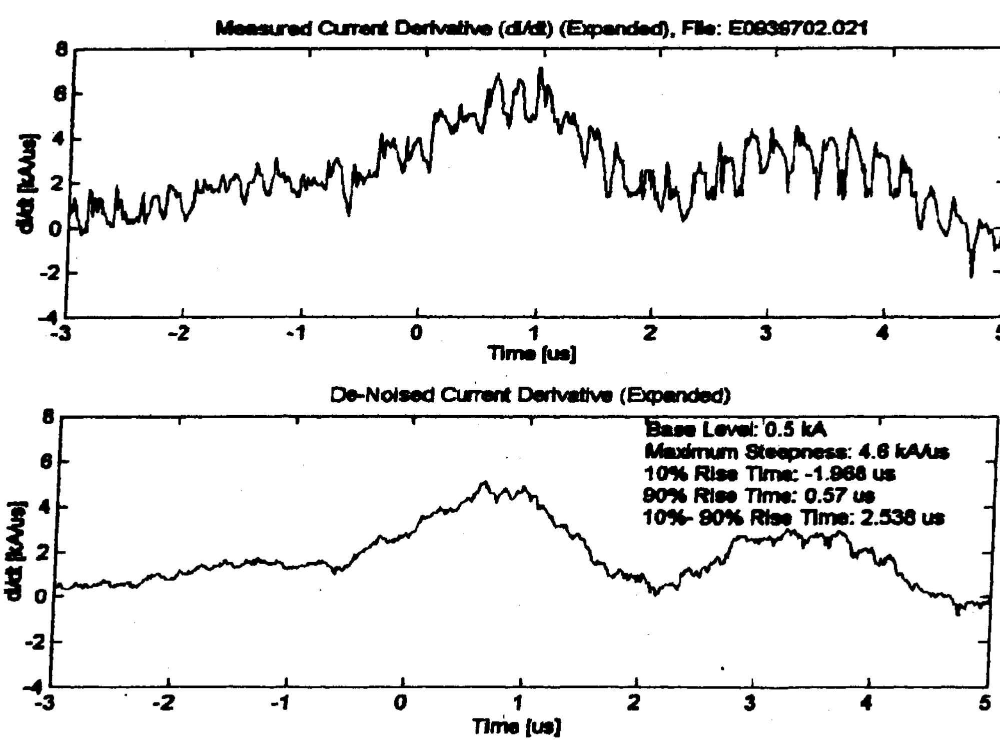

Figure 4.24: Expanded form of measured and de-noised *di/dt* and its parameters.

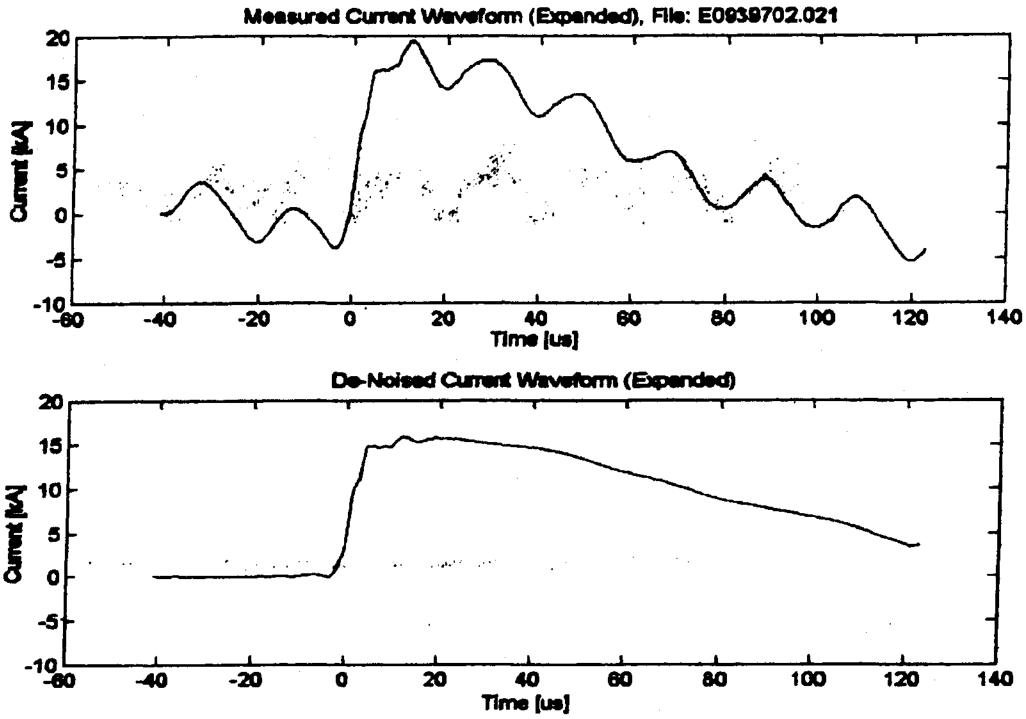

Figure 4.25: Current waveform from measured and de-noised *di/dt*, File: E0939702.021.

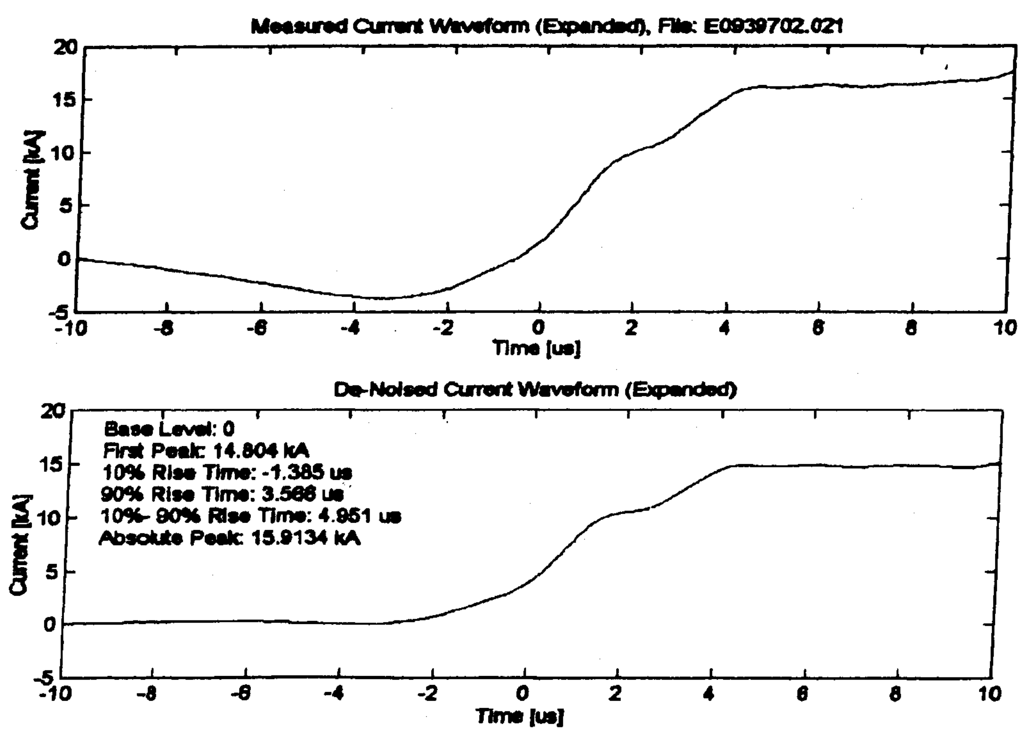

Figure 4.26: Expanded form of current waveform and its parameters.

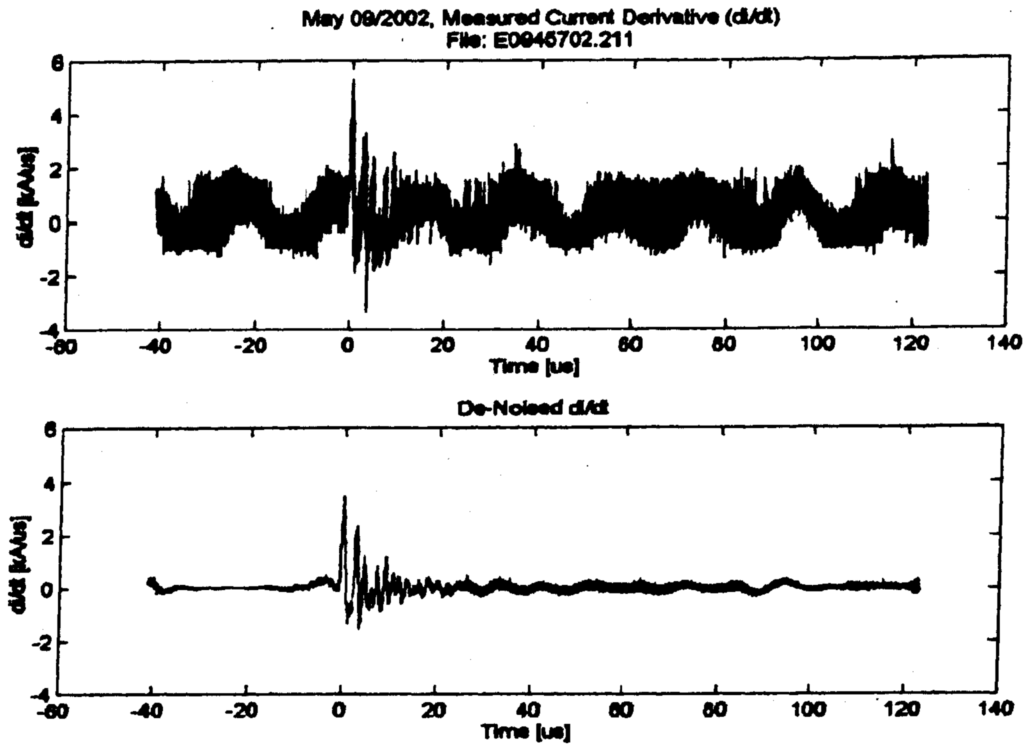

Figure 4.27: Measured and de-noised *di/dt*. File: E0939705.211.

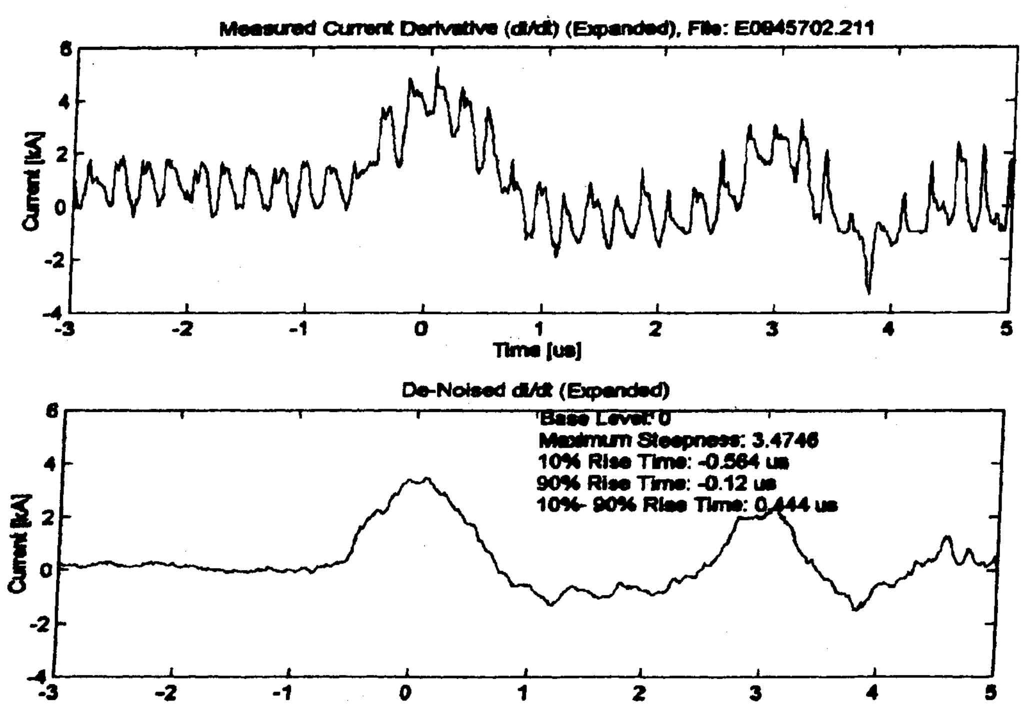

Figure 4.28: Expanded form of measured and de-noised *di/dt* and its parameters.

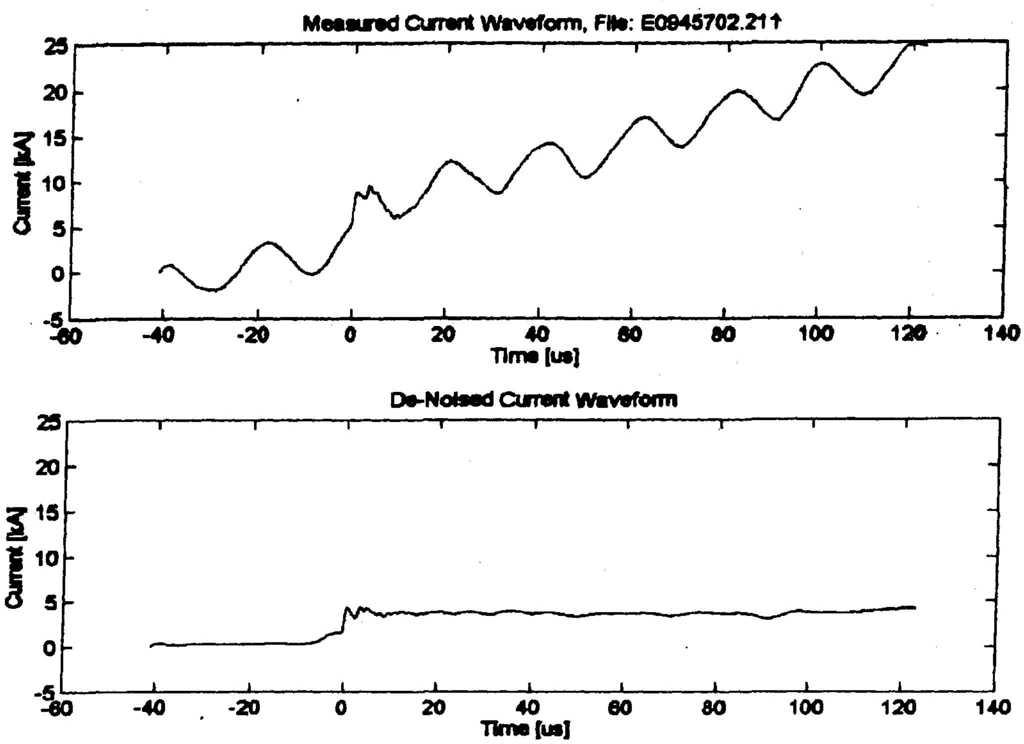

Figure 4.29: Current waveform from measured and de-noised *di/dt*. File: E0939705.211.

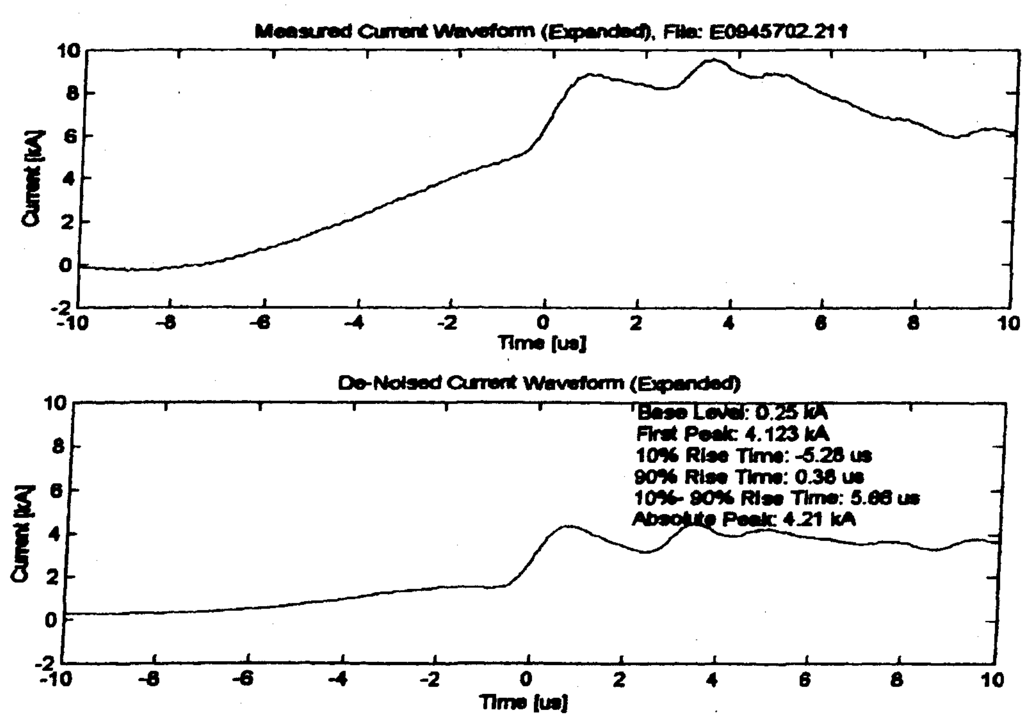

Figure 4.30: Expanded form of current waveform and its parameters.

4.2 Statistics of Current Waveform Parameters

The de-noised current derivative and current waveforms parameters and their statistics can be tabulated in the following tables for the files recorded on May 09, 2002 at the CN Tower.

Table 4.1: Waveform Parameters and their Statistics.

File Name	**Current Derivative (*di/dt*) Parameters**		**Current Waveform Parameters**		
	Maximum Steepness (kA/μs)	*10%- 90% Rise Time (μs)*	*First Peak (kA)*	*10%- 90% Rise Time (μs)*	*Absolute Peak (kA)*
E0909244.931	20.55	0.3885	5.92	0.973	6.8127
E0909245.022	19.78	0.6639	6.92	0.646	7.51
E0909245.073	24.59	0.1305	5.7095	5.1585	6.21
E0909245.234	18.6225	0.4117	8.65	5.0538	9.5665
E0909245.496	19.016	0.5288	3.68	0.619	4.26
E0909702.021	4.6	2.538	14.804	4.951	15.9134
E0909705.211	3.4746	0.444	4.123	5.66	4.21
Mean	15.80	0.73	7.12	3.30	7.78

4.3 Field Waveform Parameters

STFT-based spectral subtraction is applied on lightning generated magnetic *(H)* and electric fields *(E)* that are measured at the University of Toronto, 2 km north from the CN Tower. The electric and magnetic field waveforms, generated by CN Tower lightning strikes, are mostly corrupted by high frequency noise components. When the proposed method is applied on *E* and *H* fields, it became easier to obtain the waveform parameters from the de-noised signal. In this application a Hanning window is used. Since the frame length is application dependent, we tried different window lengths to select the appropriate window length and compared their SPNPR as it was done with lightning current derivative and current waveforms. The following table gives the comparison of SPNPR of E and H fields resulting from different window sizes.

Table 4.2: SPNPR using different window sizes.

Frame Size (Points)	**SPNPR**		**Comments**
	E	**H**	
Original (Full Length)	9.52	2.93	Measured Signal
512	104.53	32.39	2nd Highest SPNPR
1024	224.30	51.51	Highest SPNPR
2048	35.60	11.11	3rd Highest SPNPR
3072	22.43	7.18	Lowest SPNPR

From the above table, it is clear that window size 1024 (1 kB) gives the best SPNPR. Therefore, we used this size in this application. Using Hanning window of different sizes, after applying the STFT-based spectral subtraction on electric field (E) files that were measured at the University of Toronto and the de-noised signal waveforms (E) are shown in Figs. 4.31-4.34.

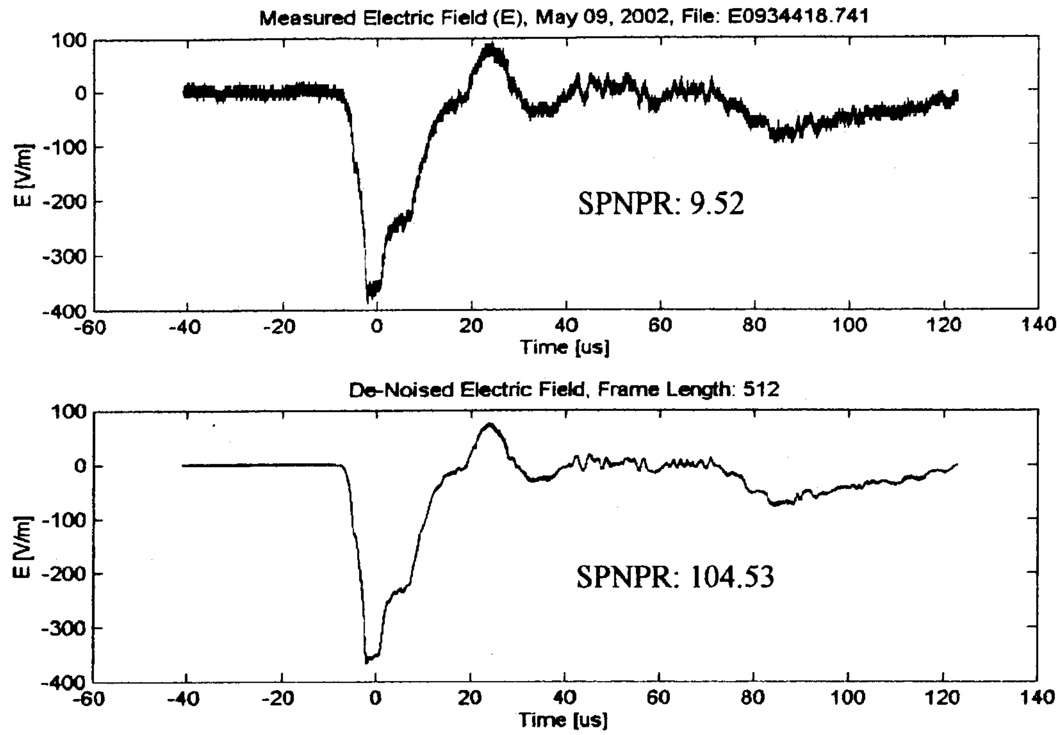

Figure 4.31: Measured and de-noised electric field. Frame length: 512.

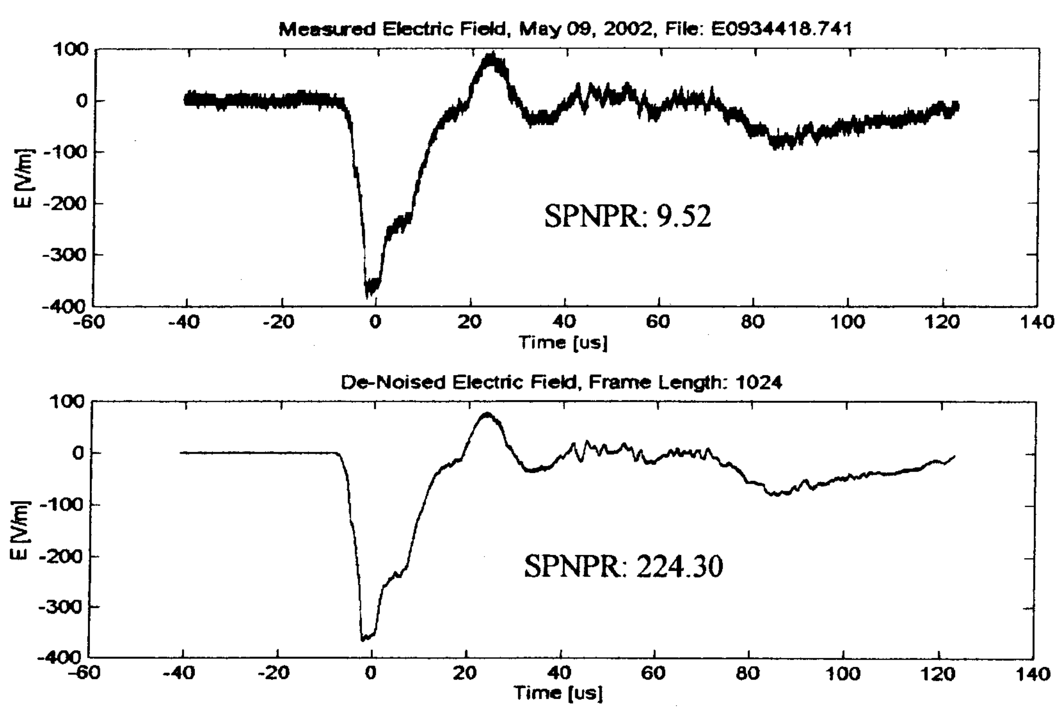

Figure 4.32: Measured and de-noised electric field. Frame length: 1024.

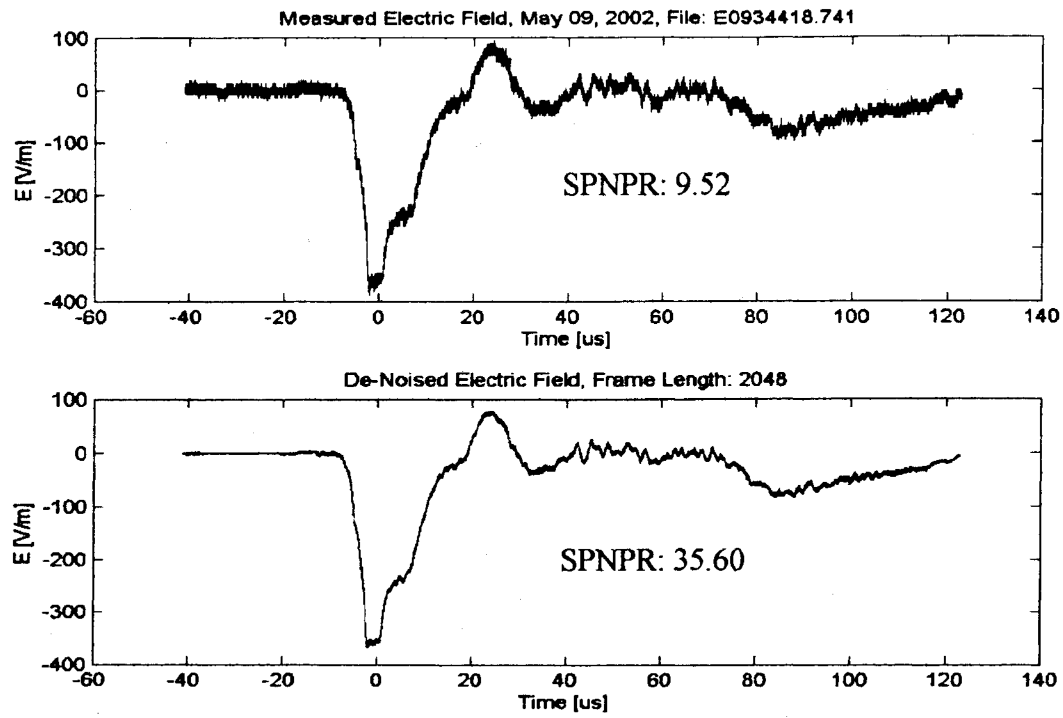

Figure 4.33: Measured and de-noised electric field. Frame length: 2048.

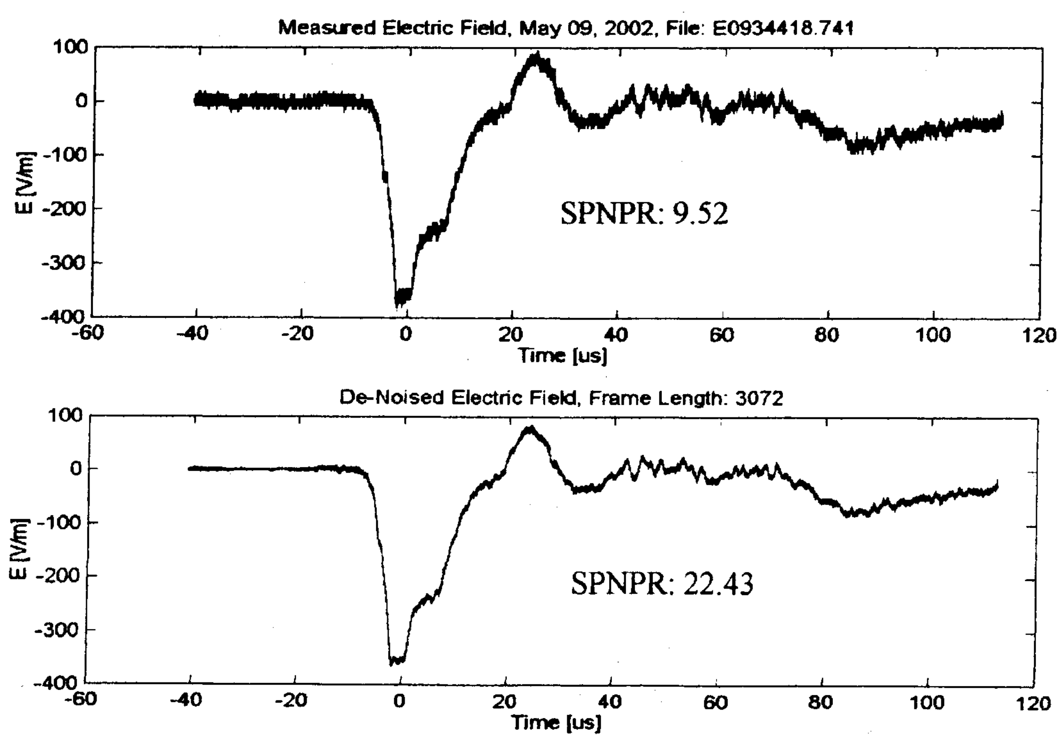

Figure 4.34: Measured and de-noised electric field. Frame length: 3072.

When the STFT-based spectral subtraction is applied on the magnetic field *(H)*, the de-noised waveforms are shown Figs. 4.35-4.38 for different frame lengths:

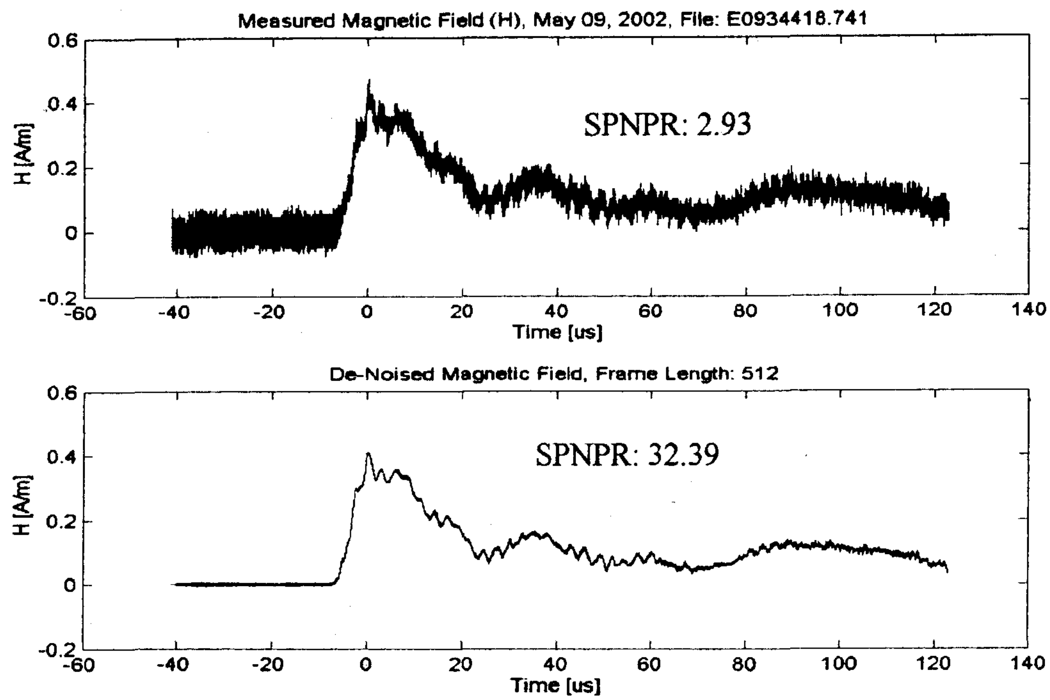

Figure 4.35: Measured and de-noised magnetic field. Frame length: 512.

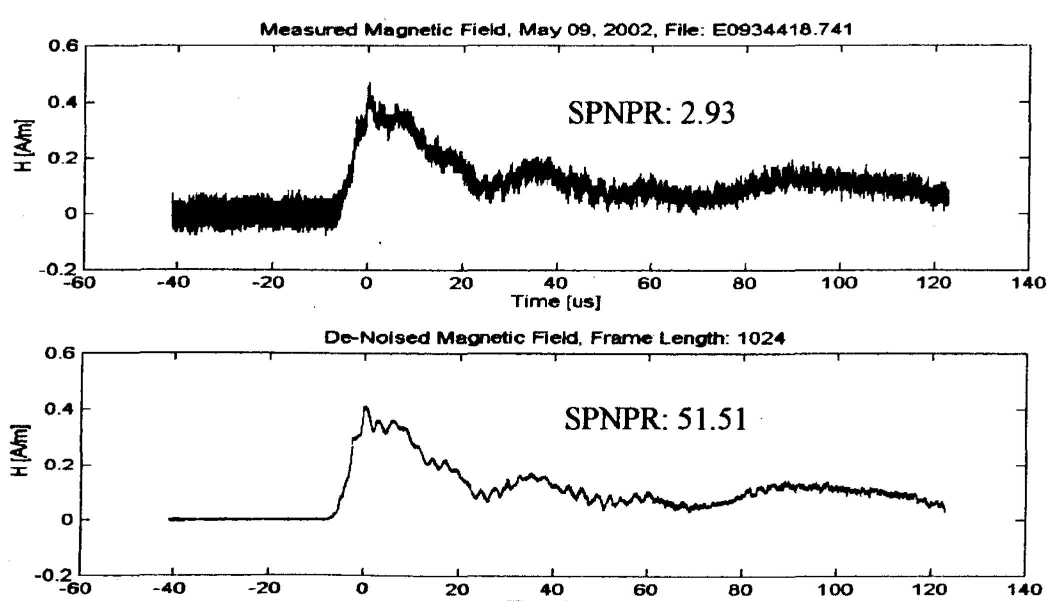

Figure 4.36: Measured and de-noised magnetic field, Frame length: 1024.

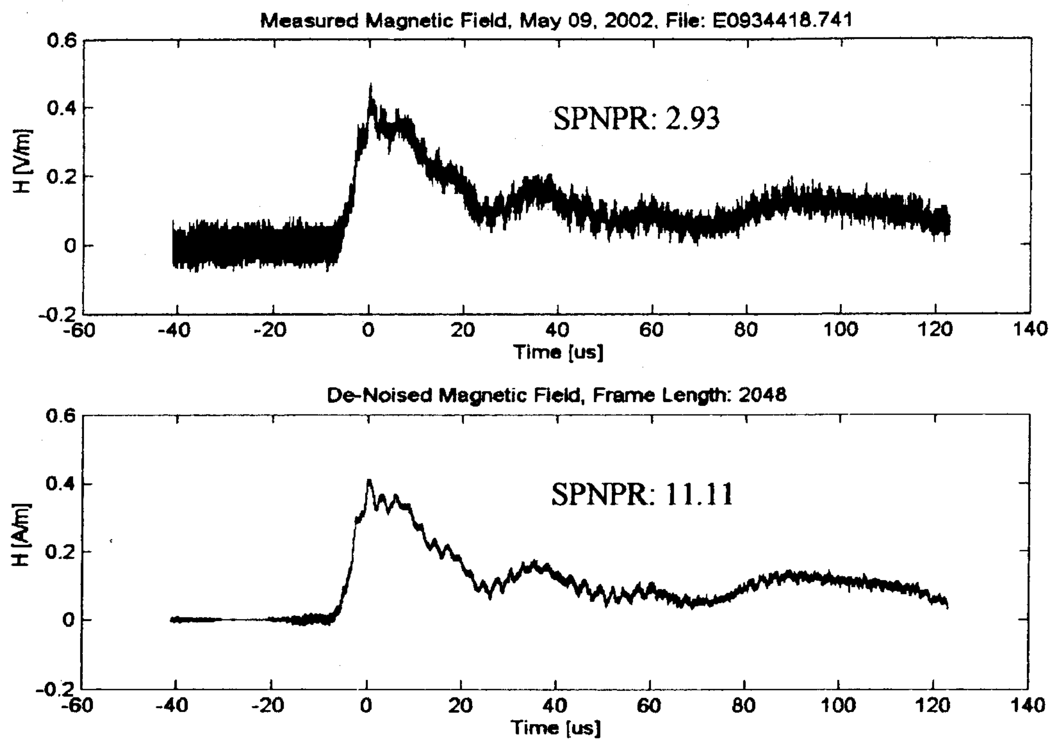

Figure 4.37: Measured and de-noised magnetic field, Frame length: 2048.

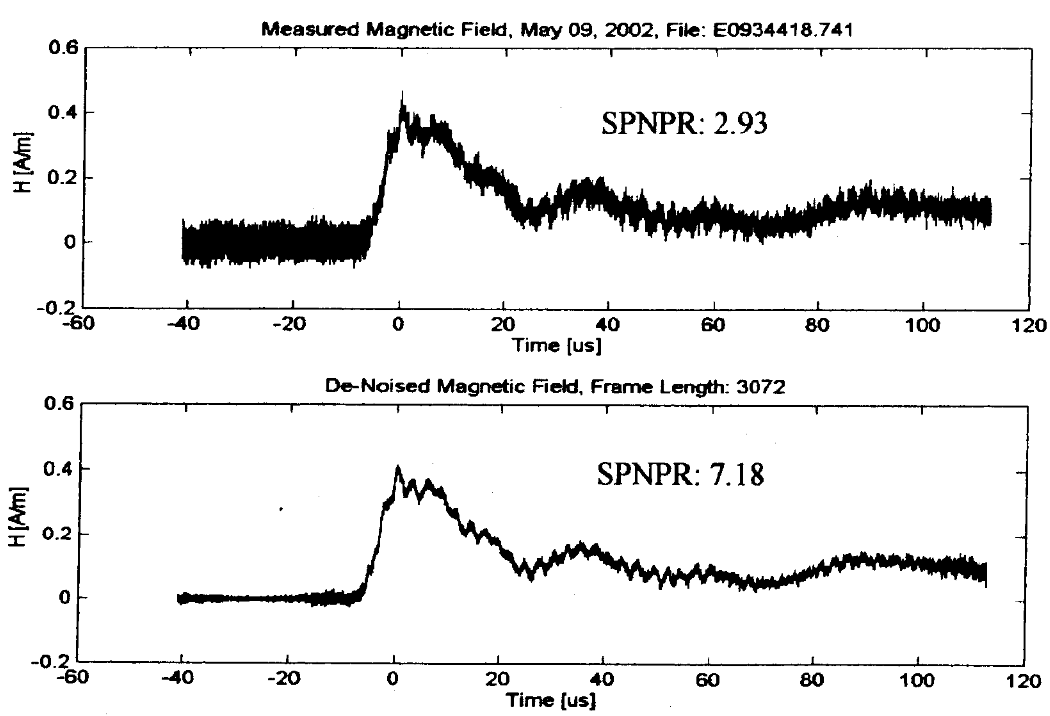

Figure 4.38: Measured and de-noised magnetic field, Frame length: 3072.

It is evident from the above figures and SPNPR values, the frame length 1024 gives the best result for both E and H fields..

When the proposed method is applied on *E* and *H* field measured on May 09, 2002, the de-noised waveforms and their corresponding parameters are shown below:

Electric Field Parameters

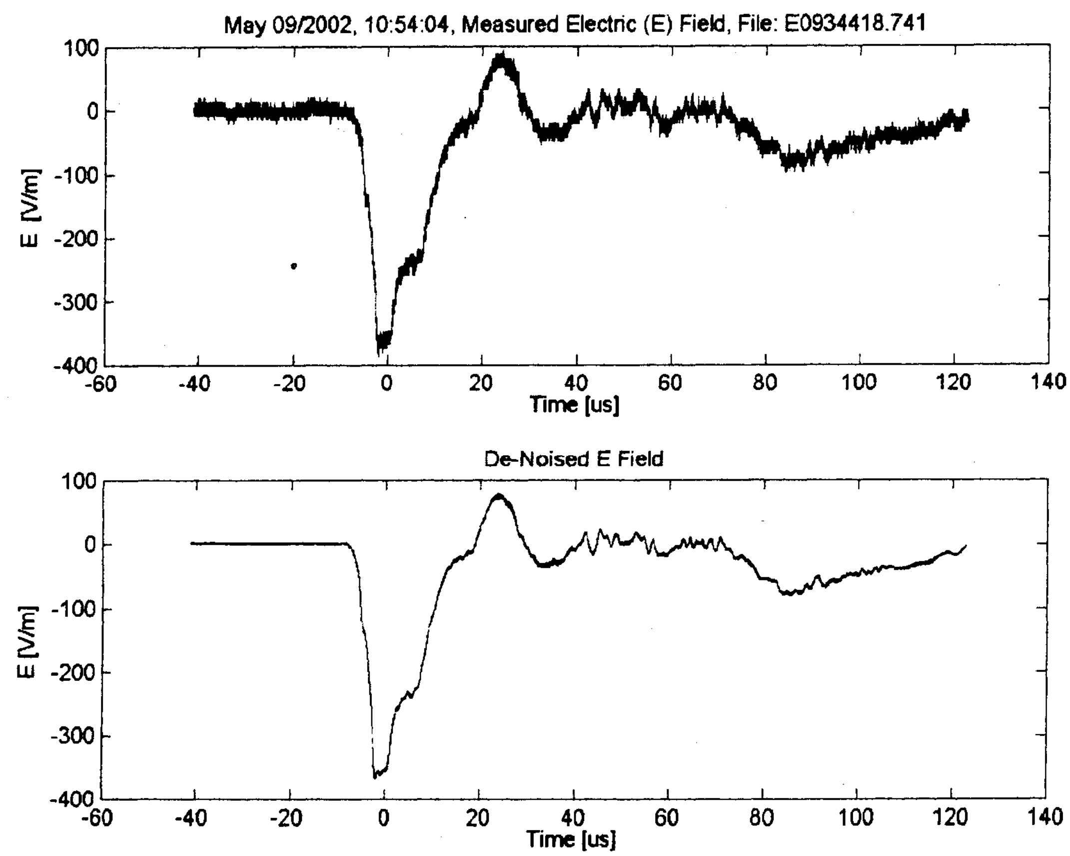

Figure 4.39: Measured and de-noised electric field. File: E0937718.741.

Table 4.3: Electric field waveform parameters. File: E0934418.741.

Maximum Steepness (V/m/μs)	*Peak (V/m)*	*10%- 90% Rise Time (μs)*	*Pulse Width (μs)*
-58.06	-368.102	3.635	11.673

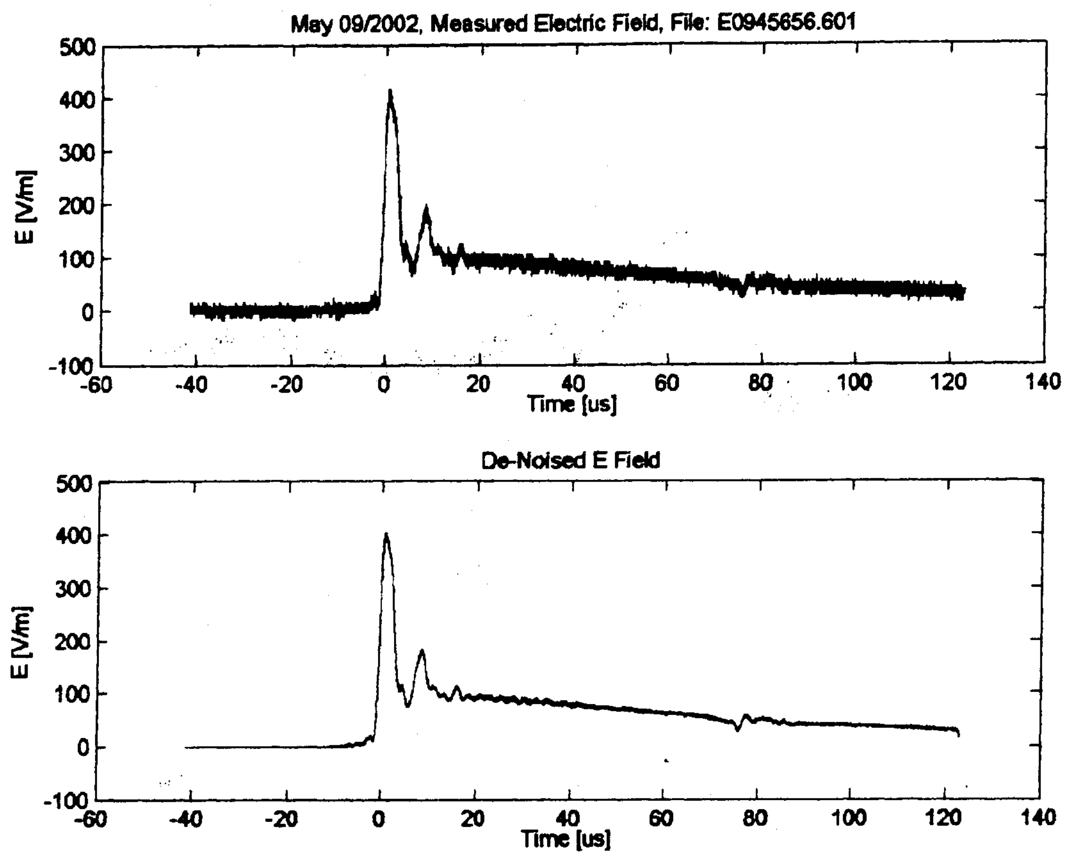

Figure 4.40: Measured and de-noised electric field. Time: 12.40:56. File: E0945656.601.

Table 4.4: Electric field waveform parameters. File: E0945656.601.

Maximum Steepness (V/m/μs)	*Peak (V/m)*	*10%- 90% Rise Time (μs)*	*Pulse Width (μs)*
46.73	404.285	1.336	3.2774

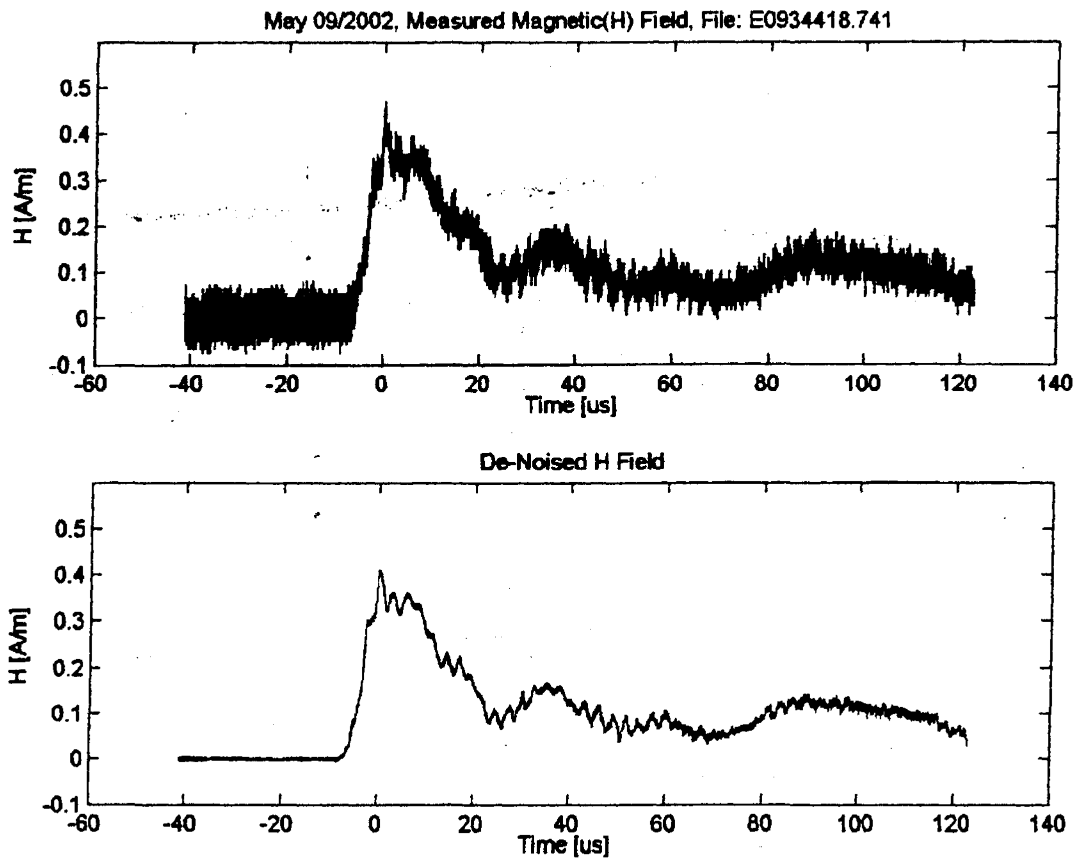

Figure 4.41: Measured and de-noised magnetic field, File: E0934418.741.

Table 4.5: Magnetic field waveform parameters. File: E0934418.741.

Maximum Steepness (A/m/μs)	*Peak (A/m)*	*10%- 90% Rise Time (μs)*	*Pulse Width (μs)*
0.05	0.412	5.3234	19.45

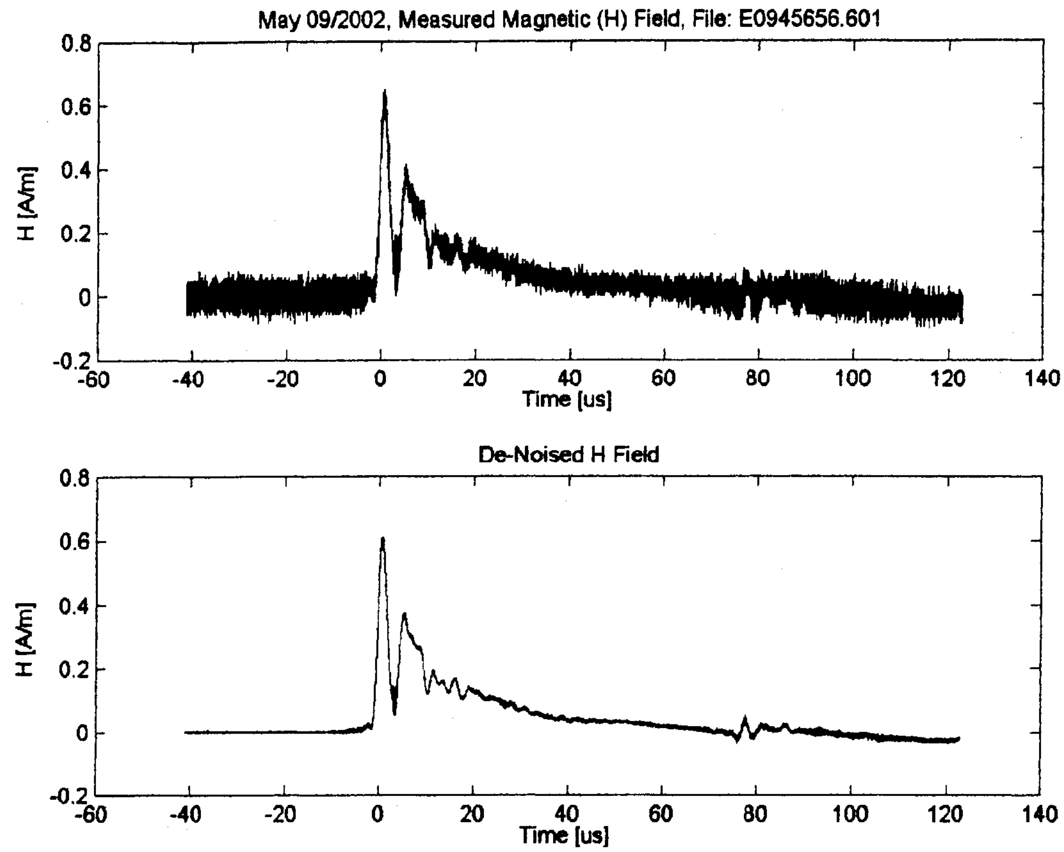

Figure 4.42: Measured and de-noised magnetic field, File: E0945656.601.

Table 4.6: Magnetic field waveform parameters. File: E0945656.601.

Maximum Steepness (A/m/μs)	*Peak (A/m)*	*10%- 90% Rise Time (μs)*	*Pulse Width (μs)*
0.07	0.6092	1.33	2.1431

From the above de-noised waveforms it is obvious that the proposed de-noising method makes it possible to obtain the field waveform parameters. The summary of the parameters obtained from the de-noised field waveforms are tabulated in Table 4.7.

Table 4.7: Field waveform parameters, May 09, 2002

Field Name	**File Name**	**Parameters**			
		Maximum Steepness *(V/m/µs)*	**Peak *(V/m)***	**10%- 90% Risetime *(µs)***	**Pulse Width *(µs)***
Electric Field *(E)*	E0934418.741	-58.06	-368.102	3.635	11.673
	E0945656.601	46.73	404.285	1.336	3.2774
		(A/m/µs)	***(A/m)***	***(µs)***	***(µs)***
Magnetic Field *(H)*	E0934418.741	0.05	0.412	5.3234	19.45
	E0945656.601	0.07	0.6092	1.33	2.1431

Chapter 5

Conclusions

In this thesis we proposed an STFT-based Spectral Subtraction de-noising algorithm to minimize the effect of the unwanted interferences from the lightning current derivative signals measured at the CN Tower. We successfully applied the proposed method for de-noising the current derivative signals as well as the electric and magnetic field signals generated by lightning strikes to the CN Tower. This chapter presents the conclusions of the thesis and discusses directions of future work.

5.1 General Conclusions and Discussions

In chapter 3 we delineated the suppression of quasi-periodic interferences. DC offset, high frequency and low frequency noise in recorded CN Tower lightning current derivative waveforms were removed or substantially minimized. In the summer of 1997, a new Rogowski coil was installed and was connected to the recording station through an optical fiber link, which renders the above types of noise almost insignificant. However, current derivative signals captured by the old Rogowski coil are important for the derivation of extensive statistics that are of interest to scientists working in the area of lightning protection. Aside from the limited data captured by the new Rogowski coil, it has been showing deterioration in its performance during the last several years. That is why de-noising the signals recorded by the old Rogowski coil is important.

Heidler function is used to model the lightning current measured at the CN Tower, as described in chapter 3. The derivative of the Heidler function is artificially distorted by an actual noise derivative signal, measured at the CN Tower in the absence of lightning. Then the Spectral Subtraction method is used to remove the added noise.

The proposed method gives better output when it is applied on the current derivative *(di/dt)* signals rather than the current signals, as discussed in chapter 3. A new measure, signal-peak to noise-peak ratio (SPNPR) for analyzing the CN Tower lightning current signal is defined and calculated before and after the de-noising process. For example, for a typical measured CN Tower lightning current derivative signal, the SPNPR before de-noising was found to be 7.27, and after de-noising it became 151.30. Similarly for its current waveform (obtained by numerical integration), the SPNPR before de-noising was 20.16 and it became 361.39 after de-noising.

A de-noised old coil current derivative waveform compares well with the simultaneously measured new noise-protected coil current derivative waveform. Furthermore, the current waveform, obtained by numerical integration of the de-noised current derivative waveform, proved close to that of the new coil.

The current parameters obtained from the de-noised waveforms are reported in chapter 4. These parameters will assist in designing systems for protection from the hazards of the lightning discharge. It always proved difficult to even make an estimate of the waveform parameters for low level lightning current derivative and current waveforms obtained through the old coil (e.g., signals captured on May 09, 2002). However, applying the proposed method facilitated the determination of these parameters.

When the Spectral Subtraction method was applied to a noise signal measured in the absence of lightning, it was found that allocating one third of the record to the pre-stroke lightning portion helps to characterize the noise signal and eventually de-noising it, as described in chapter 3.

5.2 Original Contributions

Original contributions of this thesis can be summarized as follows:

1. The successful application of STFT-based Spectral Subtraction method for de-noising non-stationary noise, such as the noise embedded in the CN Tower lightning current signal and its associated electric and magnetic fields.
2. Using Heidler function to simulate the lightning signal.
3. Simulating the noisy current signal by a combination of the derivative of Heidler function and a measured noise file in the absence of lightning.
4. Identification of future work.

5.3 Main Features

In conclusion, the main features of the proposed method are summarized as:

1. **Capability of analyzing signals of non-stationary nature:** The algorithm is essentially a signal processing tool which is capable of analyzing non-stationary signals.
2. **Capability of de-noising the signals of non-stationary noise:** The core method directly decomposes the signal into segments and estimates the average noise spectrum during the non-lightning period. The average noise spectrum is then subtracted from the signal to obtain the de-noised waveform.
3. **Simplicity of the algorithm and programming:** The algorithm is easy to implement using Matlab programming software.

5.4 Future Work

More work is needed to improve and expand the area of application of the proposed de-noising method to reach following goals:

1. **Noise cancellation without affecting the peak and rate of rise:** The method should work in such a way so that the peak and rate of rise of both the current derivative and current waveforms remain completely intact. The proposed method was found to very slightly affect the peak and rate of rise which is of concern.

2. **Calculating the pulse width and the total charge introduced by lightning:** Reflections should be estimated and cancelled out from the lighting current signals which will help in calculating the current pulse width and the total impulse charge generated by lightning.

3. **Electromagnetic interference source identification:** A major research trend in electromagnetic compatibility (EMC) engineering is the application of signal processing in interference characterization, source identification and EMI mitigation. Characterization of interferences is useful as it helps in the identification of potential sources within or outside a system, tracing noise and interference and suppression or mitigation of the interferences [7, 19]. The proposed method, by virtue of its ability to decompose a signal into segments while tracking its time variations, is expected to be applicable in the area of interference analysis and cancellation.

Publications and Awards

During the span of the thesis, the published papers and received awards are as follows:

[p1] M.J. Islam and A.M. Hussein, "De-noising the CN Tower Lightning Current Signal by Modifying Its Fast Fourier Transform", *CAGE Club Student Conference on High Voltage Engineering and Applied Electrostatics,* University of Western Ontario, London, ON, August 20, 2002.

Note: Received **Best Graduate Student Paper Award**.

[p2] M.J. Islam and A.M. Hussein, "A Novel Technique for De-noising the CN Tower Lightning Current Signal by Modifying Its Fast Fourier Transform", *International Signal Processing Conference (ISPC)' 2003,* Paper# 287, pp. 1-5, Dallas, TX, USA, March 31- April 3, 2003.

[p3] M.J. Islam and A.M. Hussein, "Frequency Analysis of CN Tower Lightning Current Signals Using Short Term Fourier Transform", *International Conference for Upcoming Engineers (ICUE)*, Paper# 2, Maxwell Session, pp. 1-4, Ryerson University, Toronto, ON, May 1-2, 2003.

Note: Received **Best Graduate Student Paper Award**.

[p4] M.J. Islam and A.M. Hussein, "De-Noising the CN Tower Lightning Current Signal Using Short Term Fourier Transform-Based Spectral Subtraction", in preparation to submit to *Journal of Applied Signal Processing (The European Association for Signal Processing).*

References

[1] M.A. Uman, The Lightning Discharge, Academic Press, Inc., 1987.

[2] A.M. Hussein, W. Janischewskyj, J.S. Chang, V. Shostak, W. Chisholm, P. Dzurevych, and Z.I. Kawasaki, "Simultaneous Measurement of Lightning Parameters for Strokes to the Toronto CN Tower," *Journal of Geophysical Research-Atmosphere*, vol. 100, no. 5, pp. 8853-8861, May 1995.

[3] W. Janischewskyj, A.M. Hussein, V. Shostak, I. Rusan, J.X. Li and J.S. Chang, "Statistics of Lightning Strikes to the Toronto CN Tower (1978-1995)," *IEEE Trans. Power Delivery*, vol. 12, no. 3, pp. 1210-1221, July 1997.

[4] P. Dzurevych, "Measurement and Analysis of Lightning Strokes to the CN Tower in Toronto", *MASc. Thesis, Electrical and Computer Engineering Department*, University of Toronto, ON, 1993.

[5] J.R. Barrat, "Influence of Reflections within Instrumental Towers on the measurement of Lightning Current ", *BASc. Thesis*, University of Toronto, Toronto, ON, Dec., 1995.

[6] A. Obaid, "Improving the SNR of lightning Records Captured at the CN Tower using Linear Filtering Techniques", *BASc. Thesis*, University of Toronto, Toronto, ON, Apr., 1993.

[7] A.K. Ziarani, "Extraction of Non-Stationary Sinusoids", *PhD thesis, Electrical and Computer Engineering*, University of Toronto, Tornoto, ON, December, 2002.

[8] A.A. Girgis, F.M. Ham, "A Quantitative Study of Pitfalls in the FFT", *IEEE Transactions on Aerospace and Electronic Systems*, vol. 16, no. 4, pp. 434-439, 1980.

[9] M.J. Islam, A.M. Hussein, "Frequency Analysis of CN Tower Lightning Current Signals Using Short Term Fourier Transform", *International Conference for Upcoming Engineers (ICUE)*, Paper# 2, Maxwell Session, pp. 1-4, Ryerson University, Toronto, ON, May 1 and 2, 2003.

[10] S.K. Mitra, Digital Signal Processing: A Computer- Based Approach, Second Edition, New York: McGraw-Hill, 2001.

[11] J.B. Allen, " Short Term Spectral Analysis, Synthesis, and Modification by Discrete Fourier Transform", *IEEE Transactions On Acoustics, Speech and Sig. Processing*, vol. ASSP- 25(3), pp. 235-238, 1977.

[12] J.B. Allen, L.R. Rabiner, "A Unified Approach to Short Time Fourier Analysis and Synthesis", *IEEE Transactions On Acoustics, Speech and Sig. Processing*, vol. 65, pp. 1558-1564, 1977.

[13] http://engineering.rowan.edu/~polikar/~wavelets

[14] http://cnmat.berkeley.edu/~alan/MS-html/MSv2.html

[15] S.F. Boll, "Suppression of Acoustic Noise in Speech Using Spectral Subtraction", *IEEE Transactions on Acoustics, Speech, and Signal Processing*, vol. ASSP-27, no. 2, pp. 113-120, April 1979.

[16] F. Heidler, "Lightning Electromagnetic Impulse", *Theorie und Messungen, Thesis dissertation, Fakultät der Elektrotechnik*, Universität der Bundeswehr, München, 1987.

[17] M.J. Islam, A.M. Hussein, "A Novel Technique for De-Noising the CN Tower Lightning Current Signal by Modifying Its Fast Fourier Transform", *International Signal Processing Conference (ISPC)*, Paper# 287, pp. 1-5, Dallas, TX, USA, April 31- May 3, 2003.

[18] I. Rusan, "CN Tower Lightning Parameters", *MASc. Thesis*, University of Western Ontario, London, ON, May 1996.

[19] G. Antonini, A. Orlandi, "Wavelet packet-based EMI signal processing and source identification", *IEEE Transactions on Electromagnetic Compatibility*, vol. 43, no. 2, pp. 140-148, 2001.

Appendix

Spectral Subtraction Implementation Code in Matlab:

```
% signal is the variable that contains the dc removed di/dt
i2=signal;
% Half of window length Zero is inserted in front and back end
i1=[zeros(1,1024),i2,zeros(1,1024)];
w=hanning(2048); % Hanning window of size 2048 for segmentation
k=1;
% Segmenting the signal into frames of length 2048 each one
for n=1:1024:length(i1)-2047
    sp(k,n:n+2047)=fft(w.*i1(n:(n+2047))); % FFT of each frame
    abs_sp(k,n:n+2047)=abs(sp(k,n:n+2047)); % Magnitude of FFT
    angle_sp(k,n:n+2047)=angle(sp(k,n:n+2047)); % Phase angle
    k=k+1;
end
s=size(sp);
%Bias Estimation
test_abs=(abs_sp(2,1025:3072)+abs_sp(3,2049:4096))./2;
k=1; % Subtraction only magnitude in Frequency domain
for n=1:1024:length(i1)-2047
   abs_sp(k,n:n+2047)=abs_sp(k,n:n+2047)-test_abs;
    k=k+1;
end
```

```
% Half Wave Rectification
for k=1:s(1)
    for n=1:length(i1)
        if(abs_sp(k,n)<0)
            abs_sp(k,n)=0;
        end
    end

% Signal Reconstruction Using Overlap Add Method
x_hat=zeros(1,length(i1));
j=sqrt(-1);
k=1;
for n=1:1024:length(i1)-2047
    x_hat(:,n:n+2047)=x_hat(:,n:n+2047)+real(ifft(abs_sp(k,n:n
                    +2047).*exp(j*angle_sp(k,n:n+2047))));
    k=k+1;
end
% Ignoring the zeros that was inserted in front and back end
no_dc_sig1=x_hat(1025:length(i1)-1024); % De-Noised di/dt
% Integration of di/dt
integ_sig1=zeros(1,length(signal));
% dt1 is the initial time step in μs that is 0.01
integ_sig1=cumsum(no_dc_sig1)*dt1; % De-noised Current
```